THE ROLE OF THE ENERGY CONSERVING HYDROGENASE B IN AUTOTROPHY AND THE CHARACTERIZATION OF SULFUR METABOLISM IN *METHANOCOCCUS MARIPALUDIS*

by

TIFFANY ANN MAJOR

(Under the Direction of William B. Whitman)

ABSTRACT

The energy-conserving hydrogenase b (Ehb) in hydrogenotrophic methanogens such as *Methanococcus maripaludis* couples the oxidation of H_2 to the production of a proton motive force. The electrons and energy generated by the Ehb are used by enzymes involved in carbon fixation, which catalyze endergonic reactions requiring low-potential electrons. To characterize the Ehb function, several *ehb* genes were deleted. Most *ehb* deletion strains exhibited reduced growth phenotypes under autotrophic conditions (i.e., in minimal medium). Furthermore, growth of the Ehb large hydrogenase mutant strain S965 was inhibited by aryl acids. The indolepyruvate oxidoreductase (Ior) is a carbon assimilatory enzyme that converts aryl acids into amino acids. The lack of S965 growth on aryl acids provides the first physiological evidence that the Ehb activity is associated with the Ior function.

Electron transport from the Ehb is performed by ferredoxins. The sequenced methanogen genomes contain a large number of open reading frames that contain $CX_2CX_2CX_3C$ motifs, which bind 4Fe-4S clusters. Two proteins predicted to shuttle electrons between the Ehb and the pyruvate oxidoreductase are the PorE and PorF. Characterization of recombinant histidine-

tagged PorE and PorF from *E. coli* was attempted; however, results were inconclusive due to protein insolubility during purification and the lack of PorE- or PorF-specific assays.

Sulfur assimilation is necessary to produce both iron-sulfur clusters and cysteine. A pathway was proposed where cysteine biosynthesis occurs by tRNA-loading in the hydrogenotrophic methanogens. *In vivo* characterization of this pathway involved the deletion of the *sepS* gene in *M. maripaludis*, which encodes a protein that converts *O*-phosphoserine-tRNA^{Cys} to cysteine-tRNA^{Cys} *in vitro*. The Δ*sepS* deletion strain S210 was a cysteine auxotroph, suggesting that no other mechanism of cysteine biosynthesis exists in this organism. Attempts to delete the gene encoding the second enzyme in this pathway were unsuccessful, suggesting that this gene may be essential. The quantity of cysteine necessary for S210 growth is less than the calculated value for the total thiols within *M. maripaludis*. As free cysteine is the sulfur source for thiol-containing cofactors and prosthetic groups in other organisms, this result suggests that this organism also uses an alternative method of sulfur assimilation. Current studies are underway to quantify cellular pools of free cysteine and homocysteine.

INDEX WORDS: electron transport, archaea, methanogen, hydrogenase, membrane-bound, ferredoxin, iron-sulfur cluster, cysteine biosynthesis, cysteine metabolism

THE ROLE OF THE ENERGY CONSERVING HYDROGENASE B IN AUTOTROPHY AND THE CHARACTERIZATION OF SULFUR METABOLISM IN *METHANOCOCCUS MARIPALUDIS*

by

TIFFANY ANN MAJOR

B.S., Grand Valley State University, 2000

A Dissertation Submitted to the Graduate Faculty of The University of Georgia in Partial Fulfillment of the Requirements for the Degree

DOCTOR OF PHILOSOPHY

ATHENS, GEORGIA

2006

THE ROLE OF THE ENERGY CONSERVING HYDROGENASE B IN AUTOTROPHY AND THE CHARACTERIZATION OF SULFUR METABOLISM IN *METHANOCOCCUS MARIPALUDIS*

by

TIFFANY ANN MAJOR

Major Professor: William B. Whitman

Committee: Robert J. Maier
Joy B. Peterson
Lawrence J. Shimkets

Electronic Version Approved:

Maureen Grasso
Dean of the Graduate School
The University of Georgia
August 2006

TABLE OF CONTENTS

Page

CHAPTER

CHAPTER 1

INTRODUCTION AND LITERATURE REVIEW

Methanogens are an interesting group of organisms for several reasons. First, they are found in diverse habitats, from freshwater to saturated brine, in glacers and around oceanic hydrothermal vents, in gasterointestinal tracts, rice paddies and salt marshes (6, 17, 44, 51, 98). Second, methanogens are a phylogenetically diverse group that are categorized by the obligate use of methanogenesis for energy production (121). Biochemically, these organisms are interesting due to their novel enzymes and cofactors, many of which are used to obtain energy through methane production (111). Methanogens have an agricultural relevance because of the generation of methane in the rumen of cattle and in rice paddies. Finally, methanogens are ecologically relevant in the carbon cycle and environmentally significant in the production of the greenhouse gas methane, of which 27 teragrams per year are predicted to be biologically generated in the United States by the year 2010 (113).

Phylogeny and categorization of Archaea

Methanogens are found in the domain Archaea (122). Archaea differ from bacteria and eukarya by a number of features. First, archaeal lipids are formed of isoprenoid chains and are ether-linked to glycerol as opposed to bacterial lipids, which are fatty acyl chains with ester links. Archaea have unusual tRNA modifications, ribosome structure and novel cell walls (often comprised of the S-layer protein), which gives the archaea a range of antibiotic sensitivities different from bacteria or eukarya. Archaea also have some similarities to eukaryotes, primarily in the RNA polymerases and promoter structures.

Archaea are comprised of three phyla with isolated representatives, Crenarchaeota and Euryarchaeota. *Nanoarchaeum equitans* may represent a third archaeal phylum (12, 39). This hyperthermophilic archaeon is a parasite of *Ignicoccus,* from which this organism obtains its amino acids, nucleotides and lipids (116). A fourth phylum (Korarchaeota) is predicted to exist from environmental 16S rDNA sequences. *Crenarchaeota* are all within a single class (*Thermoprotei*), which include the three orders *Desulfurococcales*, *Thermoproteales*, and *Sulfolobales*. The archaea in the Crenacrchaeota are obligately thermophilic chemoheterotrophs that are mostly hyperthermophilic, acidophilic and/or sulfur-dependent. The phylum *Euryarchaeota* consists of seven classes: *Methanobacteria, Methanococci, Methanopyri, Halobacteria, Thermoplasmata, Thermococci,* and *Archaeoglobi*. Of these groups, the first three are comprised of methanogens. Other physiological groups of Euryarchaeota include halophiles, Archaea lacking a cell wall, sulfate reducers and thermophilic sulfur metabolizers (31).

Phylogeny and physiology of methanogens

There are five orders of methanogenic archaea: *Methanobacteriales, Methanococcales, Methanomicrobiales, Methanopyrales,* and *Methanosarcinales*. Table 1 displays the characteristics of each order of methanogens, including cell wall structure, lipid head group composition, and substrates utilized for methanogenesis.

Methanogens are divided into three groups according to the substrates utilized as carbon and energy sources for methanogenesis. Hydrogenotrophic methanogens use H_2 and/or formate as an electron donor and CO_2 is reduced to methane (9, 87). Methylotrophic methanogens reduce the methyl group of a one-carbon compound (such as methanol). The methyl groups can also be electron donors upon oxidation to CO_2; alternatively, H_2 can be used as an electron donor (9). Aceticlastic methanogens split acetate to form CO_2 and CH_4 (9). No methanogens are able

to utilize more complex organic substrates than acetate and/or secondary alcohols for methanogenesis.

Our model organism is *Methanococcus maripaludis*. This species is a member of the order *Methanococcales*. *M. maripaludis* cells are irregular cocci that are motile by flagella (50). The cell wall of *M. maripaludis* is comprised of protein, primarily the surface layer protein. The genomic DNA of methanococci has a mol G+C% of approximately 32-34%. These organisms can only use H_2 plus CO_2 or formate for methanogenesis. *M. maripaludis* can grow autotrophically using a modified Ljungdahl-Wood pathway or heterotrophically by the assimilation of acetate (119).

Methanococcus autotrophy

The methanococci utilize CO_2 as a source of carbon for biomass production. This is performed via a modification of the reductive acetyl-CoA pathway, also known as the Ljungdahl-Wood pathway (Figure 1).

Ljungdahl-Wood pathway

Forms of the Ljungdahl-Wood pathway are performed by methanogens, some acetogens and some sulfate-reducing bacteria. In this pathway, acetyl-CoA is synthesized from two carbon dioxide molecules, one of which is reduced to the methyl state while the other is converted to a carbonyl group.

The modified Ljungdahl-Wood pathway in methanogens is associated with the methanogenesis pathway. In the first step, CO_2 is bound to methanofuran by the formylmethanofuran dehydrogenase (Fmd). This reaction requires low potential electrons. In *Methanosarcina barkeri*, these electrons are generated by the Ech hydrogenase, which couples a

proton gradient to low potential electron generation from H_2 (68). Ferredoxin is the physiological electron transport protein between the Ehb and the Fmd (68).

The formyl group is transferred to tetrahydromethanopterin, where it is reduced in a step-wise fashion to methyltetrahydromethanopterin (Figure 1). The methyl group from this compound is then transferred to the carbon monoxide dehydrogenase/acetyl-CoA synthase (CODH/ACS). The CODH/ACS enzyme has two activities: to reduce CO_2 to CO and to condense the bound CO, CH_3 and a HS-CoA molecule to form acetyl-CoA.

Carbon Monoxide Dehydrogenase/Acetyl-CoA Synthase

Most methanogenic CODH/ACS enzymes contain five subunits, αβγδε, which have been resolved into three enzyme components (49). The first enzyme component, at which the primary CODH reactions occur, is the nickel/iron-sulfur component (83). This component, which contains the αε subunits, is structurally and functionally similar to the clostridial CODH Clusters B and C (49, 93). The second enzyme component, the β subunit, contains Cluster A, the site of acetyl-CoA synthesis (70, 93). The third component, composed of the δγ subunits, is a corrinoid/iron-sulfur component (64, 70). *C. thermoaceticum* has a similar protein that functions as a methyl carrier in the synthesis of acetyl-CoA, but unlike the methanogenic CODH, the clostridial corrinoid protein does not co-purify with the CODH/ACS enzyme (66).

The *cdh* genes, which encode for the CODH subunits, form a single multicistronic operon in most methanogens (64). For example, in *Methanosarcina thermophila*, the *cdhABCDE* operon encodes the αεβδγ subunits, respectively, to form a CODH/ACS with the quarternary structure $(\alpha\varepsilon\beta\delta\gamma)_8$ (64). Annotation of the *M. maripaludis* genome sequence identified 5 genes for the CODH/ACS enzyme that were members of a gene cluster (Table 2; 38). Two additional genes were found that correspond to a Ni-insertion protein and a potential ferredoxin. The ORF

cdhD is related to the nickel-insertion gene *cooC* of the carbon monoxide dehydrogenase of *Rhodospirillum rubrum* and may be involved in biosynthesis or maturation of the prosthetic group (42). MMP0979 (*cdhG*) is similar to *porE* and *porF*, which are associated with the pyruvate oxidoreductase (58). These proteins are low molecular weight iron-sulfur containing proteins, which are predicted to transfer electrons from the energy-conserving hydrogenase B (Ehb) to their respective enzymes (58, 79).

Pyruvate Oxidoreductase

In the methanococci, acetyl-CoA is reductively carboxylated to pyruvate by the pyruvate oxidoreductase (Por). The midpoint potential of the acetyl-CoA/pyruvate couple is approximately -500 mV under physiological conditions, and the pyruvate synthesis reaction is endergonic. In order to generate pyruvate, the pyruvate oxidoreductase must be coupled to an energy-providing source. Meuer (68) demonstrated that pyruvate biosynthesis is linked to the energy-conserving hydrogenase in *Methanosarcina barkeri*. The energy-conserving hydrogenases (Ech) couple the oxidation or reduction of low potential electron carriers to the proton motive force. Ferredoxins were found to be the physiological electron acceptors for the Ech of *Methanosarcina* (68) as well as the electron donors for the Por of *Moorella* (65). As yet, no ferredoxin(s) have been identified that directly link the Ech to the Por.

Most Pors from anaerobic archaea contain four subunits. The purified *M. maripaludis* Por enzyme was found to contain five polypeptides (59). Furthermore, the *M. maripaludis* genome contains a cluster of six contiguous *por* genes (Table 3): the standard four found in anaerobic archaea as well as two extra genes, which are are predicted to be ferredoxins (38, 58, 59). It is predicted that the PorE and/or the PorF are involved in the electron transport from the Ehb to the Por (58).

Incomplete Reductive Tricarboxylic Acid Cycle

Pyruvate is converted to phosphoenolpyruvate and oxaloacetate, which is shuttled into the incomplete reductive tricarboxylic acid (IR-TCA) cycle (Figure 2). The methanococci utilize the IR-TCA cycle to convert oxaloacetate to 2-ketoglutarate through a series of reductions. In methanococcal autotrophy, most of the amino acids are derived from pyruvate, oxaloacetate or 2-ketoglutarate.

Amino acid biosynthesis

Several pathways of amino acid biosynthesis in methanogens are similar to those found in bacteria and eukaryotes. Three pathways that differ in some methanogens are the biosynthesis pathways for the aromatic amino acids, isoleucine and cysteine.

Aromatic amino acid biosynthesis

Two pathways exist in *M. maripaludis* for synthesizing the aromatic amino acids tryptophan, phenylalanine and tyrosine (Figure 3). One pathway is the aryl acid pathway, where exogenous aryl acids are assimilated and converted to aromatic amino acids. In this pathway, the aryl acids (indoleacetate, phenylacetate and *p*-hydroxyphenylacetate) are first activated with coenzyme A to yield a thioester (81). Next, the thioester is reductively carboxylated by the indolepyruvate oxidoreductase (Ior) to indolepyruvate, phenylpyruvate or *p*-hydroxyphenylpyruvate. This substrate is then reductively transaminated to its amino acid form.

The second pathway for aromatic amino acid biosynthesis is called the *de novo* aromatic amino acid biosynthetic pathway (Figure 3). As the early steps of the *de novo* pathway are novel, these steps have only recently been elucidated in the methanogens (118). Incorporation of $U^{13}C$-labeled acetate generated a phenylalanine isotopic labeling pattern consistant with a 6-deoxy-5-ketofructose 1-phosphate (DKFP) pathway of aromatic amino acid biosynthesis (80). In

this pathway, fructose-1,6-bisphosphate is a precursor for DKFP, 2-amino-3,7-dideoxy-*D*-threo-hept-6-ulosonate (ADTH), and 3-dehydroquinate (80). A gene from *Methanocaldococcus jannaschii* predicted to encode fructose-1,6-bisphosphate aldolase was expressed in *E. coli* (80). The enzyme catalyzed the conversion of FBP to DKFP (80). Deletions were made in two genes that were predicted to encode the next two steps of the DKFP pathway, *aroA'* and *aroB*' (80). These genes were found to encode ADTH synthase and dehydroquinate synthase II, respectively (118). The *aroA'* mutant required aromatic amino acids for growth, suggesting that this is directly involved in the aromatic amino acid biosynthesis pathway (80). The *aroB'* mutant did not require aromatic amino acids for growth, which suggests that there is an isozyme to the dehydroquinate synthase capable of performing the same biochemical reaction (80). Later steps of the *de novo* aromatic amino acid biosynthesis pathway are described in Figure 3 (81).

Interestingly, several of the steps of the aromatic amino acid biosynthesis pathway are either feedback or transcriptionally regulated (80, 81). Prephenate dehydratase, which converts prephenate to phenylalanine, is feedback inhibited by phenylalanine but activated by tyrosine (81). Both tyrosine and *p*-hydroxyphenylpyruvate cause feedback inhibition of prephenate dehydrogenase, which converts prephenate to *p*-hydroxyphenylpyruvate, the precursor of tyrosine (81). Growth with aryl acids reduces the expression of ADTH synthase and FBP aldolase (80, 81). The 3-dehydroquinate dehydratase enzyme catalyzes the conversion of 3-dehydroquinate to 3-dehydroshikimate (81).

Branched chain amino acid biosynthesis

Similarly to the aromatic amino acids, two pathways for branched chain amino acid (BCAA) biosynthesis also exist in *Methanococcus maripaludis*, a *de novo* pathway and a pathway for branched chain fatty acid (BCFA) incorporation (23, 94, 120). The biosynthesis of

leucine, isoleucine and valine occurs using the acetohydroxyacid pathway, which is similar to that found in bacteria (22). However, in the methanogens, isoleucine is derived from a different source. In the most common bacterial pathway, isoleucine is derived from threonine. In methanogens and some bacteria, isoleucine is generated from 2-ketobutyrate, which is produced via the citramalate pathway (20, 21, 23). 2-Ketobutyrate is shuttled into the acetohydroxyacid pathway (22). The methanococci contain the four enzymes involved in the acetohydroxyacid pathway: acetohydroxyacid synthase, acetohydroxyacid isomeroreductase, dihydroxyacid dehydratase and branched chain aminotransferase (124, 125).

The second pathway of branched chain amino acid biosynthesis involves the BCFAs isovalerate, 2-methylbutyrate and isobutyrate, in a pathway analagous to the aryl acid pathway. Notably, in the BCFA incorporation pathway, the 2-oxoisovalerate oxidoreductase (VOR) is utilized to carboxylate the BCFA-thioesters (108).

Ferredoxin-dependent Oxidoreductases

Oxidoreductases reductively carboxylate acyl-CoA derivatives to 2-oxoacids in the methanogens. Seven gene clusters corresponding to ferredoxin-dependent oxidoreductases were found in *Methanococcus maripaludis* (Tables 3 and 4). These include open reading frames encoding the 2-oxoisovalerate oxidoreductase (Vor), pyruvate oxidoreductase (Por), 2-oxoglutarate oxidoreductase (Kor), two gene clusters for indolepyruvate oxidoreductase (Ior), and a gene cluster homologous to a non-specific oxidoreductase of *Sulfolobus* (108, 127). An open reading frame corresponding to the *Pyrococcus furiosus* glyceraldehyde-3-phosphate oxidoreductase (Gapor) has also been identified.

Cysteine

Cysteine is one of the 22 amino acids translationally inserted during protein production. Of the amino acids, cysteine has some of the most complex chemical interactions within the protein, including formation of disulfide bonds and coordination to metal active sites. Furthermore, cysteine is the primary sulfur source for biosynthesis of a variety of cofactors and prosthetic groups including iron-sulfur clusters, biotin, molybdopterins, thiamin, lipoic acid, 4-thiouridine and several coenzymes (45, 47, 56, 57, 74, 106).

Bacterial cysteine biosynthesis

Cysteine biosynthesis in *E. coli* and other bacteria starts with the uptake and reduction of sulfate (52). Extracellular sulfate binds to the sulfate permease and is transported into the cell. Once inside the cell, ATP sulfurylase reacts with the sulfate to form adensine 5'-phosphosulfate (APS). APS kinase then adds a second phosphate group to APS, generating 3'-phosphoadenosine 5'-phosphosulfate or PAPS. PAPS sulfotransferase converts the PAPS to sulfite, which is subsequently reduced by sulfite reductase to sulfide. Concurrently, serine transacetylase activates serine with acetyl-CoA, producing O-acetylserine. O-acetylserine and sulfide are finally converted to cysteine via the O-acetylserine sulfhydrolases A and B.

Cysteine biosynthesis in mammals

Mammals synthesize cysteine through a transsulfuration of the sulfhydryl of methionine to serine (32). In the first reaction, methionine is activated by ATP to form S-adenosyl-methionine (SAM), which is catalyzed by methionine adenosyltransferase MAT1A and MAT2A. A variety of cellular methyltranferases then convert SAM to S-adenosyl-homocysteine (SAH). SAH hydrolase generates adenosine and free homocysteine. Cystathione β-synthase condenses

homocysteine and serine to form cystathionine. Finally, cysteine and α-ketobutyrate are generated due to the activity of cystathionine γ-lyase.

Cysteine biosynthesis in *Saccharomyces cerevisiae*

The biosynthesis of cysteine in the yeast *S. cerevisiae* appears to be a hybrid of the bacterial and mammalian pathways (112). In this pathway, homoserine is first activated through esterification to *O*-acetylhomoserine by the homocysteine transacetylase enzyme. Sulfide is incorporated into *O*-acetylhomoserine by *O*-acetylhomoserine sulfhydryls, generating homocysteine. The remainder of the steps converting homocysteine to cysteine is performed as in the mammalian pathway.

Cysteine biosynthesis in methanogens

Some aceticlastic methanogens such as *Methanosarcina barkeri* and *Methanosarcina thermophila* were found to have homologs to the bacterial cysteine biosynthesis genes (3, 10, 48). However, in the genome sequences of hydrogenotrophic methanogens *Methanothermobacter thermautotrophicus*, *Methanocaldococcus jannaschii*, and *Methanopyrus kandleri*, no homologs were found to the serine *O*-acetyltransferase, *O*-acetylserine sulfhydrylase, cystathionine β-synthase or cystathionine γ-lyase (3, 15, 99, 100). White (117) found in vitro cysteine production was dependent upon homocysteine, cystathionine and *O*-phosphoserine. Although these possible intermediates could be used to generate cysteine, neither the natural presence of these intermediates nor the enzymes catalyzing these reactions were identified (117).

A second hypothesized method for cysteine biosynthesis was through Cys-tRNA^{cys} formation. Sauerwald *et al.* (90) identified *O*-phosphoserine as the substrate that binds the tRNA^{Cys} through the purification of low molecular weight filtration of *M. jannaschii* cell-free

extracts. Purification of *M. jannaschii* proteins along with liquid chromatography-repeated mass spectrometry analysis identified SepS, an *O*-phosphoseryl-tRNA synthetase that was subsequently shown to catalyze the binding of *O*-phosphoserine to $tRNA^{Cys}$ (90). A deletion in the *Methanococcus maripaludis sepS* gene, which encodes the *O*-phosphoseryl-tRNA synthetase, generated a cysteine auxotroph (90). This mutation was not lethal because *M. maripaludis* has a copy of the canonical bacterial *cysS* gene, which is the typical Cys-$tRNA^{cys}$ synthetase. This gene had previously been deleted in *M. maripaludis*, demonstrating that a second system for loading cysteine into tRNA is present (103). The proposed second step of cysteine-$tRNA^{Cys}$ synthesis is the conversion of *O*-phosphoserine-$tRNA^{Cys}$ to cysteine-$tRNA^{Cys}$ by a NifS homolog named SepCysS. Production of recombinant SepCysS, in the presence of sodium sulfide and pyridoxal phosphate, catalyzed the conversion of *O*-phosphoserine-$tRNA^{Cys}$ to cysteine-$tRNA^{Cys}$ (90). Although the gene encoding SepCysS, *pscS*, has been identified, the role of the *pscS* gene product has not yet been shown *in vivo*.

Sulfur assimilation from cysteine

The incorporation of sulfur into proteins, cofactors and prosthetic groups is of primary importance because sulfur is typically the catalytic site of biochemical reactions (43). The first step of sulfur assimilation in plants and bacteria is the assimilation or biosynthesis of cysteine (32, 52, 62, 63). Cysteine is the sulfur donor for a variety of prosthetic groups and cofactors for proteins. These include iron-sulfur clusters, thiamine, biotin, lipoic acid and molybdopterins (45, 47, 56, 57, 106).

Biosynthesis of iron-sulfur clusters

Iron-sulfur cluster-containing proteins are found throughout the three domains of life. The Fe-S cluster is commonly used during electron transport and is found in proteins such as

ferredoxin, hydratase, nitrogenase, various reductases, hydrogenase and biotin synthase. Clusters vary by the number of Fe and S units, with the most common combinations being [2Fe-2S], [3Fe-4S], [4Fe-4S] or [8Fe-7S] (43). Furthermore, several enzymes use Fe-S clusters along with additional metal ions to form complex active sites. Some examples of this are the nickel and cobalt active sites of the carbon monoxide dehydrogenase/acetyl-CoA synthase enzyme and the di-iron center of the iron-sulfur hydrogenase (19, 73).

The formation of iron-sulfur clusters has only recently been studied. When making deletions in the nitrogenase (*nif*) genes, Δ*nifS* and Δ*nifU* mutants were deficient in nitrogenase [Fe-S] cluster biosynthesis (41). NifU was found to be a scaffold protein. This homodimeric protein contains two [2Fe-2S] clusters, one of which is permanent while the other is transferred to the target protein (30, 126). Characterization of the *nifS* gene product revealed that NifS is a pyridoxal 5'-phosphate (PLP)-dependent cysteine desulfurase (130). This type of enzyme catalzxyes the breakdown of cysteine to alanine and sulfide, providing the sulfur groups for Fe-S clusters. *M. maripaludis* contains a *nifS* homolog called *pscS*. As discussed above, it is believed to catalyze the transformation of *O*-phosphoserine-bound to Cys-tRNA to cysteine (90). The *pscS* is the only *nifS* homolog found in *M. maripaludis*.

Other NifS homologs include IscS (128) and SufS (76). Purified IscS was found to have cysteine desulfurase activity (25). IscS was subsequently shown to transfer sulfur from cysteine to form 4-thiouridine tRNA (45), thiamin and NAD (56) in *E. coli*. SufS appears to have similar biochemical activity as IscS under conditions of oxidative stress or iron limitation (72, 75, 76, 129).

Recently, a novel enzyme catalyzing the breakdown of L-cysteine was detected in *Methanocaldococcus jannaschii*. This enzyme, L-cysteine desulfidase, converts cysteine to

pyruvate, ammonia and sulfide (107). Cysteine desulfidase shows no sequence homology to the known cysteine desulfurases and is devoid of PLP, suggesting that this enzyme uses a different mechanism for sulfur removal than the cysteine desulfurases. It has been proposed that this enzyme is used to produce sulfide for Fe-S clusters, although this activity has not yet been shown.

Hydrogenases

Hydrogenases catalyze the reversible reaction $H_2 \leftrightarrow 2H^+ + 2e^-$. The direction in which this reaction proceeds depends on the physiological role: whether to act as an electron sink or to generate electrons for redox reactions. Hydrogenases are widespread among the prokaryotes. The number of accessory and maturation proteins involved varies widely, as does the cellular localization of the hydrogenase, depending on the type of hydrogenase. There are three general categories of hydrogenase, characterized by the metal in the active site of the enzyme. These are the nickel-iron hydrogenases, the iron-sulfur hydrogenases, and the iron-sulfur cluster-free hydrogenases (also known as metal-free hydrogenases).

Iron-sulfur hydrogenases

The first characterized hydrogenases were of the iron-sulfur type (16). The number of catalytic subunits varies from one to four, where most FeS hydrogenses are monomeric (114). The metal active site structure is composed of a Fe_4S_4 cluster linked via a cysteinyl residue to a Fe_2S_3 cluster (77). The FeS hydrogenases of several *Clostridium* species additionally harbor 3 FeS cluster-containing domains (2). Other species, such as *Desulfovibrio fructosovorans* contain an additional FeS cluster-containing accessory proteins (61). The variations in FeS hydrogenase structure reflect the physiological diversity of the organisms harboring these enzymes.

Fe-S cluster-free hydrogenases

So called "metal-free' hydrogenases or H_2-forming N^5, N^{10}-methylenetetrahydromethanopterin dehydrogenases (Hmd) are only found in methanogenic archaea. This hydrogenase does not contain nickel or iron-sulfur clusters in its active site (132). However, it does contain an iron-bound low molecular mass cofactor (60). Although the cofactor structure is unknown, irradiation of the cofactor generates two CO molecules, an iron ion and a pyridone derivative linked to a guanosine base (95).

In methanogenesis, CO_2 is reduced in a stepwise fashion to produce methane. The Hmd is involved in the reversible reduction of methylenetetrahydromethanopterin (methylene-H_4MPT) to methyltetrahydromethanopterin, transferring a hydride from H_2 (92). Hmd purified from *M. thermautotrophicus* was found to be a homodimer (131). Recently, the crystal structure of the *M. jannaschii* and *M. kandleri* Hmd apoenzymes were resolved (78). Molecular modeling suggests a likely position for the methylene-H_4MPT, which could be coordinated via an H_2 molecule to Cys176-Fe (78). Furthermore, mutational analysis of the four cysteinyl residues in Hmd showed that only Cys176 is necessary for enzymatic activity (78). These results suggest that Cys176 is the site for iron binding (78).

Nickel-iron hydrogenases

The first organism from which nickel was associated with hydrogenase activity was *Alcaligenes eutrophus* (29). Since then, a large number of hydrogenases have been identified that contain nickel in their active site. The crystal structure of the *Desulfovibrio gigas* nickel-iron hydrogenase shows that the catalytic site contains a dinuclear thiolate-bridged nickel-iron complex (115). The Ni and Fe atoms are coordinated by four and two cysteinyl residues,

respectively (115). One [3Fe-4S] and 2 [4Fe-4S] clusters as well as cyanide and carbon monoxide molecules are also found within the hydrogenase active site (115).

Ni-FeS hydrogenases can be classified by the sequence alignments of the large subunits, which correlate well with the cellular functions (82). Table 5 lists the four groups of hydrogenases and gives some characteristics of these hydrogenases as described by Wu (123) and Vignais (14).

Cytoplasmic nickel-iron hydrogenases in *Methanococcus maripaludis*

The F_{420}-reducing and F_{420}-nonreducing hydrogenases are utilized in the methanogenesis pathway (Figure 1). F_{420} is a coenzyme that carries electrons to the methylenetetrahydromethanopterin dehydrogenase and the methylenetetrahydromethanopterin reductase. The F_{420}-reducing hydrogenase then oxidizes H_2 for the reduction of coenzyme F_{420}. The F_{420}-nonreducing hydrogenases are involved in regenerating the coenzyme M molecule after the final, methane-producing step of methanogenesis. In the final step of methanogenesis, the methyl group of methyl-coenzyme M is reduced by the methyl-coenzyme M reductase. (33, 110). The electron donor for the reduction of the methyl-CoM is coenzyme B (CoB-SH). This reduction generates a heterodisulfide, CoB-S-S-CoM (33, 110). This heterodisulfide is reduced by the heterodisulfide reductase to regenerate coenzymes M and B. In *Methanosaricina*, the electrons for this heterodisulfide reduction are provided by the F_{420}-nonreducing hydrogenase (37). In contrast, in *M. voltae*, the heterodisulfide reduction is coupled to the F_{420}-reducing Fru hydrogenase (14). The reduction of the heterodisulfide is coupled to ATP synthesis via the production of an electrochemical proton potential associated with an ATP synthase (33, 110). Previous analysis of the cellular localization of the F_{420}-reducing and -nonreducing hydrogenases in *Methanothermobacter thermautotrophicus* suggest that both enzymes are membrane

associated, facing the cytoplasm (11). Recent studies found that the F_{420}-nonreducing hydrogenase is directly associated with the heterodisulfide reductase in *Methanothermobacter marburgensis* (105).

The genome sequence of *M. maripaludis* contains seven hydrogenases, one FeS cluster-free hydrogenase and six nickel-iron hydrogenases. Of the six nickel-containing hydrogenases, four are considered cytoplasmic while two are membrane-spanning.

Table 6 lists the genes encoding the four cytoplasmic [NiFe] hydrogenases in *M. maripaludis*. Homologs of these four hydrogenases have been studied in *M. voltae*; three of which have been purified (34). Two gene clusters encode hydrogenases that are F_{420}-reducing, *fru* (14) and *frc* (7, 71). Two other gene clusters encode the F_{420}-nonreducing hydrogenases: *vhu* (102) and *vhc* (7). Of these four hydrogenases, Fru and Vhu are selenium-dependent enzymes, while the other two are selenium-independent. The genes *fruA* (14), *vhuA* (102), *vhuE* (102), and *vhuD* (86) contain selenocysteinyl residues. The *vhcA* gene appears to be a gene fusion of the *vhuA* and *vhuU* genes (101). VhuE is a novel hydrogenase subunit that contains a selenocysteinyl residue and is post-translationally processed (101). This subunit appears to be part of the Vhu active site (101).

Most of the predictions about *M. maripaludis* hydrogenase subunit composition are based upon studies performed on the cytoplasmic hydrogenases in the related organism *Methanococcus voltae*. The *M. voltae* hydrogenase gene clusters encode both structural hydrogenase subunits as well as proteases, polyferredoxins and proteins of unknown function. The *frcB* and *fruB* genes encode hydrogenase maturation proteases (85). Two genes encode for polyferredoxins, *vhcD* and *vhuE* (35). Although part of the operons, the protein products of *frcB* (71), *fruB* (14), and *vhuD* (101) do not co-purify with the enzymes. The products of *vhcA* and *vhuA* are

uncharacterized. The *M. maripaludis* genome also contains an open reading frame that does not cluster with the hydrogenase genes but is similar to the *frcB* and *fruB* genes (MMP1337).

Energy-conserving hydrogenases

Homologs to *Escherichia coli* type 3 hydrogenases have been found in a variety of prokaryotes (Table 7). These include the *Escherichia coli* type 4 hydrogenase (4, 8, 91), the CO dehydrogenase from *Rhodospirillum rubrum* and *Desulfovibrio vulgaris* (27, 28, 36), the Ech from *Methanosarcina barkeri* (54, 67) and *Desulfovibrio gigas* (84), the Mbh and Mbx hydrogenases from *Pyrococcus furiosus* (88, 89, 96), and the Eha and Ehb from *Methanothermobacter thermautotrophicus* (109) and *Methanococcus maripaludis* (38). There is a wide variety in the number of genes in each operon, as well as in the physiological role of the complex.

Under anaerobic, glycolytic conditions, *E. coli* undergoes mixed acid fermentation, generating formic acid, acetic acid, succinic acid, lactic acid and ethanol. Formic acid can be converted to carbon dioxide and hydrogen by the formate hydrogenlyase. The *E. coli* type 3 hydrogenase is part of the formate hydrogenlyase H complex, along with the formate dehydrogenase. This complex disproportionates formate to carbon dioxide and hydrogen gas. These reactions are driven by a proton motive force generated by the F_0F_1-ATPase (5).

E. coli has a homolog of the type 3 hydrogenase: the type 4 hydrogenase (91). The type 4 hydrogenase is part of a second formate hydrogenlyase system. The activity of these two formate hydrogenlyases is pH dependent. At slightly acidic pH, the active complex involves the type 3 hydrogenase. At slighly alkaline pH, the type 4 hydrogenase dominates (5).

The type 3 hydrogenase has sequence similarity to the carbon monoxide hydrogen lyase (Coo) of *Rhodospirillum rubrum* (28). This enzyme complex contains a carbon monoxide

dehydrogenase along with the Coo hydrogenase (24). In the absence of light, the complex oxidizes CO as a sole source of energy (24). Like the type 3 hydrogenase, it is believed that the Coo hydrogenase is linked to a proton pump (27). In addition, several of the Coo hydrogenase subunits show sequence similarity to the NADH:ubiquinone oxidoreductase (respiratory complex I, 27).

The energy-conserving hydrogenase of the fermentative archaeon *Pyrococcus furiosus* also plays a large role in metabolism. Here, the production of hydrogen gas by Mbh acts as an electron sink following glyceraldehyde 3-phosphate oxidation (88). Furthermore, the Mbh couples this reaction to energy production via a proton motive force (88). This is the first example of respiration in *Pyrococcus*. A second operon for a homologous hydrogenase (*mbx*) has been observed, but its function is unclear (96).

Energy-conserving hydrogenases in methanogens

Energy-conserving hydrogenases in methanogens were first identified in *Methanosarcina barkeri* (54). These Ni-FeS hydrogenases are composed of six subunits (EchABCDEF). The putative functions of the hydrogenase subunits are EchE, large hydrogenase subunit; EchC, small hydrogenase subunit; EchF, electron transfer protein; EchA and EchB, integral membrane proteins; EchA, putative proton translocator; and EchD, small hydrophilic protein (54). The large and small hydrogenase subunits (EchE and EchC, respectively) have 34% and 45% sequence identity to HycE and HycG of *E. coli* (54).

The *M. barkeri* Ech was purified and found to reduce ferredoxin (67). The enzyme contains 0.9 mol Ni, 11.3 mol of non-heme iron and 10.8 mol of acid-labile sulfur per mol hydrogenase (67). Electron paramagentic resonance spectra displayed three different [4Fe-4S] cluster signals, one of which was assigned to the Ech (small hydrogenase) subunit, while the

other two were assigned to the EchF (putative electron transfer) protein (55). The EchF and one of the EchC iron-sulfur clusters were found to be pH-dependent (55). Site-directed mutations of cysteinyl residues with the [4Fe-4S] clusters of *M. barkeri echC* and *echF* demonstrated that the two pH-dependent FeS clusters are directly involved in the redox activity of the Ech enzyme (26). It was concluded that the pH-dependence of the midpoint potential of these clusters reflects the simultaneous electron and proton transfer to a nearby acidic amino acid residue (26, 55).

To elucidate the physiological role of Ech in *Methanosarcina barkeri*, a mutational analysis was performed (68). First, an Ech deletion mutant was constructed and the various conditions for growth were tested. Typically, *M. barkeri* can utilize a relatively broad range of 1 or 2 carbon compounds, including CO, CO_2, methanol, acetate, and methylamines. The Ech mutant displayed no growth on methanol/H_2/CO_2, H_2/CO_2 or acetate as sole carbon sources; however, the mutant could grow on methanol alone (68). Furthermore, it was found that the Ech hydrogenase interacts with ferredoxins, which are associated with the pyruvate oxidoreductase, the carbon monoxide dehydrogenase/acetyl-CoA synthase, and the formylmethanofuran dehydrogenase (68, 104).

Ech hydrogenases are also found in hydrogenotrophic methanogens such as *Methanothermobacter thermautotrophicus* (109). Unlike the *Methanosarcina* Ech, *Methanothermobacter* contains gene clusters for two membrane-bound hydrogenases, designated *eha* and *ehb* (109). These operons encoding the *eha* and *ehb* hydrogenases contain 20 and 17 genes, respectively (109). The genome of *Methanococcus maripaludis* contains homologs to the *eha* and *ehb* genes; however, only 9 of the *ehb* open reading frames are found in a gene cluster (38). Sequence similarities to other Ni-FeS hydrogenases suggest that the Eha and Ehb each contain a large and small hydrogenase subunit and two integral membrane proteins (109).

Furthermore, the *eha* operon encodes two polyferredoxins, four nonconserved hydrophilic subunits and 10 nonconserved integral membrane proteins. The *ehb* operon encodes a polyferredoxin, a ferredoxin, two nonconserved hydrophilic subunits and nine nonconserved integral membrane proteins.

Competitive RT-PCR transcription levels were used to predict the relative abundance of the hydrogenase proteins relative to proteins involved in methanogenesis (109). From this analysis, the Eha hydrogenase was predicted to be involved in the synthesis of formylmethanofuran (109, 68). The Ehb hydrogenase was predicted to generate low potential electrons for anabolic enzymes such as the CODH/ACS, Por and Kor (109). A deletion of the *ehbF* gene in *M. maripaludis* confirmed the association of the Ehb hydrogenase in CO_2 assimilation (79). The Δ*ehbF* mutant displayed increased CODH and Por activity, increased quantities of *cdh* and *por* transcript and CODH/ACS and POR protein concentration and decreased levels of methanogenesis by resting cells using pyruvate as electron donor (79).

Rationale for this work

Energy metabolism is a complex phenomenon in any organism. Only now, with the large number of genomes currently sequenced, is it possible to identify many components of the energy-producing systems. It is particularly interesting that many important enzymes and pathways were not identified until the organism's genomic DNA sequence was analyzed. This is particularly true in the case of the energy-conserving hydrogenases of the organisms listed in Table 7. The *P. furiosus mbh* and *mbx*, the *E. coli hyf*, the methanothermobacterial *eha* and *ehb*, the methanococcal *eha* and *ehb*, and the *Desulfovibrio gigas ech* have all been primarily identified through genome sequencing. Interestingly, although generally grouped together as "energy-conserving hydrogenases," the enzymes are substantially different, even at the amino

acid sequence level. For example, phylogenetic trees based on the large hydrogenase subunit show deep branching (Figure 4). This suggests that there is a wide diversity of structure and function of this group of hydrogenases. Analysis of some of the characteristics of individual energy-conserving hydrogenases displays even more clearly that these enzymes are different from one another. Table 8 contrasts the methanococcal, methanosarcinal, pyrococcal, and *E. coli* energy-conserving hydrogenases. The physiological use of the hydrogenases, the number of subunits and the percent amino acid similarity between subunits of these hydrogenases are clearly different between the complexes. In fact, even whether the hydrogenase generates hydrogen gas or oxidizes it varies depending on the physiology of the organism. Even between *M. maripaludis* and *M. mazei*, whose hydrogenases have similar functions, there is substantial diversity. Why does *M. maripaludis* contain two energy-conserving hydrogenases when *M. mazei* can perform the same reactions with only one? Why do the *M. maripaludis* hydrogenases have so many subunits when the *M. mazei* enzyme is composed of only six subunits? These questions can only be answered with further characterization of the enzymes.

Among the methanogens, energy conservation and electron transport has best been characterized in the *Methanosarcina* species. One example is the H_2:heterodisulfide oxidoreductase system for the reduction of the coenzyme M:coenzyme B heterodisulfide (37). Here, the F_{420}-nonreducing hydrogenase oxidizes hydrogen to produce electrons (46). The electrons generated in this reaction are shuttled to the heterodisulfide reductase by methanophenazine (1). Both the reduction of methanophenazine and the reduction of the heterodisulfide are coupled to a proton motive force (40), which is utilized by the A_1A_0-type ATP synthase (69). The *Methanosarcina* have a second, similar reaction scheme that is

catalyzed by the F_{420}-reducing hydrogenase (1, 18). Cytochromes are the primary electron accepting components of the heterodisulfide reductase and the hydrogenases (13, 97).

Unlike the *Methanosarcina,* electron transport within the hydrogenotrophic methanogens is largely undescribed. Methanophenazine and cytochromes are not found in the methanococci or other hydrogenotrophic methanogens (53). Clearly, different mechanisms for electron transport and energy conservation are required.

Due to the lack of methanophenazine and cytochromes, ferredoxins and polyferredoxins appear to be the primary electron transporting proteins in the hydrogenotrophic methanogens. During the annotation of the *Methanococcus maripaludis* genome, it was noted that this genome sequence contained a large number of open reading frames with the 4Fe-4S amino acid motif $CX_2CX_2CX_3C$ (Table 9). Several of these motifs are found in genes encoding either biochemically characterized proteins or homologs of characterized proteins, such as the oxidoreductases. Even in those proteins, the function of these Fe-S clusters is unknown. The pyruvate oxidoreductase of *Methanococcus maripaludis* is a primary example of a purified enzyme that is involved in electron transport but the mechanism of electron shuttling to the Por is unknown. Our hypothesis is that electrons are generated by the Ehb and are transferred to the PorF, which shuttles electrons to the PorE-Por complex. In order to analyze this this electron transport pathway, it is first necessary to characterize the PorE and PorF proteins. In this work, attempts were made to produce histidine-tagged PorE and PorF for further analysis.

Furthermore, the energy-conserving hydrogenases have largely gone uncharacterized. Even in the pyrococcal Mbh and the methanosarcinal Ech, which have both been purified to homogeniety (67, 89), little is known about the structure and functional mechanism of the hydrogenase. It is also unclear how the hydrogenases shuttle electrons both throughout the

enzyme or to proteins that are not part of the hydrogenase complex. In this work, we analyzed the structure and function of the *Methanococcus maripaludis* Ehb through the deletion of several subunits. The work presented here focuses more on the function of the Ehb: how *ehb* gene deletions affect the growth of *M. maripaludis*, which reflects the importance of the Ehb on this organism's physiology. Furthermore, the strong inhibition of the *de novo* aromatic amino acid biosynthesis pathway by the aryl acids provides an opportunity to characterize whether the Ehb is coupled to the Ior. Current and future work by other lab members focuses on the structural aspects of the Ehb complex, particularly how and whether deletions of *ehb* genes affect the Ehb structure.

References

1. **Abken, H. J., M. Tietze, J. Brodersen, S. Bäumer, U. Beifuss, and U. Deppenmeier.** 1998. Isolation and characterization of methanophenazine and funciton of phenazines in membrane-bound electron transport of *Methanosarcina mazei* Gö1. J. Bacteriol. **180:**2027-2032.

2. **Adams, M.W.W.** 1990. The structure and mechanisms of iron-hydrogenases. Biochim. Biophys. Acta **1020:**115-145.

3. **Ambrogelly, A., S. Kametkar, A. Sauerwald, B. Ruan, D. Tumbula-Hansen, D. Kennedy, I. Ahel, D. Söll.** 2004. Cys-tRNA^{Cys} formation and cysteine biosynthesis in methanogenic archaea: Two faces of the same problem? Cell. Mol. Life Sci. **61:**2437-2445.

4. **Andrews, S. C., B. C. Berks, J. McClay, A. Ambler, M. A. Quail, P. Golby, and J. R. Guest.** 1997. A 12-cistron *Escherichia coli*operon (*hyf*) encoding a putative proton-translocating formate hydrogenlyase system. Microbiology **143:**3633-3647.

5. **Bagramyan, K., N. Mnatsakanyan, A. Poladian, A. Vassilian, and A Trchounian.** 2002. The roles of hydrogenases 3 and 4, and the F_0F_1-ATPase, in H_2 production by *Escherichia coli* at alkaline and acidic pH. FEBS Lett. **516:**172-178.

6. **Beijer, W. H.** 1952. Methane fermentation in the rumen of cattle. Nature **170:**576-577.

7. **Berghöfer, Y., K. Agha-Amiri, and A. Klein.** 1994. Selenium is involved in the negative regulation of the expression of selenium-free [NiFe] hydrogenases in *Methanococcus voltae*. Mol. Gen. Genet. **242**:369-373.

8. **Böhm, R., M. Sauter, and A. Bock.** 1990. Nucleotide sequence and expression of an operon in *Escherichia coli* coding for formate hydrogenlyase components. Mol. Microbiol. **4:**231-243.

9. **Boone, D. R., W. B. Whitman, and P. Rouviére.** 1993. Diversity and taxonomy of methanogens, pp. 35-80. *In* Ferry, J. G (ed.), Methanogenesis: Ecology, Physiology, Biochemistry, and Genetics. Chapman and Hall, New York.

10. **Borup, B., and J. G. Ferry.** 2000. Cysteine biosynthesis in the archaea: *Methanosarcina thermophila* utilizes O-acetylserine sulfhydrylase. FEMS Micrbiol. Lett. **189:**205-210.

11. **Braks, I. J., M. Hoppert, S. Roge, and F. Mayer.** 1994. Structural aspects and immunolocalization of the F_{420}-reducing and non-F_{420}-reducing hydrogenases from *Methanobacterium thermautotrophicum* Marburg. J. Bacteriol. **176:**7677-7687.

12. **Brochier, C., S. Gribaldo, Y. Zivanovic, F. Confalonieri, and P. Forterre.** 2005. Nanoarchaea: representatives of a novel archaeal phylum or a fast-evolving euryarchaeal lineage related to *Thermococcales*? Genome Biol. **6:**R42.

13. **Brodersen, J., S. Bäumer, H. J. Abken, G. Gottschalk, and U. Deppenmeier.** 1999. Inhbition of membrane-bound electron transport of the methanogenic archaeon *Methanosarcina mazei* Gö1 by diphenyleneiodonium. Eur. J. Biochem. **259:**218-224.

14. **Brodersen, J., G. Gottschalk, and U. Deppenmeier.** 1999. Membrane-bound $F_{420}H_2$-dependent heterodisulfide reduction in *Methanococcus voltae*. Arch. Microbiol. **171**:115-21.

15. **Bult, C. J., O. White, G. J. Olsen, L. Zhou, R. D. Fleischmann, G. G. Sutton, J. A. Blake, L. M. FitzGerald, R. A. Clayton, J. D. Gocayne, A. R. Kerlavage, B. A. Dougherty, J. F. Tomb, M. D. Adams, C. I. Reich, R. Overbeek, E. F. Kirkness, K. G. Weinstock, J. M. Merrick, A. Glodek, J. L. Scott, N. S. M. Geoghagen, J. F. Weidman, J. L. Fuhrmann, D. Nguyen, T. R. Utterback, J. M. Kelley, J. D. Peterson, P. W. Sadow, M. C. Hanna, M. D. Cotton, K. M. Roberts, M. A. Hurst, B. P. Kaine, M. Borodovsky, H.-P. Klenk, C. M. Fraser, H. O. Smith, C. R. Woese, and J. C. Venter.** 1996. Complete genome sequence of the methanogenic archaeon, *Methanococcus jannaschii*. Science **273:**1058-1073.

16. **Chen, J.-S., and L. E. Mortenson.** 1974. Purification and properties of hydrogenase from *Clostridium pasteurianum* W5. Biochim. Biophys. Acta **371:**283-298.

17. **Childress, J. J. and C. R. Fisher.** 1992. The biology of hydrothermal vent animals: physiology, biochemistry and autotrophic symbioses. Oceanogr. Mar. Biol. Annu. Rev. **30:**337-441.

18. **Deppenmeier, U., V. Müller, and G. Gottschalk.** 1996. Pathways of energy conservation in methanogenic archaea. Arch. Microbiol. **165:**149-163.

19. **Dobbek H., V. Svetlitchnyi, L. Gremer, R. Huber, and O. Meyer.** 2001. Crystal structure of a carbon monoxide dehydrogenase reveals a [Ni-4Fe-5S] cluster. Science **293:**1281-1285.

20. **Eikmanns, B., R. Jaenchen, and R. K. Thauer.** 1983. Propionate assimilation by methanogenic bacteria. Arch. Microbiol. **136:**106-110.

21. **Eikmanns, B. D. Linder, and R. K. Thauer.** 1983. Unusual pathway of isoleucine biosynthesis in *Methanobacterium thermoautotrophicum*. Arch. Microbiol. **136:**111-113.

22. **Ekiel, I., I. C. P. Smith, and G. D. Sprott.** 1983. Biosynthetic pathways in *Methanospirillum hungatei* as determined by ^{13}C nuclear magnetic resonance. J. Bacteriol. **156:**316-326.

23. **Ekiel, I., I. C. P. Smith, and G. D. Sprott.** 1984. Biosynthesis of isoleucine in methanogenic bacteria: a ^{13}C NMR study. Biochemistry **23:**1683-1687.

24. **Ensign, S. A., and P. W. Ludden.** 1991. Characterization of the CO oxidation/H_2 evolution system of *Rhodospirillum rubrum*. Role of a 22-kDa iron-sulfur protein in mediating electron transfer between carbon monoxide dehydrogenase and hydrogenase. J. Biol. Chem. **266:**18395–18403.

25. **Flint, D. H.** 1996. *Escherichia coli* contains a protein that is homologous in function and N-terminal sequence to the protein encoded by the *nifS* gene of *Azotobacter vinelandii* and that can participate in the synthesis of the Fe-S cluster of dihydroxyacid dehydratase. J. Biol. Chem. **271:**16068-16074.

26. **Forzi, L., J. Koch, A. M. Guss, C. G. Radsevich, W. W. Metcalf, and R. Hedderich.** 2005. Assignment of the [4Fe-4S] clusters of Ech hydrogenase from *Methanosarcina barkeri* to individual subunits via the characterization of site-directed mutants. FEBS J. **272:**4741-4753.

27. **Fox, J. D., Y. He, D. Shelver, G. P. Roberts, and P. W. Ludden.** 1996. Characterization of the region encoding the CO-induced hydrogenase of *Rhodospirillum rubrum*. J. Bacteriol. **178:** 6200-6208.

28. **Fox, J. D., R. L. Kerby, G. P. Roberts, and P. W. Ludden.** 1996. Characterization of the CO-induced, CO-tolerant hydrogenase from *Rhodospirillum rubrum* and the gene encoding the large subunit of the enzyme. J. Bacteriol. **178:**1515-1524.

29. **Friedrich, B., E. Heine, A. Finck, and C. G. Friedrich.** 1981. Nickel requirement for active hydrogenase formation in *Alcaligenes eutrophus*. J. Bacteriol. **145:**1144-1149.

30. **Fu. W., R. F. Jack, T. V. Morgan, D. R. Dean, and M. K. Johnson.** 1994. *nifU* gene product from *Azotobacter vinelandii* is a homodimer that contains two identical [2Fe-2S] cluters. Biochemistry **33:**13455-13463.

31. **Garrity, G. M., and J. G. Holt.** 2001. Phylum AII. Euryarchaeota *phy. nov.,* p. 211. *In* Garrity, G. M. (ed.-in-chief) Bergey's Manual of Systematic Bacteriology, 2nd ed. Springer, New York.

32. **Griffith, O. W.** 1987. Mammalian sulfur amino acid metabolism: an overview. Methods Enzymol. **143:**366-376.

33. **Gottschalk, G. and M. Blaut.** 1990. Generation of proton and sodium motive forces in methaogenic bacteria. Biochim. Biophys. Acta. **1018:**263-266.

34. **Halboth, S., and Klein, A.** 1992. *Methanococcus voltae* harbors four gene clusters potentially encoding two [NiFe] and two [NiFeSe] hydrogenases, each of the cofactor F420-reducing or F420-non-reducing types. Mol. Gen. Genet. **233:**217-224.

35. **Hedderich, R., S. P. J. Albracht, D. Linder, J. Koch, and R. K. Thauer.** 1992. Isolation and characterization of polyferredoxin from *Methanobacterium thermoautotrophicum*. FEBS Lett. **298**:65-68.

36. **Heidelberg, J. F., R. Seshadri, S. A. Haveman, C. L. Hemme, I. T. Paulsen, J. F. Kolonay, J. A. Eisen, N. Ward, B. Methe, L.M. Brinkac, S. C. Daughtery, R. T. Deboy, R. J. Dodson, A. S. Durkin, R. Madupu, W. C. Nelson, S. A. Sullivan, D. Fouts, D. H. Haft, J. Selengut, J. D. Peterson, T. M. Davidsen, N. Zafar, L. Zhou, D. Radune, G. Dimitrov, M. Hance, K. Tran, H. Khouri, J. Gill, T. R. Utterback, T. V. Feldblyum, J. D. Wall, G. Voordouw, and C. M. Fraser.** 2004. The genome sequence of the anaerobic, sulfate-reducing bacterium *Desulfovibrio vulgaris* Hildenborough. Nat. Biotech. **22:**554-559.

37. **Heiden, S., R. Hedderich, E. Setzke, and R. K. Thauer.** 1993. Purification of a cytochrome b containing H_2:heterodisulfide oxidoreductase complex from membranes of *Methanosarcina barkeri*. Eur. J. Biochem. **213:**529-535.

38. **Hendrickson E. L., R.,Kaul, Y. Zhou, D. Bovee, P. Chapman, J. Chung, E. Conway de Macario, J. A. Dodsworth, W. Gillett, D. E. Graham, M. Hackett, A. K. Haydock, A. Kang, M. L. Land, R. Levy, T. J. Lie, T. A.Major, B. C. Moore, I. Porat, A. Palmeiri, G. Rouse, C. Saenphimmachak, D. Söll, S. Van Dien, T. Wang, W. B. Whitman, Q. Xia, Y. Zhang, F. W. Larimer, M. V. Olson, and J. A. Leigh.** 2004. Complete genome sequence of the genetically tractable hydrogenotrophic methanogen *Methanococcus maripaludis*. J. Bacteriol. **186:**6956-6969.

39. **Huber, H., M. J. Hohn, R. Rachel, T. Fuchs, V. C. Wimmer, and K. O. Stetter.** 2002. A new phylum of Archaea represented by a nanosized hyperthermophilic symbiont. Nature **417:**63-67.

40. **Ide, T., S. Bäumer, and U. Deppenmeier.** 1999. Energy conservation by the H_2:heterodisulfide oxidoreductase from *Methanosarcina mazei* Gö1: identification of two proton-translocating segments. J. Bacteriol. **181:**4076-4080.

41. **Jacobson, M. R., V. L. Cash, M. C. Weiss, N. F. Laird, W. E. Newton, and D. R. Dean.** 1989. Biochemical and genetic analysis of the *nifUSVWZM* cluster from *Azotobacter vinelandii*. Mol. Gen. Genet. **219:**49-57.

42. **Jeon, W. B., J. Cheng, and P. W. Ludden.** 2001. Purification and characterization of membrane-associated CooC protein and its functinoal role in the insertion of nickel into carbon monoxide dehydrogenase from *Rhodospirillum rubrum*. J. Biol. Chem. **276**:38602-38609.

43. **Johnson, D. C., D. R. Dean, A. D. Smith, and M. K. Johnson.** 2005. Structure, function and formation of biological iron-sulfur clusters. Annu. Rev. Biochem. **74:**247-281.

44. **Jones, W. J., and M. J. Paynter.** 1980. Populations of methane-producing bacteria and *in vitro* methanogenesis in salt marsh and esturaine sediments. Appl. Environ. Microbiol. **39:**864-871.

45. **Kambampati, R., and C. T. Lauhon.** 1999. IscS is a sulfurtransferase for the in vitro biosynthesis of 4-thiouridine in *Escherichia coli* tRNA. Biochemistry **38:**16561-16568.

46. **Kemner, J. M., and J. G. Zeikus.** 1994. Regulation and function of ferrdoxin-linked versus cytrochrome b-linked hydrogenase in electron transfer and energy metabolism in *Methanosarcina barkeri* MS. Arch. Micrbiol. **162:**26-32.

47. **Kiyasu, T., A. Asakura, Y. Nagahashi, and T. Hoshino.** 2000. Contribution of cysteine desulfurase (NifS protein) to the biotin synthase reaction of *Escherichia coli*. J. Bacteriol. **182:**2879-2885.

48. **Kitabatake, M., M. W. So, D. L. Tumbula, and D. Söll.** 2000. Cysteine biosynthesis pathway in the archaeon *Methanosarcina barkeri* encoded by acquired bacterial genes? J. Bacteriol. **182:**143-145.

49. **Kocsis, E., M. Kessel, E. DeMoll, and D. A. Grahame.** 1999. Structure of the Ni/Fe-S protein subcomponent of the Acetyl-CoA decarbonylase/synthase complex from *Methanocarcina thermophila* at 26-Å resolution. J. Struct. Biol. **128:**165-174.

50. **Koval, S. F., and K. F. Jarrell.** 1987. Ultrastructure and biochemistry of the cell wall of *Methanococcus maripaludis*. J. Bacteriol. **169:**1298-1306.

51. **Koyama, T.** 1963. Gaseous metabolism in the lake sediments and paddy soils and the production of atmospheric methane and hydrogen. J. Geophys. Res. **68:**3971-3973.

52. **Kredich, N. M.** 1996. Biosynthesis of Cysteine, p. 514-527. *In* Neidhardt, F.C. (chief ed.) *Escherichia coli* and *Salmonella*: Cellular and Molecular Biology, 2nd ed. ASM Press, Washington, D.C.

53. **Kühn, W., and G. Gottschalk.** 1983. Characterization of the cytochromes occurring in *Methanosarcina* species. Eur. J. Biochem. **135:**89-94.

54. **Künkel, A., J. A. Vorholt, R. K. Thauer, and R. Hedderich.** 1998. An *Escherichia coli* hydrogenase-3-type hydrogenase in methanogenic archaea. Eur. J. Biochem. **252:**467-476.

55. **Kurkin, S., J. Meuer, J. Koch, R. Hedderich, and S. P. J. Albracht.** 2002. The membrane-bound [Ni-Fe] hydrogenase (Ech) from *Methanosarcina barkeri*: unusual properties of the iron-sulfur clusters. Eur. J. Biochem. **269:**6101-6111.

56. **Lauhon C. T., and R. Kambampati.** 2000. The *iscS* gene in *Escherichia coli* is required for the biosynthesis of 4-thiouridine, thiamin, and NAD. J. Biol. Chem. **275:**20096-20103.

57. **Leimkuhler, S., and K. V. Rajagopalan.** 2001. A sulfurtransferase is required in the transfer of cysteine sulfur in the *in vitro* synthesis of molybdopterin from precursor Z in *Escherichia coli*. J. Biol. Chem. **276:**22024-22031.

58. **Lin, W. C., and W. B. Whitman.** 2004. The importance of *porE* and *porF* in the anabolic pyruvate oxidoreductase of *Methanococcus maripaludis.* Arch. Microbiol. **179:**444-456.

59. **Lin, W. C., Y.-L. Yang, and W. B. Whitman.** 2003. The anabolic pyruvate oxidoreductase from *Methanococcus maripaludis*. Arch. Microbiol. **179:**444-456.

60. **Lyon, E. J., S. Shima, G. Buurman, S. Chowdhuri, A. Batschauer, K. Steinbach, and R. K. Thauer.** 2004. UV-A/blue-light inactivation of the 'metal-free' hydrogenase (Hmd) from methanogenic archaea: The enzyme contains functional iron after all. Eur. J. Biochem. **271:**195-204.

61. **Malki S., I. Saimmaime, G. De Luca, M. Rousset, Z. Dermoun, and J.-P. Belaich.** 1995. Characterization of an operon encoding an NADP-reducing hydrogenase in *Desulfovibrio fructosovorans*. J. Bacteriol. **177:**2628-2636.

62. **Marquet A.** 2001. Enzymology of carbon-sulfur bond formation. Curr. Opin. Chem. Biol. **5:**541-549.

63. **Marquet, A., B. Tse Sum Bui, and D. Florentin.** 2001. Biosynthesis of biotin and lipoic acid, pp. 51-101. *In* T.P. Begley (ed.) Vitamins and Hormones, Vol. 61. Academic Press, San Diego, CA.

64. **Maupin-Furlow, J. A., and J. G. Ferry.** 1996. Analysis of the CO dehydrogenase/acetyl-Coenzyme A synthase operon of *Methanosarcina thermophila*. J. Bacteriol. **178:**6849-6856.

65. **Menon, S., and S. W. Ragsdale.** 1997. Mechanism of the *Clostridium thermaceticum* pyruvate:ferredoxin oxidoreductase: Evidence for the common catalytic intermediacy of the hydroxyethylamine pyrophosphate radical. Biochemistry **36:**8484-8494.

66. **Menon, S., and S. W. Ragsdale.** 1999. The role of an iron-sulfur cluster in an enzymatic methylation reaction: methylation of CO dehydrogenase/acetyl-CoA synthase by the methylated corrinoid iron-sulfur protein. J. Biol. Chem. **274:**11513-11518.

67. **Meuer, J., S. Bartoschek, J. Koch, A. Künkel, and R. Hedderich.** 1999. Purification and catalytic properties of Ech hydrogenase from *Methanosarcina barkeri*. Eur. J. Biochem. **265:**325-335.

68. **Meuer, J., H. C. Kuettner, J. K. Zhang, R. Hedderich, and W. W. Metcalf.** 2002. Genetic analysis of the archaeon *Methanosarcina barkeri* Fusaro reveals a central role for Ech hydrogenase and ferredoxin in methanogenesis and carbon fixation. Proc. Natl. Acad. Sci. USA **999:**5632-5637.

69. **Müller, V, C. Ruppert, and T. Lemker.** 1999. Structure and function of the A_1A_0-ATPases from methanogenic archaea. J. Bioenerg. Biomembr. **31:**15-27.

70. **Murakami, E., and S. W. Ragsdale.** 2000. Evidence for intersubunit communication during acetyl-CoA cleavage by the multienzyume CO dehydrogenase/acetyl-CoA synthase complex from *Methanosarcina thermophila*. J. Biol. Chem. **275:**4699-4707.

71. **Muth, E., E. Mörschel, and A. Klein.** 1987. Purification and characterization of an 8-hydroxy-5-deazaflavin-reducing hydrogenase from the archaebacterium *Methanococcus voltae*. Eur. J. Biochem. **169**:571-577.

72. **Nachin, L., M. El Hassouni, L. Loisean, D. Expert, and F. Barras.** 2001. SoxR-dependent response to oxidative stress and virulence of *Erwinia chrysanthemi*: the key role of SufC, and orphan ABC ATPase. Mol. Microbiol. **39:**960-972.

73. **Nicolet, Y., C. Cavazza, and J. C. Fontecilla-Camps.** 2002. Fe-only hydrogenases: structure, function and evolution. J. Inorg. Biochem. **91:**1-8.

74. **Ollagnier-de Choudens, S., and M. Fontecave.** 1999. The lipoate synthase from *Escherichia coli* is an iron-sulfur protein. FEBS Lett. **453:**25-28.

75. **Outten, F. W., O. Djaman, and G. Storz.** 2004. A suf operon requirement for Fe-S cluster assembly during iron starvation in *Escherichia coli*. Mol. Microbiol. **52:**861-872.

76. **Patzer, S. I., and K. Hantke.** 1999. SufS is a NifS-like protein and SufD is necessary for stability of the [2Fe-2S] FhuF protein in *Escherichia coli*. J. Bacteriol. **181:**3307-3309.

77. **Peters, J. W., W. N. Lanzilotta, B. J. Lemon, and L. C. Seefeldt.** 1998. X-ray crystal structure of the Fe-only hydrogenase (CpI) from *Clostridium pasterianum* to 1.8 angstrom resolution. Science **282:**1853-1858.

78. **Pilak, O., B. Mamat, S. Vogt, C. H. Hagemeier, R. K. Thauer, S. Shima, C. Vonrhein, E. Warkentin, and U. Ermler.** 2006. The crystal structure of the apoenzyme of the iron-sulphur cluster-free hydrogenase. J. Mol. Biol. **358:**798-809.

79. **Porat, I., W. Kim, E. L. Hendrikson, Q. Xia, Y. Zhang, T. Wang, F. Taub, B. C. Moore, I. J. Anderson, M. Hackett, J. A. Leigh and W. B. Whitman.** 2006. Disruption of the operon encoding Ehb hydrogenase limits anabolic CO2 assimilation in the archaeon *Methanococcus maripaludis*. J. Bacteriol. **188:**1373-1380.

80. **Porat, I., M. Sieprawska-Lupa, Q. Teng, F. J. Bohanon, R. H. White, and W. B. Whitman.** 2006. Biochemical and genetic characterization of an early step in a novel pathway for the biosynthesis of aromatic amino acids and *p*-aminobenzoic acid in the archaeon *Methanococcus maripaludis*. Submitted J. Bacteriol.

81. **Porat, I., B. W. Waters, Q. Teng, and W. B. Whitman.** 2004. Two biosynthetic pathways for aromatic amino acids in the archaeon *Methanococcus maripaludis*. J. Bacteriol. **186:**4940-4950.

82. **Przybyla, A. E., J. Robbins, N. Menon, and H. D. Peck, Jr.** 1992. Structure-function relationships amont the nickel-containing hydrogenases. FEMS Microbiol. Rev. **88:**109-135.

83. **Ragsdale, S. W., and C. G. Riordan.** 1996. The role of nickel in acetyl-CoA synthesis by the bifunctional enzyme CO dehydrogenase/acetyl-CoA synthase: enzymology and model chemistry. J. Biol. Inorg. Chem. **1:**489-493.

84. **Rodrigues, R., F. M. A. Valente, I. A. C. Pereira, S. Oliveira, and C. Rodrigues-Pousada.** 2003. A novel membrane-bound Ech [NiFe] hydrogenase in *Desulfovibrio gigas*. Biochem. Biophys. Res. Comm. **306:**366-375.

85. **Rossmann, R., T. Maier, F. Lottspeich, and A. Böck.** 1995. Characterisation of a protease from *Escherichia coli* involved in hydrogenase maturation. Eur. J. Biochem. **227**:545-550.

86. **Rother, M., A. Resch, W. L. Gardner, W. B. Whitman, and A. Böck.** 2001. Heterologous expression of archaeal selenoprotein genes directed by the SECIS element located in the 3' non-translated region. Mol. Microbiol. **40**:900-908.

87. **Rouviére, P. E., and R. S. Wolfe.** 1988. Novel biochemistry of methanogenesis. J. Biol. Chem. **263:**72-83.

88. **Sapra, R., K. Bagramyan, and M. W. Adams.** 2003. A simple energy-conserving system: proton reduction coupled to proton translocation. Proc. Natl. Acad. Sci. USA **100:**7545-7550.

89. **Sapra, R., M. F. J. M. Verhagen, and M. W. W. Adams.** 2000. Purification and characterization of a membrane-bound hydrogenase from the hyperthermophilic archaeon *Pyrococcus furiosus*. J. Bacteriol. **182:**3423-3428.

90. **Sauerwald A., W. Zhu, T. A. Major, H. Roy, S. Palioura, D. Jahn, W. B. Whitman, J. R. Yates 3rd, M. Ibba, and D. Söll.** 2005. RNA-dependent cysteine biosynthesis in archaea. Science **307:**1969-1972.

91. **Sauter, M., R. Böhm, and A. Bock.** 1992. Mutational analysis of the operon (*hyc*) determining hydrogenase 3 formation in *Escherichia coli*. Mol. Micro. **6:**1523-1532.

92. **Schleucher, J., C. Griesinger, B. Schwörer, and R. K. Thauer.** 1994. H2-forming N5, N10-methylenetetrahydromethanopterin dehydrogenase from *Methanobacterium thermoautotrophicum* catalyzes a stereoselective hydride transfer as determined by two-dimensional NMR spectroscopy. Biochemistry **33:**3986-3993.

93. **Seravalli, J., and S. W. Ragsdale.** 2000. Channeling of carbon monoxide during anaerobic carbon dioxide fixation. Biochemistry **39:**1274-1277.

94. **Shieh, J. S., and W. B. Whitman.** 1988. Autotrophic acetyl-conezyme A biosynthesis in *Methanococcus maripaludis*. J. Bacteriol. **170:**3072-3079.

95. **Shima, S., E. J. Lyon, M. S. Sordel-Klippert, M. Kauss, J. Kahnt, R. K. Thauer, K. Steinbach, X. Xie, L. Verdier, and C. Griesinger.** 2004. The cofactor of the iron-sulfur cluster free hydrogenase Hmd: Structure of the light-inactivation product. Angew. Chem. Int. Ed. **43:**2547-2551.

96. **Silva, P. J., E. C. D. van den Ban, H. Wassink, H. Haaker, B. de Castro, F. T. Robb, and W. R. Hagen.** 2000. Enzymes of hydrogen metabolism in *Pyrococcus furiosus*. Eur. J. Biochem. **267:**6541-6551.

97. **Simianu, M., E. Murakami, J. M. Brewer, and S. W. Ragsdale.** 1998. Purification and properities of the heme- and iron-sulfur-containing heterodisulfide reductase from *Methanosarcina thermophila*. Biochemistry **37:**10027-10039.

98. **Skidmore, M. L., J. M. Foght, and M. J. Sharp.** 2000. Microbial life beneath a high arctic glacier. Appl. Environ. Microbiol. **66:**3214-3220.

99. **Slesarev A. I., K. V. Mezhevaya, K. S. Makarova, N. N. Polushin, O. V. Shcherbinina, V. V. Shakhova, G. I. Belova, L. Aravind, D. A. Natale, I. B. Rogozin, R. L. Tatusov, Y. I. Wolf, K. O. Stetter, A. G. Malykh, E. V. Koonin, and S. A. Kozyavkin.** 2003. The complete genome of hyperthermophile *Methanopyrus kandleri*

AV19 and monophyly of archaeal methanogens. Proc. Natl. Acad. Sci. USA **99:**4644-4649.

100. **Smith, D. R., L. A. Doucette-Stamm, C. Deloughery, H. Lee, J. Dubois, T. Aldredge, R. Bashirzadeh, D. Blakely, R. Cook, K. Gilbert, D. Harrison, L. Hoang, P. Keagle, W. Lumm, B. Pothier, D. Qiu, R. Spadafora, R. Vicaire, Y. Wang, J. Wierzbowski, R. Gibson, N. Jiwani, A. Caruso, D. Bush, H. Safer, D. Patwell, S. Prabhakar, S. McDougall, G. Shimer, A. Goyal, S. Pietrokovski, G. M. Church, C. J. Daniels, J. Mao, P. Rice, J. Nölling, and J. N. Reeve.** 1997. Complete genome sequence of *Methanobacterium thermoautotrophicum* ΔH: Functional analysis and comparative genomics. J. Bacteriol. **179:**7135-7155.

101. **Sorgenfrei, O., D. Linder, M. Karas, and A. Klein.** 1993. A novel very small subunit of a selenium containing [NiFe] hydrogenase of *Methanococcus voltae* is postranslationally processed by cleavage at a defined position. FEBS Lett. **332**:291-297.

102. **Sorgenfrei, O., S. Müller, M. Pfeiffer, I. Sniezko, and A. Klein.** 1997. The [NiFe] hydrogenases of *Methanococcus voltae*: genes, enzymes and regulation. Arch. Microbiol. **167:**189-195.

103. **Stathopoulos, C., W. Kim, T. Li, I. Anderson, B. Deutsch, S. Palioura, W. Whitman, and D. Söll.** 2001. Cysteinyl-tRNA synthetase is not essential for viability of the archaeon *Methanococcus maripaludis*. Proc. Natl. Acad. Sci. USA **98:**14292-14297.

104. **Stojanowic, A., and R. Hedderich.** 2004. CO2 reduction to the level of formylmethanofuran in *Methanosarcina barkeri* is non-energy driven when CO is the electron donor. FEMS Microbiol. Lett. **235:**163-167.

105. **Stojanowic, A., G. J. Mander, E. C. Duin, and R. Hedderich.** 2003. Physiolgoical role of the F_{420}-non-reducing hydrogenase (Mvh) from *Methanothermobacter marburgensis*. Arch. Microbiol. **180:**194-203.

106. **Takahashi, Y., and M. Nakamura.** 1999. Functional assignment of the ORF2-*iscS*-*iscU*-*iscA*-*hscB*-*hscA*-*fdx*-ORF3 gene cluster involved in the assembly of Fe-S clusters in *Escherichia coli*. **126:**917-926.

107. **Tchong, S.-I., H. Xu, and R. H. White.** 2005. L-cysteine desulfidase: An [4Fe-4S] enzyme isolated from *Methanocaldococcus jannaschii* that catalzyes the breakdown of L-cysteine into pyruvate, ammonia, and sulfide. Biochemistry **44:**1659-1670.

108. **Tersteegen, A., D. Linder, R. K. Thauer, and R. Hedderich.** 1997. Structures and functions of four anabolic 2-oxoacid oxidoreductases in *Methanobacterium thermoautotrophicum*. Eur. J. Biochem. **244:**862-868.

109. **Tersteegen, A., and R. Hedderich.** 1999. *Methanobacterium thermoautotrophicum* encodes two multisubunit membrane-bound [NiFe] hydrogenases: Transcription of the operons and ssequence analysis of the deduced proteins. Eur. J. Biochem. **264:**930-943.

110. **Thauer, R. K.** 1990. Energy metabolism of methanogenic bacteria. **1018:**256-259.

111. **Thauer, R. K.** 1998. Biochemistry of methanogenesis: a tribute to Marjory Stephenson. Microbiol. **144:**2377-2406.

112. **Thomas, D., and Y. Surdin-Kerjan.** 1997. Metabolism of sulfur amino acids in *Saccharomyces cerevisiae*. Microbiol. Mol. Biol. Rev. **61:**503-532.

113. **United States Environmental Protection Agency.** 18 March 2006. Anthropogenic methane emissions in the United States: Estimates for 1990. http:://www.epa.gov/nonco2/reports/anthrosummary.html.

114. **Vignais, P. M., B. Billoud, and J. Meyer.** 2001. Classificiation and phylogeny of hydrogenase. FEMS Microbiol. Rev. **25:**455-501.

115. **Volbeda, A., M.-H. Charon, C. Piras, E. C. Hatchikian, M. Frey, and J. C. Fontecilla-Camps.** 1995. Crystal structure of the nickel-iron hydrogenase from *Desulfovibrio gigas*. Nature **373:**580-587.

116. **Waters, E., M. J. Hohn, I. Ahel, D. E. Graham, M. D. Adams, M. Barnstead, K. Y. Beeson, L. Bibbs, R. Bolanos, M. Keller, K. Kretz, X. Lin, E. Mathur, J. Ni, M. Podar, T. Richardson, G. G. Sutton, M. Simon, D. Söll, K. O. Stetter, L. M. Short, and M. Noordeweier.** 2003. The genome of *Nanoarchaeum equitans*: insights into early archaeal evolution and derived parasitism. Proc. Natl. Acad. Sci. USA **100:**12984-12988.

117. **White, R. H.** 2003. The biosynthesis of cysteine and homocysteine in *Methanococcus jannaschii*. Biochim. Biophys. Acta. **1624:**46-53.

118. **White, R. H.** 2004. L-Aspartate semialdehyde and a 6-deoxy-5-ketohexose 1-phosphate are the precursors to the aromatic amino acids in *Methanocaldococcus jannaschii*. Biochemistry **43:**7618-7627.

119. **Whitman, W. B.** 1985. Methanogenic bacteria pp. 2-84. *In* Woese, C. R., and R. S. Wolfe (eds.), The Bacteria, Vol. VIII. Academic Press, New York.

120. **Whitman, W. B., E. Ankwanda, and R. S. Wolfe.** 1982. Nutrition and carbon metabolism of *Methanococcus voltae*. J. Bacteriol. **149:**852-863.

121. **Whitman, W. B., D. R. Boone, Y. Koga, and J. Keswani.** 2001. Taxonomy of Methanogenic *Archaea* p. 211-213. *In* G. Garrity (ed.), Bergey's manual of systematic bacteriology, 2nd edition. Springer-Verlag, New York.

122. **Woese, C. R., and G. E. Fox.** 1977. Phylogenetic structure of the prokaryotic domain: the primary kingdoms. Proc. Natl. Acad. Sci. USA **74:**5088-5090.

123. **Wu, L. F., and M. A. Mandrand.** 1993. Microbial hydrogenses: primary structure, classification, signatures and phylogeny. FEMS Microbiol. Rev. **10:**243-269.

124. **Xing, R., and W. B. Whitman.** 1991. Characterization of enzymes of the branched chain amino acids biosynthetic pathway in *Methanococcus* spp. J. Bacteriol. **173:**2086-2092.

125. **Xing, R., and W. B. Whitman.** 1992. Characterization of amino acid transferases of *Methanococcus aeolicus*. J. Bacteriol. **174:**541-548.

126. **Yuraniyama, P., J. N. Agar, V. L. Cash, M. K. Johnson, and D. R. Dean.** 2000. NifS-directed assembly of a transient [2Fe-2S] cluster within the NifU protein. Proc. Natl. Acad. Sci. USA **97:**599-604.

127. **Zhang, Q., T. Iwasaki, T. Wakagi, and T. Oshima.** 1996. 2-Oxoacid:ferredoxin oxidoreductase from the thermoacidophlic archaeon, *Sulfolobus* sp. strain 7. J. Biochem. **120**:587-599.

128. **Zheng, L., V. L. Cash, D. H. Flint, and D. R. Dean.** 1998. Assembly of iron-sulfur clusters. Identification of an *iscSUA-hscBA-fdx* gene cluster from *Azotobacter vinelandii*. J. Biol. Chem. **273:**13264-13272.

129. **Zheng, M., X. Wang, L. J. Templeton, D. R. Smulski, R. A. LaRossa, and G. Storz.** 2001. DNA microarray-mediated transcriptional profiling of the *Escherichia coli* resonse to hydrogen peroxide. J. Bacteriol. **183:**4562-4570.

130. **Zheng, L., R. H. White, V. L. Cash, R. F. Jack, and D. R. Dean.** 1993. Cysteine desulfurase activity indicates a role for NIFS in metallocluster biosynthesis. Proc. Natl. Acad. Sci. USA **90:**2754-2758.

131. **Zirngibl, C., R. Hedderich, and R. K. Thauer.** 1990. N5, N10-methylenetetrahydromethanopterin dehydrogenase from *Methanobacterium thermoautotrophicum* has hydrogenase activity. FEBS Lett. **261:**112-116.

132. **Zirngibl, C., W. van Dongen, B. Schwörer, R. von Bünau, M. Richter, A. Klein, and R. K. Thauer.** 1992. H2-forming methylenetetrahydromethanopterin dehydrogenase, a novel type of hydrogenase without iron-sulfur clusters in methanogenic archaea. Eur. J. Biochem. **208:**511-520.

Table 1-1. Description of the five methanogen orders.

Order	Cell wall structure	Lipid composition	Electron acceptors	Reductants
Methanobacteriales	pseudomurein	caldarchaeol myo-inositol	CO_2 sometimes methyl compounds	H_2 formate secondary alcohols
Methanococcales	protein S-layers	*N*-acetylglucosamine hydroxyarchaeol caldarchaeol cyclic archaeol	CO_2	H_2 formate
Methanomicrobiales	glycoprotein S-layers sometimes exterior sheath	aminopentanetetrols galactose	CO_2	H_2 formate sometimes secondary alcohols
Methanopyrales	pseudomurein	archaetidylcholine	CO_2	H_2
Methanosarcinales	S-layer	hydroxyarchaeol galactose	methyl compounds acetate sometimes CO_2	methyl compounds acetate H_2

Table 1-2. *Methanococcus maripaludis* genes encoding the carbon monoxide dehydrogenase/acetyl-CoA synthase.

ORF Name	Protein Name	EC Number	Gene Name
MMP0985	CO dehydrogenase/acetyl-CoA synthase complex alpha subunit	1.2.99.2	*cdhA*
MMP0984	CO dehydrogenase/acetyl-CoA synthase complex epsilon subunit	1.2.99.2	*cdhB*
MMP0983	CO dehydrogenase/acetyl-CoA synthase complex beta subunit	1.2.99.2	*cdhC*
MMP0982	Conserved hypothetical protein		*cdhD*
MMP0981	CO dehydrogenase/acetyl-CoA synthase complex delta subunit	1.2.99.2	*cdhE*
MMP0980	CO dehydrogenase/acetyl-CoA synthase complex gamma subunit	1.2.99.2	*cdhF*
MMP0979	Conserved archaeal protein		*cdhG*

Table 1-3. *Methanococcus maripaludis* pyruvate oxidoreductase gene cluster.

ORF Name	Protein Name	EC Number	Gene Name
MMP1507	pyruvate oxidoreductase (synthase) subunit delta	1.2.7.1	*porA*
MMP1506	pyruvate oxidoreductase (synthase) subunit gamma	1.2.7.1	*porB*
MMP1505	pyruvate oxidoreductase (synthase) subunit	1.2.7.1	*porC*
MMP1504	pyruvate oxidoreductase (synthase) subunit beta	1.2.7.1	*porD*
MMP1503	Conserved archaeal protein		*porE*
MMP1502	Conserved archaeal protein		*porF*

Table 1-4. Genes encoding oxidoreductases (excluding Por) found in *Methanococcus maripaludis*.

ORF Name	Protein Name	EC Number	Gene Name
MMP0305	oxidoreductase family member subunit beta	1.2.7.-	
MMP0306	oxidoreductase family member subunit alpha	1.2.7.-	
MMP0003	2-oxoglutarate oxidoreductase subunit alpha	1.2.7.3	*korA*
MMP1316	2-oxoglutarate oxidoreductase subunit beta	1.2.7.3	*korB*
MMP1315	2-oxoglutarate oxidoreductase subunit gamma	1.2.7.3	*korG*
MMP1296	glyceraldehyde-3-phosphate oxidoreductase	1.2.7.6	*pfkC*
MMP1271	2-oxoisovalarate oxidoreductase, subunit alpha	1.2.7.7	*vorA*
MMP1272	2-oxoisovalarate oxidoreductase, subunit beta	1.2.7.7	*vorB*
MMP1273	2-oxoisovalarate oxidoreductase, subunit gamma	1.2.7.7	*vorC*
MMP0316	indolepyruvate oxidoreductase subunit alpha	1.2.7.8	*iorA1*
MMP0315	indolepyruvate oxidoreductase subunit beta	1.2.7.8	*iorB1*
MMP0714	indolepyruvate oxidoreductase subunit beta	1.2.7.8	*iorA2*
MMP0713	indolepyruvate oxidoreductase subunit alpha	1.2.7.8	*iorB2*

Table 1-5. The four groups of nickel-containing hydrogenases as described by Vignais (2001) and Wu (1993).

Hydrogenase Group	H_2 formation/consumption	Function	Cellular Localization
1	consumption	transfer electrons from H_2 to cytochrome, coupling electron formation to transmembrane proton translocation	membrane-associated
2	consumption	H_2 signal transduction	cytoplasm
3	both, dependent on conditions	electron sink/source for cofactors	cytoplasm
4	either, dependent on organism's physiology	energy conservation: couple proton motive force to the generation of low-potential electrons	membrane-spanning

Table 1-6. Open reading frames encoding the F_{420}-reducing and F_{420}-non reducing Ni-FeS hydrogenases in *M. maripaludis*.

ORF Name	Protein Name	EC Number	Gene Name
MMP0817	coenzyme F_{420} hydrogenase beta subunit (8-hydroxy-5-deazaflavin-reducing hydrogenase beta subunit)	1.12.99.1	*frcD*
MMP0818	coenzyme F_{420} hydrogenase gamma subunit (8-hydroxy-5-deazaflavin-reducing hydrogenase gamma subunit)	1.12.99.1	*frcC*
MMP0819	related to hydrogenase maturation protease, associated with coenzyme F_{420} hydrogenase		*frcB*
MMP0820	coenzyme F_{420} hydrogenase alpha subunit (8-hydroxy-5-deazaflavin-reducing hydrogenase alpha subunit)	1.12.99.1	*frcA*
MMP0821	Conserved archaeal protein, associated with F_{420}-nonreducing (methyl viologen-reducing) hydrogenase		*vhcA*
MMP0822	F_{420}-nonreducing (methyl viologen-reducing) hydrogenase subunit	1.12.99.-	*vhcB*
MMP0823	F_{420}-nonreducing (methyl viologen-reducing) hydrogenase subunit	1.12.99.-	*vhcC*
MMP0824	Polyferredoxin, associated with F_{420}-nonreducing (methyl viologen-reducing) hydrogenase		*vhcD*
MMP1337	hydrogenase maturation protease, related		
MMP1382	coenzyme F_{420} hydrogenase alpha subunit (8-hydroxy-5-deazaflavin-reducing hydrogenase alpha subunit)	1.12.99.1	*fruA*
MMP1383	related to hydrogenase maturation protease, associated with coenzyme F_{420} hydrogenase		*fruB*
MMP1384	coenzyme F_{420} hydrogenase gamma subunit (8-hydroxy-5-deazaflavin-reducing hydrogenase gamma subunit)	1.12.99.1	*fruC*
MMP1385	coenzyme F_{420} hydrogenase beta subunit (8-hydroxy-5-deazaflavin-reducing hydrogenase beta subunit)	1.12.99.1	*fruD*
MMP1696	conserved archaeal protein, associated with F_{420}-nonreducing (methyl viologen-reducing) hydrogenase		*vhuA*
MMP1695	F_{420}-nonreducing (methyl viologen-reducing) hydrogenase subunit beta	1.12.99.-	*vhuB*
MMP1694	F_{420}-nonreducing (methyl viologen-reducing) hydrogenase subunit alpha	1.12.99.-	*vhuC*
MMP1693	F_{420}-nonreducing (methyl viologen-reducing) hydrogenase subunit gamma	1.12.99.-	*vhuD*
MMP1692	Polyferredoxin, associated with F_{420}-nonreducing (methyl viologen-reducing) hydrogenase		*vhuE*

Table 1-7. Gene homologs of *Escherichia coli* type 3 hydrogenases.

	Organism			
	Methanothermobacter thermautotrophicum ΔH[f]		*Methanococcus maripaludis* S2[g]	
	eha	*ehb*	*eha*	*ehb*
large hydrogenase	*ehaO* MTH398	*ehbN* MTH1238	*ehaO* MMP1462	*ehbN* MMP1153
small hydrogenase	*ehaN* MTH397	*ehbM* MTH1239	*ehaN* MMP1461	*ehbM* MMP1622
ferredoxin/ polyferredoxin	*ehaP* MTH399 *ehaQ* MTH400/1[i]	*ehbK* MTH1241 *ehbL* MTH1240	*ehaP* MMP1463 *ehaQ* MMP1464	*ehbK* MMP1624 *ehbL* MMP1623
proton translocator	*ehaH* MTH391	*ehbF* MTH1246	*ehaH* MMP1455	*ehbF* MMP1628
transmembrane proteins	*ehaA* MTH384 *ehaB* MTH385 *ehaC* MTH386 *ehaD* MTH387 *ehaE* MTH388 *ehaF* MTH389 *ehaG* MTH390 *ehaI* MTH392 *ehaJ* MTH393 *ehaK* MTH394 *ehaL* MTH395	*ehbA* MTH1251 *ehbB* MTH1250 *ehbC* MTH1249 *ehbD* MTH1248 *ehbE* MTH1247 *ehbG* MTH1245 *ehbH* MTH1244 *ehbI* MTH1243 *ehbJ* MTH1242 *ehbO* MTH1237	*ehaA* MMP1448 *ehaB* MMP1449 *ehaC* MMP1450 *ehaD* MMP1451 *ehaE* MMP1452 *ehaF* MMP1453 *ehaG* MMP1454 *ehaI* MMP1456 *ehaJ* MMP1457 *ehaK* MMP1458 *ehaL* MMP1459	*ehbA* MMP1469 *ehbB* MMP1049 *ehbC* MMP1073 *ehbD* MMP1074 *ehbE* MMP1629 *ehbG* MMP1627 *ehbH* MMP1626 *ehbJ* MMP1625 *ehbO* MMP1621
regulation	ND[j]	ND	ND	ND
hydrogenase maturation	ND	ND	ND	ND
unknown function	*ehaM* MTH396 *ehaR* MTH402 *ehaS* MTH403 *ehaT* MTH404	*ehbP* MTH1236 *ehbQ* MTH1235	*ehaM* MMP1460 *ehaR* MMP1465 *ehaS* MMP1466 *ehaT* MMP1467	*ehbP* MMP940 *ehbQ* MMP400

Table 1-7, cont.

	Organism			
	Methanosarcina barkeri fusaro[1]	*Rhodospirillum rubrum* [1]	*Pyrococcus furiosus* DSM368[d]	
	ech	*coo*	*mbh*	*mbx*
large hydrogenase	*echE* AAZ69136	*cooH* U65510-8	*mbhL* PF1434	*mbxL* PF1442
small hydrogenase	*echC* AAZ69134	*cooL* U65510-5	*mbhJ* PF1432	*mbxJ* PF1444
ferredoxin/ polyferredoxin	*echF* AAZ69137	*cooX* U65510-6 *cooF* U65510-9	*mbhN* PF1436	*mbxN* PF1441
proton translocator	*echA* AAZ69132	ND	*mbhM* PF1435	*mbxM* PF1445
transmembrane proteins	*echB* AAZ69133	*cooK* U65510-4 *cooM* U65510-3	*mbhA* PF1423 *mbhB* PF1424 *mbhC* PF1425 *mbhD* PF1426 *mbhE* PF1427 *mbhF* PF1428 *mbhG* PF1429 *mbhH* PF1430 *mbhI* PF1431	*mbxA* PF1453 *mbxB* PF1452 *mbxC* PF1451 *mbxD* PF1450 *mbxF* PF1449 *mbxG* PF1448 *mbxH* PF1446 *mbxH'* PF1447
regulation	ND	ND	ND	ND
hydrogenase maturation	ND	ND	ND	ND
unknown function	*echD* AAZ69135	*cooU* U65510-7	*mbhK* PF1433	*mbxK* PF1443

Table 1-7, cont.

	Organism			
	Escherichia coli K12[a]		*Desulfovibrio gigas* Hildenborough	
	hyc	*hyf*	*ech*	*coo*
large hydrogenase	*hycE* b2721	*hyfG* b2487	*echE* DVU0430	*cooH* DVU2291
small hydrogenase	*hycG* b2719	*hyfI* b2489	*echC* DVU0432	*cooL* DVU2288
ferredoxin/ polyferredoxin	*hycB* b2724 *hycF* b2720	*hyfA* b2481 *hyfH* b2488	*echF* DVU0429	*cooX* DVU2289 *cooF* DVU2293
proton translocator	ND	*hyfB* b2482 *hyfD* b2484 *hyfF* b2486	*echA* DVU0434	ND
transmembrane proteins	*hycC* b2723 *hycD* b2722	*hyfC* b2483 *hyfE* b2485	*echB* DVU0433	*cooK* DVU2287 *cooM* DVU2286
regulation	*hycA* b2725	*hyfR* b2491	ND	ND
hydrogenase maturation	*hycI* b2717	ND	ND	ND
unknown function	*hycH* b2718	*hyfJ* b2490	*echD* DVU0431	*cooU* DVU2290

[a]Andrews 1997, Sauter 1992
[b]Rodrigues 2003, Heidelberg 2004
[c] genome sequenced by US DOE Joint Genome Institute
[d]Silva 2000, Sapra 2000
[e]Kunkel 1998
[f]Tersteegan 1999
[g]Hendrickson 2004
[i]Possible frameshift.
[j]ND, none detected.

Table 1-8. Comparison of several energy conserving hydrogenases to *M. maripaludis* Ehb.

	Methanococcus maripaludis		*Methanosarcina barkeri*	*Pyrococcus furiosus*		*Escherichia coli*	
	Eha	Ehb	Ech	Mbh	Mbx	Hyc	Nuo
Predicted physiological role of complex	provide electrons for Fmd (methanogenesis)	provide electrons for enzymes involved in carbon assimilation	provide electrons for Fmd, Por, CODH/ACS; electron sink in aceticlastic reactions	electron sink from Gapor	undescribed	part of the formate hydrogenlyase complex (fermentation)	NADH:ubiquinone oxidoreductase, first step in the electron transport chain
Number of genes in gene cluster	20	9	6	14	13	9	13
Percent similarity of large hydrogenase subunit homolog to EhbN	49.2	100	40.1	41	33.7	28	22.3
Percent similarity of proton translocator subunit homolog(s) to EhbF	14.2	100	27.9	39.9 41.0	30	no homolog	30.0 33.0 32.3
Number of homologs with >30% amino acid similarity to individual Ehb subunits	2	17	2	5	11	1	4

Table 1-9. *Methanococcus maripaludis* open reading frames containing $CX_2CX_2CX_3$ motifs.

ORF name	Protein name
MMP0078	conserved hypothetical protein
MMP0081	glutamate synthase, large subunit
MMP0083	conserved archaeal protein
MMP0098	ferredoxin
MMP0104	polyferredoxin
MMP0139	formate dehydrogenase beta subunit
MMP0208	conserved hypothetical protein, oxidoreductase
MMP0270	conserved archaeal protein
MMP0316	indolepyruvate oxidoreductase subunit alpha
MMP0382	RNase L inhibitor
MMP0389	ferredoxin
MMP0449	conserved hypothetical protein
MMP0450	conserved hypothetical protein
MMP0614	related to iron-sulfur flavoproteins of *Methanosarcina thermophila*
MMP0660	Adenine phosphoribosyltransferase
MMP0690	conserved hypothetical protein
MMP0713	indolepyruvate oxidoreductase subunit alpha
MMP0721	conserved hypothetical protein
MMP0722	conserved archaeal protein
MMP0800	conserved archaeal protein
MMP0803	conserved archaeal protein
MMP0808	conserved hypothetical protein
MMP0818	Coenzyme F_{420} hydrogenase subunit gamma [*frcG*]
MMP0824	F_{420}-non-reducing hydrogenase subunit beta [*vhcD*]
MMP0825	conserved archaeal protein
MMP0851	conserved archaeal protein
MMP0911	related to iron-sulfur flavoproteins of *Methanosarcina thermophila*
MMP0945	glyceraldehyde-3-phosphate ferredoxin oxidoreductase
MMP0979	conserved archaeal protein [*cdhG*]
MMP0985	Carbon monoxide dehydrogenase/acetyl-CoA synthase subunit alpha
MMP0986	thymidylate synthase
MMP1054	heterodisulfide reductase C
MMP1067	Succinate dehydrogenase/fumarate reductase iron-sulfur subunit/ methanosarcinal type heterodisulfide reductase subunit D
MMP1140	ferredoxin
MMP1154	heterosulfide reductase, subunit C1
MMP1166	related to iron-sulfur flavoproteins of *Methanosarcina thermophila*
MMP1244	tungsten containing formylmethanofuran dehydrogenase, subunit H
MMP1245	tungsten containing formylmethanofuran dehydrogenase, subunit F
MMP1246	tungsten containing formylmethanofuran dehydrogenase, subunit G
MMP1273	2-oxoisovalerate oxidoreductase subunit gamma
MMP1311	ferredoxin
MMP1329	ferredoxin
MMP1356	conserved hypothetical protein
MMP1358	ferredoxin
MMP1359	conserved hypothetical protein

Table 9, cont.

ORF name	Protein name
MMP1384	coenzyme F_{420} hydrogenase subunit gamma [*fruG*]
MMP1463	polyferredoxin [*ehaP*]
MMP1464	conserved hypothetical protein [*ehaQ*]
MMP1465	conserved hypothetical protein [*ehaR*]
MMP1502	conserved archaeal protein [*porE*]
MMP1503	conserved archaeal protein [*porF*]
MMP1506	pyruvate oxidoreductase (synthase) subunit gamma
MMP1603	conserved archaeal protein
MMP1623	ferredoxin [*ehbH]*
MMP1624	polyferredoxin [*ehbG*]
MMP1679	conserved archaeal protein
MMP1687	2-oxoglutarate oxidoreductase delta subunit
MMP1692	F_{420}-non-reducing hydrogenase subunit beta [*vhuE*]

Figure 1-1. The modified Ljungdahl-Wood pathway is coupled to methanogenesis in hydrogenotrophic methanogens. The methanogenesis pathway (in bold) reduces carbon dioxide in a stepwise fashion to a methyl group, which is incorporated into acetyl-CoA by the carbon monoxide dehydrogenase/acetyl-CoA synthase (CODH/ACS) enzyme. The CODH/ACS reduces CO_2 to CO, which is bound to the enzyme. Coenzyme A is also bound to the CODH/ACS. Finally, the carbonyl group, the CoA, and the methyl group are condensed to form acetyl-CoA. Enzymes catalyzing each step: 1, formyl methanofuran dehydrogenase; 2, formylmethanofuran:tetrahydromethanopterin formyltransferase; 3, N^5,N^{10}-methenyltetrahydromethanopterin cyclohydrolase; 4, and 4', methylenetetrahydromethanopterin dehydrogenases; 5, methylenetetrahydrofolate reductase; 6, methyltransferase; 7, methyl-coenzyme M reductase; 8, carbon monoxide dehydrogenase/acetyl-CoA synthase; 9, energy conserving hydrogenase A; 10, F_{420}-reducing hydrogenases; 11, heterodisulfide reductase; 12, energy conserving hydrogenase B.

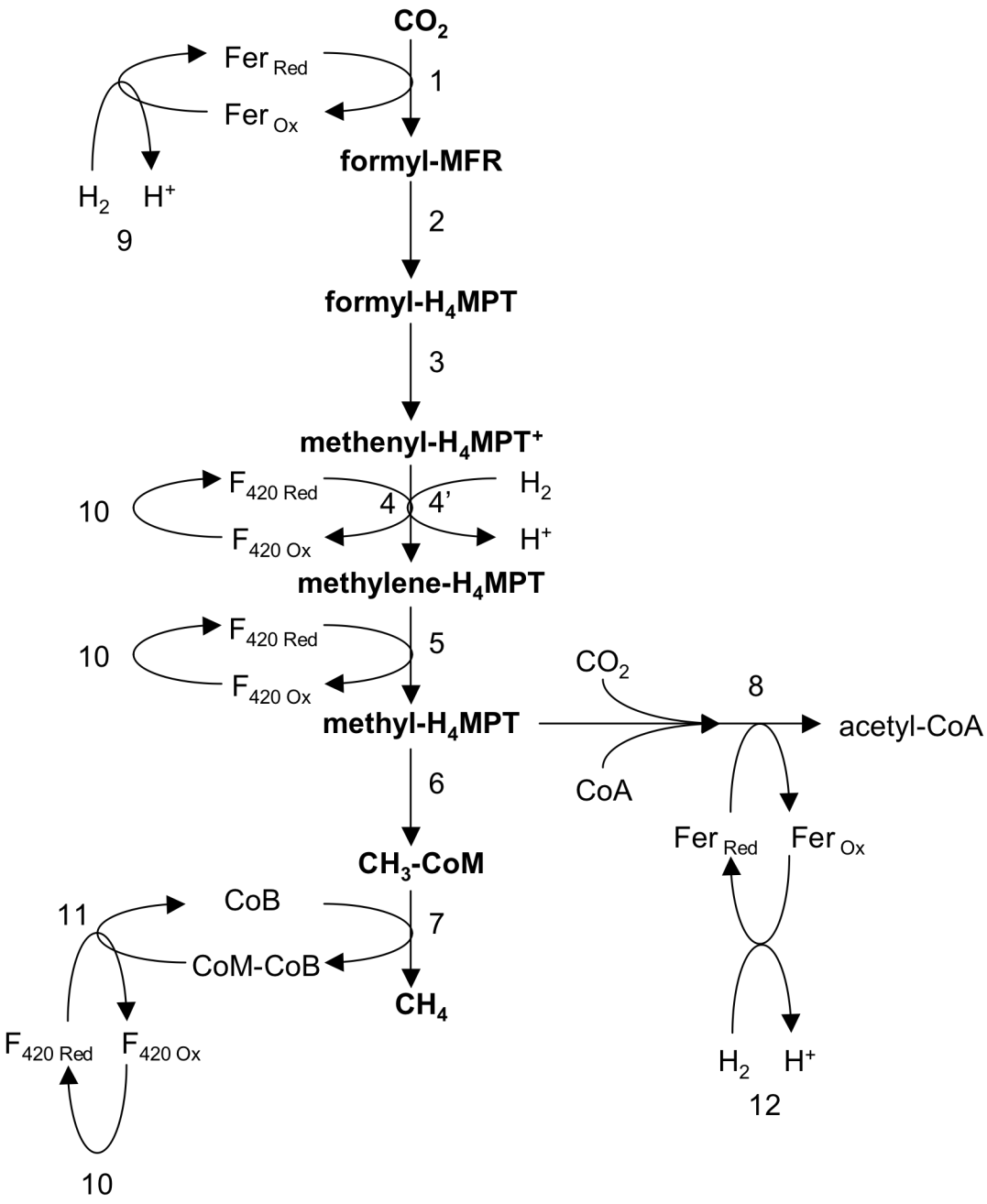
CO2
Fer Red
Fer Ox
1
formyl-MFR
H2
H+
9
2
formyl-H4MPT
3
methenyl-H4MPT+
F420 Red
F420 Ox
10
4
4'
H2
H+
methylene-H4MPT
F420 Red
F420 Ox
10
5
CO2
8
acetyl-CoA
methyl-H4MPT
CoA
6
CH3-CoM
Fer Red
Fer Ox
CoB
11
7
CoM-CoB
CH4
F420 Red
F420 Ox
H2
H+
12
10

Figure 1-2. *Methanococcus maripaludis* autotrophy depends upon the modified Ljungdahl-Wood pathway and the incomplete reductive tricarboxylic acid cycle. Most of the amino acids are derived from the biochemical intermediates generated in these pathways. The conversion of pyruvate to oxaloacetate is performed by the pyruvate carboxylase in the methanococci. Enzymes involved in the IR-TCA cycle include malate dehydrogenase, fumarase, fumarate reductase, succinyl-CoA synthetase and 2-ketoglutarate oxidoreductase. Several key enzymes in this pathway require low potential electrons, including the carbon monoxide dehydrogenase/acetyl-CoA synthase (CODH/ACS), the pyruvate oxidoreductase (POR) and the 2-ketoglutarate oxidoreductase (KOR). Other abbreviations: PEP, phosphoenolpyruvate; FBP, fructose bisphosphate. Adapted from Simpson and Whitman (1993).

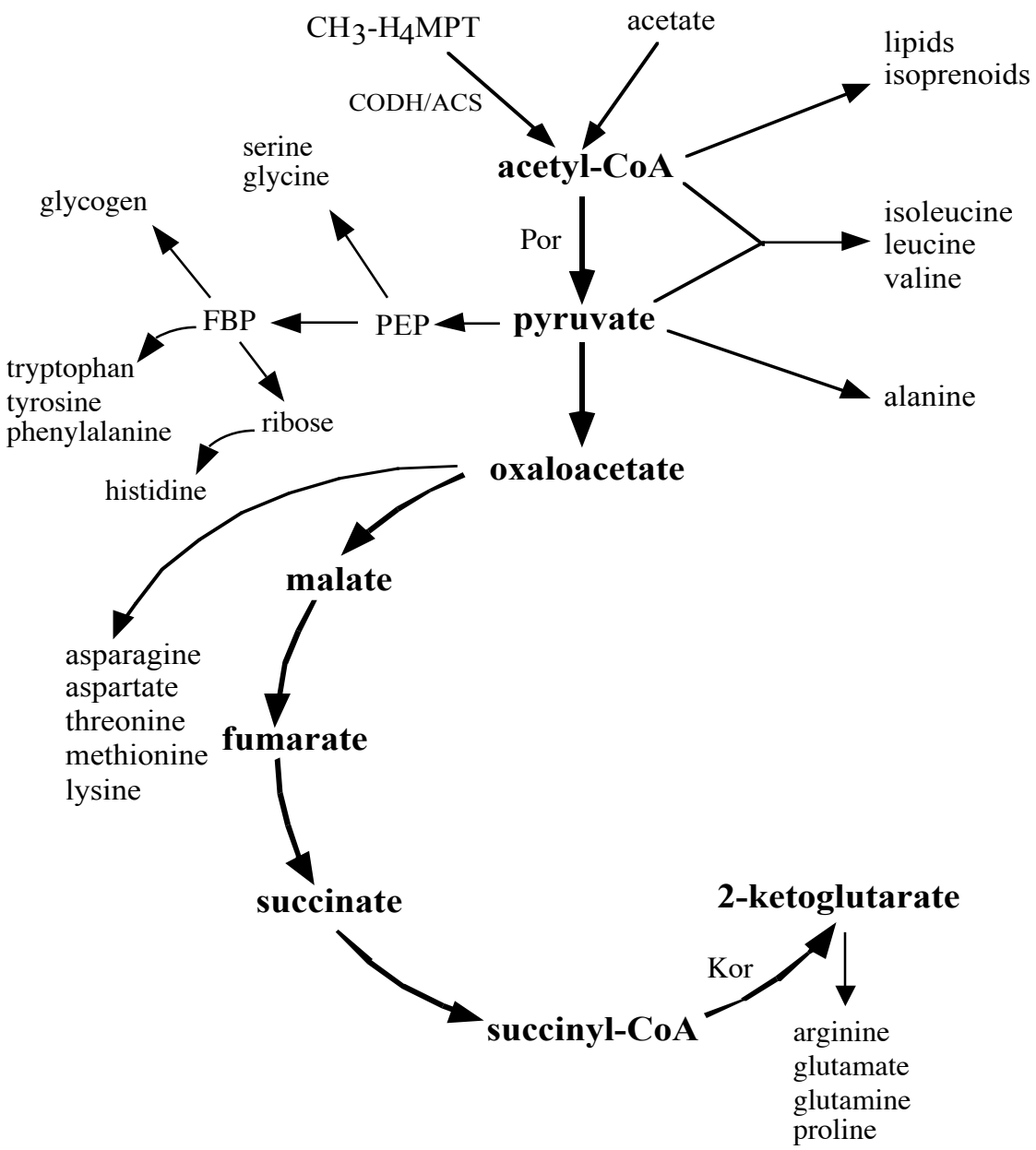
CH3-H4MPT
acetate
CODH/ACS
lipids
isoprenoids
serine
glycine
acetyl-CoA
glycogen
Por
isoleucine
leucine
valine
FBP
PEP
pyruvate
tryptophan
tyrosine
phenylalanine
ribose
alanine
histidine
oxaloacetate
malate
asparagine
aspartate
threonine
methionine
lysine
fumarate
succinate
2-ketoglutarate
Kor
succinyl-CoA
arginine
glutamate
glutamine
proline

Figure 1-3. Aromatic amino acid biosynthesis in *Methanococcus maripaludis*. Enzymes: 1, fructose bisphosphate aldolase; 2, 2-amino-3,7-dideoxy-D-threo-hept-6-ulosonate (ADTH) synthase; 3, dehydroquinate synthase; 4, 3-dehydroquinate dehydratase; 5, shikimate 5-dehydrogenase; 6, shikimate kinase; 7, 3-phosphoshikimate 1-carboxyvinyltransferase; 8, chorismate synthase; 9, chorismate mutase; 10, prephenate dehydratase; 11, prephenate dehydrogenase; 12,acetyl-CoA transferase ; 13, indolepyruvate oxidoreductase; 14, aminotransferase; 15, anthranilate synthase; 16, anthranilate phosphoribosyl transferase; 17, phosphoribosylanthranilate isomerase; 18, indole-3-glycerol-phosphate synthase; 19, tryptophan synthase. Other abbreviation: DKFP, 6-deoxy-5-ketofructose 1-phosphate. Adapted from Porat *et al.*, 2004.

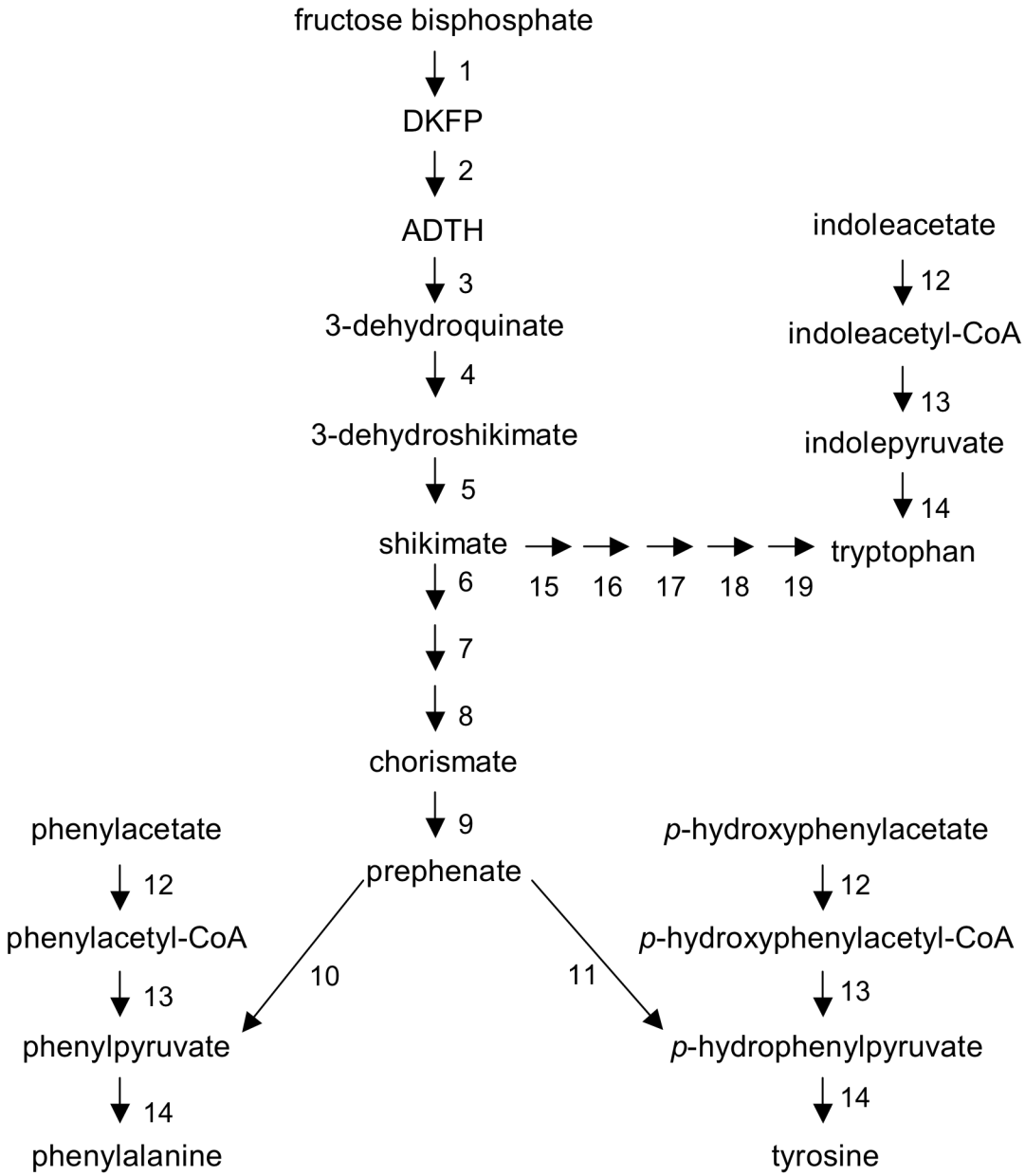
fructose bisphosphate
1
DKFP
2
ADTH
3
3-dehydroquinate
4
3-dehydroshikimate
5
shikimate
6
7
8
chorismate
9
prephenate
indoleacetate
12
indoleacetyl-CoA
13
indolepyruvate
14
tryptophan
15
16
17
18
19
phenylacetate
12
phenylacetyl-CoA
13
phenylpyruvate
14
phenylalanine
10
11
p-hydroxyphenylacetate
12
p-hydroxyphenylacetyl-CoA
13
p-hydrophenylpyruvate
14
tyrosine

Figure 1-4. Phylogenetic relationships of NiFe large hydrogenase subunits and NADH:ubiquionone oxidoreductase. Amino acid sequence alignments and trees were generated using the MEGA3.1 program. Alignments were generated using the ClustalW algorithm. The phylogenetic tree was generated using the Minimum Evolutionary distance matrix method although similar trees were generated using the Neighbor-joining and Maximum Parsimony methods (data not shown). The bootstrap values are indicated by circles at the branch points: ●, >70%; ○, 50 ≥ 70%; unlabeled, <50%. The scale bar is 0.1 expected amino acid substitutions per site. Accession numbers for the amino acid sequences (from top to bottom of tree) are NP_621827, AAS94913, AAM32020, YP_426513, NC_007503, AAS96764, AAL81566, AAC75763, AAC75540, CAF31018, NP_247493, CAB52770, NP_613748, CAB52791, YP_448457, CAF30709, NP_248021, AAL81558, YP_005886, YP_360254, AAC75346, and YP_426645.

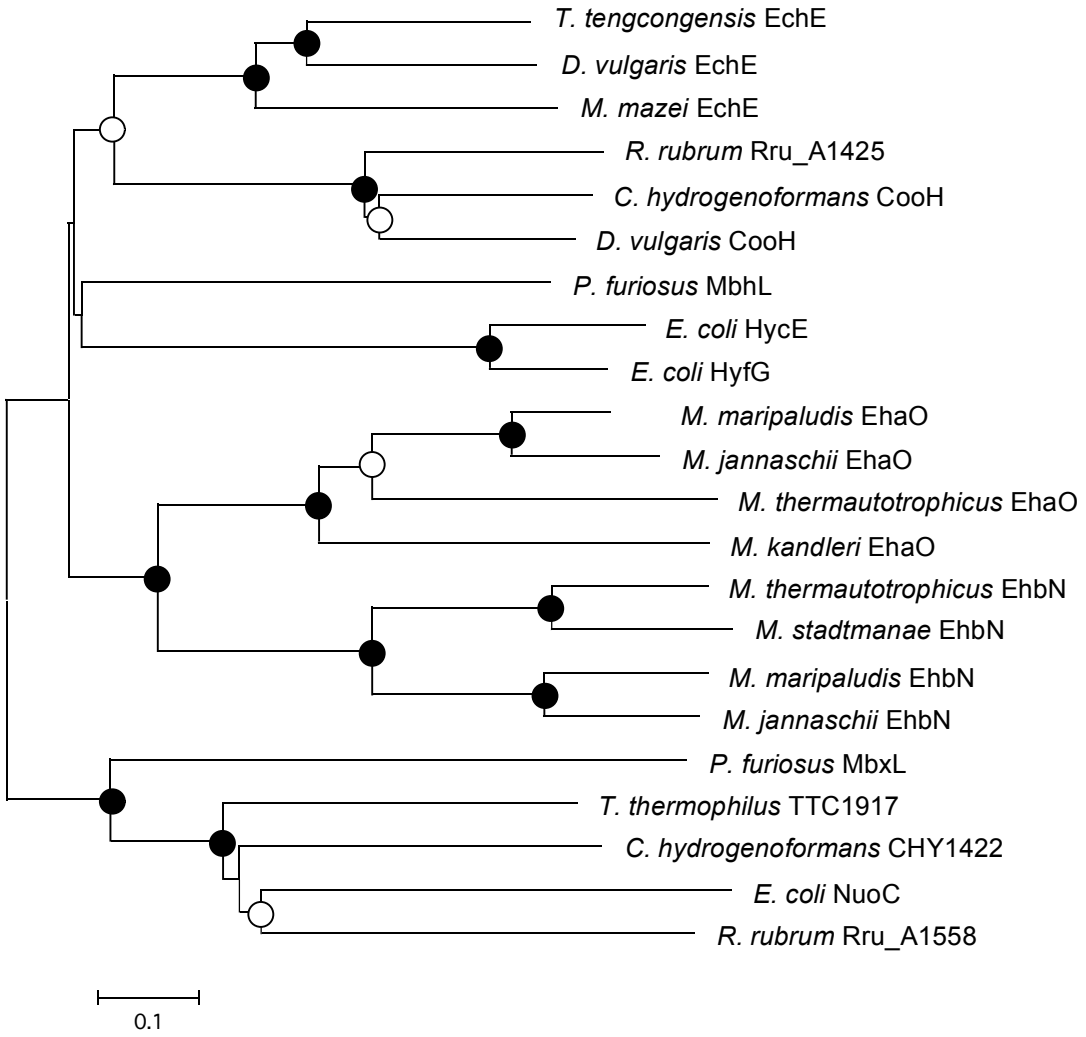
T. tengcongensis EchE
D. vulgaris EchE
M. mazei EchE
R. rubrum Rru_A1425
C. hydrogenoformans CooH
D. vulgaris CooH
P. furiosus MbhL
E. coli HycE
E. coli HyfG
M. maripaludis EhaO
M. jannaschii EhaO
M. thermautotrophicus EhaO
M. kandleri EhaO
M. thermautotrophicus EhbN
M. stadtmanae EhbN
M. maripaludis EhbN
M. jannaschii EhbN
P. furiosus MbxL
T. thermophilus TTC1917
C. hydrogenoformans CHY1422
E. coli NuoC
R. rubrum Rru_A1558
0.1

CHAPTER 2

ABUNDANCE OF 4FE-4S MOTIFS IN THE GENOMES OF METHANOGENS AND OTHER PROKARYOTES[1]

[1]Major, T.A., H. Burd, and W.B. Whitman. 2004. *FEMS Microbiol. Lett.* 239:117-123. Reprinted here with permission of Blackwell Publishing.

Abstract

The abundance of 4Fe-4S motifs of the form $CX_2CX_2CX_3C$ was analyzed in the open reading frames (ORFs) of 120 prokaryotic genomes. The abundance of ORFs containing the $CX_2CX_2CX_3C$ motif or isORFs correlated ($r = 0.82$) with methanogenesis ($p = 0.0001$), archaea ($p = 0.0173$), anaerobiosis ($p < 0.0001$) and genome size ($p < 0.0001$). Optimal growth temperature (hyperthermophily) did not correlate with the number of isORFs ($p = 0.6283$). Large numbers of $CX_2CX_2CX_3C$ motifs may be associated with unique physiologies: methanogenic archaea contained the greatest number of $CX_2CX_2CX_3C$ motifs found among the prokaryotic groups; however, only about 15% of the motifs were in genes directly involved in methanogenesis. Large numbers of $CX_2CX_2CX_3C$ motifs may also be associated with generalists such as *Desulfitobacterium hafniense*, which is an anaerobic bacterium containing multiple reductases.

Introduction

Proteins containing Fe-S clusters are ubiquitous throughout the three domains of life. However, their abundance in different physiological or phylogenetic groups is not well documented. In one example, Daniel and Danson (3) have hypothesized that Fe-S proteins are especially abundant in hyperthermophiles because they substitute for heat labile coenzymes such as NAD/P. In this proposal, the large abundance of Fe-S proteins reflects a "primitive" state since these proteins would have predated the modern development of NAD/P in less thermophilic organisms. In addition, from a physiological point of view, anaerobes may be expected to contain more Fe-S clusters than aerobes because anaerobic electron transport proteins often contain Fe-S clusters and Fe-S clusters are frequently oxygen labile. In this paper, 120 sequenced prokaryotic genomes were analyzed to determine how general physiological

characteristics such as optimum growth temperature, oxygen tolerance, and preferred respiratory pathways correlated with the distribution of $CX_2CX_2CX_3C$ 4Fe-4S motifs.

Materials and Methods

Genome-wide 4Fe-4S motif analyses. Most of the genomic analyses utilized the ERGO database, which is available through Integrated Genomics, Inc. (http://www.integratedgenomics.com). The "Query by Uploaded Pattern" command was utilized to search one hundred and fifteen publicly available draft or published genomes for motifs of the general form $CX_2CX_2CX_3C$. Individual searches for each of the 47 motifs $CX_{0-8}CX_2CX_3C$, $CX_2CX_{0-17}CX_3C$, $CX_2CX_2CX_{0-12}C$, and $CX_4CX_2CX_{6-12}C$ were performed on the genomes from *Methanococcus maripaludis* S2 (also called strain LL; pers. comm., John Leigh), *Chlorobium tepidum* TLS and *Escherichia coli* K-12. The annotations of 38 representative genomes were searched for iron-sulfur clusters not of the $CX_2CX_2CX_3C$ motif using key phrases such as "Fe-S," "2Fe-2S," "Rieske," and "iron-sulfur" using the "Query by Keywords" command.

Additional genome sequences were downloaded from The Institute for Genomic Research (*Methanosarcina mazei*, *Sulfolobus solfataricus*, and *Sulfolobus tokodaii*; http://www.tigr.org), the Center for Genome Research (*Methanosarcina acetivorans*; http://www.broad.mit.edu), and the DOE Joint Genome Institute (*Methanococcoides burtonii*; http://www.jgi.doe.gov). These five genomes were manually searched for the $CX_2CX_2CX_3C$ motif using the Find and Replace function of Microsoft Word. Using the Wildcard function of the Find command, where "?" searches for any character, searches were conducted for C??C, C???C and C????C to account for all $CX_2CX_2CX_3C$ motifs, including those motifs that wrapped to two lines. The Replace command was used to highlight the motifs for subsequent manual

confirmation. A list of the analyzed genomes with relevant groupings and motif data is located as Supplementary Material.

Numerical motif comparisons and statistical analyses. For comparisons of the number of Fe-S motifs within genomes from different physiological groups, the number of motifs was divided by the total number of open reading frames (ORFs) ($x10^3$) to normalize for genome size. The GLM procedure of SAS was used to determine how multiple characteristics correlated with the number of 4Fe-4S motif-containing ORFs (isORFs) and was the source of the reported p values. ANOVA analysis was performed to determine whether individual characteristics were significantly different at the 95% confidence level.

Results and Discussion

Preliminary motif analyses. In preliminary studies, representative genomes (*Methanococcus maripaludis* S2, *Chlorobium tepidum* TLS and *Escherichia coli* K-12) were searched for motifs of the general form $CX_2CX_2CX_3C$, $CX_2CX_4CX_3$, and $CX_2CX_{11}CX_3$, which included the major 4Fe-4S motifs identified in *E. coli* (5). Additional searches for each of the motifs $CX_{0-8}CX_2CX_3C$, $CX_2CX_{0-17}CX_3C$, and $CX_2CX_2CX_{0-12}C$ (to include motifs with varying numbers of X "bridging" amino acids) were also performed to ascertain whether other motifs identify 4Fe-4S proteins (Figure 2-1). The $CX_2CX_2CX_3C$ motif was the most prevalent, occurring 139, 49 and 72 times in the *M. maripaludis*, *C. tepidum* and *E. coli* genomes, respectively. Based solely on the amino acid composition in the absence of functional considerations, only 0.1 of each of the remaining motifs would be predicted per genome. With two exceptions, the means (and ranges) for the other 38 motifs in the three genomes were low with 2 (0-7), 2 (0-7) and 2 (0-7) occurrences, respectively. In *E. coli* two other motifs were abundant. The $CX_2CX_4CX_3C$ motif is a 4Fe-4S motif in *E. coli* and was found 20 times. The

$CX_2CX_2CX_7C$ motif was found 16 times. It was usually formed by tandem $CX_2CX_2CX_3C$ motifs, i.e., the fourth amino acid of X_7 was a C. Moreover, while some known Fe-S proteins were found with the 36 alternative motifs, most of these motifs were actually composed of tandem $CX_2CX_2CX_3C$ motifs, suggesting that these other motifs yielded largely specious identifications. Thus, only the $CX_2CX_2CX_3C$ motif consistently yielded ORFs that were annotated as Fe-S proteins.

In addition, many well-characterized Fe-S proteins contained more than one $CX_2CX_2CX_3C$ motif. A strong correlation was found between the total number of $CX_2CX_2CX_3C$ motifs found per genome and the number of open reading frames containing these motifs (data not shown). Thus, the $CX_2CX_2CX_3C$ motif appeared to be a good indicator of the relative abundance of 4Fe-4S motif-containing ORFs. Therefore, in this study, both the number of motifs and the number of iron-sulfur motif containing ORFs are used. For simplicity, ORFs containing the $CX_2CX_2CX_3C$ iron-sulfur motif are subsequently designated as isORFs.

4Fe-4S clusters are not the only iron-sulfur clusters found in prokaryotes. Rieske and 2Fe-2S clusters are also found. The $CX_4CX_2CX_{10}C$ motif is one 2Fe-2S motif in *E. coli* (5). Searches for $CX_4CX_2CX_{6\text{-}12}C$ motifs were performed on the *E. coli*, *M. maripaludis*, and *C. tepidum* genomes to approximate the number of 2Fe-2S motifs. Unfortunately, few of the known 2Fe-2S proteins were identified by this method due to the variability of the 2Fe-2S motif (5). An alternative identification method involved searching for key phrases such as “Fe-S,” “2Fe-2S,” “Rieske,” and “iron-sulfur” on the annotations of 38 representative geonmes. For 28 bacterial genomes with a small or moderate number of ORFs containing the $CX_2CX_2CX_3C$ motif (see below), the number of other ORFs annotated as Fe-S proteins was highly correlated. Thus, the number of other ORFs = 1.00 x (number of isORFs) + 3.47, with r = 0.85, which was significant

for n = 28. For genomes with large numbers of ORFs containing the $CX_2CX_2CX_3C$ motif, the number of other ORFs annotated as Fe-S proteins was always fewer. For instance, *E. coli* K-12, which contains 39 (or a high number of) isORFs, has only 14 other ORFs annotated as Fe-S proteins (see Figure 2-2). The number of other ORFs also correlates with genome size where the number of other ORFs = 0.0022 x (genome size) + 1.19 ($r = 0.735$, which is significant at $p = 0.01$ with $n = 38$). Because the number of other ORFs and isORFs correlate with each other and with genome size (discussed below), the $CX_2CX_2CX_3C$ motif search approximates the total number of Fe-S clusters, while providing quantitative information about 4Fe-4S clusters.

3.2 Correlation between the number of isORFs and genome size, anaerobiosis, and phylogeny.

Genome size correlates with the number of isORFs for all phylogenetic groups ($p < 0.0001$). Presumably, this correlation reflects that prokaryotes with larger genomes tend to be generalists with multiple metabolic capabilities (9). The possession of additional functions is then correlated with a general increase in the number of enzymes including those possessing 4Fe-4S clusters.

For the bacteria, only a few bacterial genomes are outside two standard deviations of the best fit line for the correlation with genome size: *Desulfitobacterium hafniense*, *Clostridium difficile*, *Chlorobium tepidum*, *Clostridium botulinum*, and *Escherichia coli* K-12 (Figure 2-2). Presumably, the large numbers of isORFs in these organisms are due to adaptations for special physiologies or life styles. For instance, the presence of 64 isORFs in *D. hafniense* far exceeds that found in other bacteria and suggests the presence of a unique metabolism in this fascinating halorespirer. To elucidate what these adaptations might be, the annotations for the isORFs were compared. The genomes of *Desulfitobacterium hafniense* (annotation by Integrated Genomics), *E. coli* K-12 (1), and *Vibrio cholerae* El Tor N16961 (7) are all about 4 megabases and have 64,

39, and 14 isORFs, respectively (Table 2-1). *D. hafniense*, an obligate anaerobe, has a large number of reductases and functionally uncharacterized ORFs with 4Fe-4S motifs, which may reflect the organism's physiological ability to use a variety of compounds as terminal electron acceptors. *E. coli* also contains many reductases, which reflects its ability to utilize a variety of electron acceptors. In contrast, anaerobic respiration is limited in *V. cholerae* and the number of isORFs is fewer. Both *D. hafniense* and *E. coli* are capable of proton reduction and they both possess large numbers of isORFs associated with hydrogenases and ferredoxins. *V. cholerae* has a limited ability to utilize hydrogen and has few isORFs associated with hydrogen and formate metabolism. Therefore, the possession of certain proteins involved in anaerobiosis such as hydrogenases, reductases, and ferredoxins is also correlated with an increased number of isORFs.

To further analyze these observations, several physiological traits were examined for correlation with the number of $CX_2CX_2CX_3C$ motifs. Anaerobiosis is a significant determinant of the number of 4Fe-4S motifs ($p < 0.0001$), where anaerobes have more motifs than aerobes or facultative anaerobes. Within the bacteria, the abundance of 4Fe-4S motifs in the strict anaerobes is about 7.4 motifs per 1000 ORFs and significantly higher than in the aerobes (Table 2-2). However, with 3.7 motifs per 1000 ORFs, the abundance in facultative anaerobes is not significantly different from the 2.8 motifs per 1000 ORFs found in aerobes, according to ANOVA analysis. Similarly, the abundance of Fe-S motifs in the photosynthetic bacteria, pathogenic bacteria, and proteobacteria are not significantly different from that in other bacteria (Table 2-2). Because the aerobes are such a diverse group, it is difficult to attribute with certainty the low number of isORFs to any specific character. Possibly, the O_2-sensitivity of

many isORFs and scarcity of Fe^{+3} as a nutrient in oxic environments may limit the utility of 4Fe-4S clusters in aerobes.

The number of $CX_2CX_2CX_3C$ motifs also correlates with phylogenetic domain ($p = 0.0173$), where the motifs are more abundant in archaea than bacteria (Table 2-2). Although much of this difference is due to the extraordinary abundance of isORFs in the methanogenic archaea, the higher abundance in archaea was significant even when methanogens were excluded. Thus, the average number of Fe-S motifs decreased from about 15 motifs per 1000 ORFs in all archaea to 7.4 for the non-methanogenic archaea (Table 2-2). Among non-methanogenic archaea, the aerobes and anaerobes possessed 6.4 and 8.6 motifs per 1000 ORFs, respectively, compared to 2.8 and 7.4 motifs per 1000 ORFs, respectively, found in the bacteria (Table 2-2). Therefore, the larger average number of motifs in archaea was not solely due to a greater representation of genome sequences from anaerobic archaea.

Methanogens, which are strict anaerobes, contained the most $CX_2CX_2CX_3C$ motifs of any physiological group examined ($p = 0.0001$). Methanogens contain an average of 22.2 motifs/1000 ORFs, compared with an average of 3.7 for all bacteria or 7.4 for non-methanogenic archaea (Table 2-2). Methanogens also contain large numbers of isORFs for their genome sizes (Figure 2-2), so the large number of motifs was not due to a few isORFs with multiple motifs such as polyferredoxins. Other anaerobic archaea and anaerobic bacteria contained 8.6 and 7.4 motifs/1000 ORFs, respectively, so the abundance of the motifs in methanogens cannot be ascribed solely to the anaerobic lifestyle. However, the large number of isORFs was not entirely due to genes directly associated with methanogenesis, either. In the genomes of the mesophilic methylotroph *Methanosarcina acetivorans* (*Ma*), the thermophilic hydrogenotroph *Methanothermobacter thermautotrophicus* (*Mt*), and the hyperthermophilic hydrogenotroph

Methanocaldococcus jannaschii (*Mj*), only about 13-21% of the isORFs were directly involved in methanogenesis (Table 2-1). Even including hydrogenases and formate dehydrogenases, whose functions are well known, the role of only 21-43% of the isORFs are readily explained by the methanogenic lifestyle. The remaining isORFs are primarily ferredoxins and polyferredoxins and "other" isORFs that are not easily categorized. Presumably, these non-methanogenic isORFs are also associated with methanogenesis or the strictly anaerobic life style typical of these prokaryotes but in a more complex manner that has yet to be elucidated. For instance, they may be associated with physiological adaptations necessary for growth of methanogens under environmental but not laboratory conditions.

Among the methanogens, hydrogenotrophs (organisms that require either H_2 or formate to reduce CO_2 to methane) have more 4Fe-4S motifs per 1000 ORFs than the methylotrophic methanogens, which use C1 compounds and/or acetate in addition to H_2 as substrates for methanogenesis (Table 2-2). Part of this difference is due to the absence in methylotrophs of one of the two energy conserving hydrogenases found in the hydrogenotrophic methanogens and many ferredoxins (Table 2-1; 2, 4, 6, 10). However, when comparing the absolute number of isORFs, the methylotrophs possess more because of their much larger genomes. Also, the methylotrophs tend to be "generalists" and are able to utilize a wide range of substrates. The large number of isORFs lacking a functional annotation ("unidentified" in Table 2-1) in *M. acetivorans* may, therefore, be involved in the utilization of alternative substrates (4). Similarly, *Archaeoglobus fulgidus*, a hyperthermophilic sulfate reducer, contains more isORFs than methanogens of a similar genome size (Figure 2-2). Although this organism is not capable of methanogenesis, it contains most of the genes of the tetrahydromethanopterin pathway, many of

which are isORFs (Table 2-1). In addition, this organism contains a large number of anaerobic reductases, which are necessary for sulfate reduction.

Optimal growth temperature and, in particular, hyperthermophily, was not correlated with the number of $CX_2CX_2CX_3C$ motifs ($p = 0.6283$, Table 2-2). Early life has been proposed to be both anaerobic and hyperthermophilic (11). Because of the temperature sensitivity of NAD/P, early organisms are proposed to have utilized Fe-S clusters for reactions commonly linked to pyridine nucleotides in modern organisms (3). While the presence of ferredoxin-dependent oxidoreductases in some hyperthermophiles seems to support this model (8), the abundance of Fe-S motifs is not a feature significantly correlated with hyperthermophily. Similarly, the number of isORFs in hyperthermophiles is within the range found in other prokaryotes with similar genome sizes of the same physiological or phylogenetic group (Figure 2-2). For instance, the hyperthermophilic methanogen *Methanocaldococcus jannaschii* actually has fewer isORFs than the thermophilic methanogen *Methanothermobacter thermautotrophicus* with the same genome size (Table 2-1). Also, aside from a large number of isORFs associated with the ferredoxin-dependant oxidoreductase, the number of isORFs in the heterotrophic hyperthermophile *Pyrococcus horikoshii* is similar to that in other nonmethanogenic archaea (Table 2-1, Figure 2-2). Thus, the distribution of isORFs in modern organisms is better explained by the combination of physiology and phylogeny.

Although hyperthermophily plays a relatively minor role in explaining the modern distribution of isORFs, it could explain the abundance of isORFs in the archaea. For instance, if the ancestors of the archaea contained high numbers of isORFs and were hyperthermophiles, it is possible that large numbers of isORFs were retained in modern archaea even while hyperthermophily was lost. In this case, the number of isORFs would correlate with archaea and

not hyperthermophily. Possibly, the effect of hyperthermophily would be observed with additional bacterial hyperthermophile genomes. The current data set contained only two hyperthermophilic bacteria, which possessed somewhat higher numbers of Fe-S motifs than mesophilic and thermophilic bacteria (Figure 2-2, Table 2-2). However, because of the small sample size, this increase was not significant.

Conclusion

In conclusion, searches using the $CX_2CX_2CX_3C$ motif were used to estimate the number of 4Fe-4S motifs found in 120 prokaryotic genome sequences. The number of ORFs containing these motifs correlates with genome size, anaerobiosis, phylogenetic domain, and methanogenesis. Strict anaerobes like methanogenic archaea and *Desulfitobacterium hafniense* have the largest numbers of 4Fe-4S motifs, presumably due to specialized physiological pathways. In addition, the O_2-sensitivity of many isORFs and scarcity of Fe^{+3} as a nutrient in oxic environments may limit the utility of isORFs in aerobes. As more genomes are sequenced from physiologically and phylogenetically diverse organisms, searches for the $CX_2CX_2CX_3C$ motif will identify new physiological characteristics and metabolic pathways that involve isORFs.

Acknowledgments

The authors are indebted to the annotators at Integrated Genomics and John Leigh for sharing unpublished data. The authors also thank ZhenGang Zhang for assistance in the statistical analyses. This work was supported by a contract from the US Department of Energy.

References

1. **Blattner, F. R., G. Plunkett, III, C. A. Bloch, N. T. Perna, V. Burland, M. Riley, J. Collado-Vides, J. D. Glasner, C. K. Rode, G. F. Mayhew, J. Gregor, N. W. Davis, H. A. Kirkpatrick, M. A. Goeden, D. J. Rose, B. Mau, and Y. Shao.** 1997. The complete genome sequence of *Escherichia coli* K-12. Science **277:**1453-1474.

2. **Bult, C. J., O. White, G. J. Olsen, L. Zhou, R. D. Fleischmann, G. G. Sutton, J. A. Blake, L. M. FitzGerald, R. A. Clayton, J. D. Gocayne, A. R. Kerlavage, B. A. Dougherty, J. F. Tomb, M. D. Adams, C. I. Reich, R. Overbeek, E. F. Kirkness, K. G. Weinstock, J. M. Merrick, A. Glodek, J. L. Scott, N. S. M. Geoghagen, J. F. Weidman, J. L. Fuhrmann, D. Nguyen, T. R. Utterback, J. M. Kelley, J. D. Peterson, P. W. Sadow, M. C. Hanna, M. D. Cotton, K. M. Roberts, M. A. Hurst, B. P. Kaine, M. Borodovsky, H.-P. Klenk, C. M. Fraser, H. O. Smith, C. R. Woese, and J. C. Venter.** 1996. Complete genome sequence of the methanogenic archaeon, *Methanococcus jannaschii*. Science **273:**1058-1073.

3. **Daniel, R. M., and M. J. Danson.** 1995. Did primitive microorganisms use nonhem iron proteins in place of NAD/P? J Mol Evol **40:**559-563.

4. **Galagan, J. E., C. Nusbaum, A. Roy, M. G. Endrizzi, P. Macdonald, W. FitzHugh, S. Calvo, R. Engels, S. Smirnov, D. Atnoor, A. Brown, N. Allen, J. Naylor, N. Stange-Thomann, K. DeArellano, R. Johnson, L. Linton, P. McEwan, K. McKernan, J. Talamas, A. Tirrell, W. Ye, A. Zimmer, R. D. Barber, I. Cann, D. E. Graham, D. A. Grahame, A. M. Guss, R. Hedderich, C. Ingram-Smith, H. C. Kuettner, J. A. Krzycki, J. A. Leigh, W. Li, J. Liu, B. Mukhopadhyay, J. N. Reeve, K. Smith, T. A. Springer, L. A. Umayam, O. White, R. H. White, E. Conway de Macario, J. G. Ferry, K. F. Jarrell, H. Jing, A. J. Macario, I. Paulsen, M. Pritchett, K. R. Sowers, R. V. Swanson, S. H. Zinder, E. Lander, W. W. Metcalf, and B. Birren.** 2002. The genome of *M. acetivorans* reveals extensive metabolic and physiological diversity. Genome Res **12:**532-542.

5. **Gennis, R. B., and V. Stewart.** 1996. Respiration, p. 217-261. *In* F. C. Neidhardt (ed.), *Escherichia coli* and *Salmonella*: cellular and molecular biology, 2nd ed. American Society for Microbiology, Washington, D. C.

6. **Graham, D. E., N. Kyrpides, I. J. Anderson, R. Overbeek, and W. B. Whitman.** 2001. Genome of *Methanocaldococcus* (*Methanococcus*) *jannaschii*. Methods Enzymol **330:**40-123.

7. **Heidelberg, J. F., J. A. Eisen, W. C. Nelson, R. A. Clayton, M. L. Gwinn, R. J. Dodson, D. H. Haft, E. K. Hickey, J. D. Peterson, L. Umayam, S. R. Gill, K. E. Nelson, T. D. Read, H. Tettelin, D. Richardson, M. D. Ermolaeva, J. Vamathevan, S. Bass, H. Qin, I. Dragoi, P. Sellers, L. McDonald, T. Utterback, R. D. Fleishmann, W. C. Nierman, O. White, S. L. Salzberg, H. O. Smith, R. R. Colwell, J. J. Mekalanos, J. C. Venter, and C. M. Fraser.** 2000. DNA sequence of both chromosomes of the cholera pathogen *Vibrio cholerae*. Nature **406:**477-483.

8. **Mukund, S., and M. W. Adams.** 1991. The novel tungsten-iron-sulfur protein of the hyperthermophilic archaebacterium, *Pyrococcus furiosus*, is an aldehyde ferredoxin oxidoreductase. Evidence for its participation in a unique glycolytic pathway. J Biol Chem **266:**14208-14216.

9. **Shimkets, L.J.** 1998. Structure and sizes of genomes of the archaea and bacteria. *In* de Bruijn, F.J., Lupski, J.R., Weinstock, G.M., eds., Bacterial Genomes: Physical Structure and Analysis, pp. 5-11. Chapman & Hall, New York.

10. **Smith, D. R., L. A. Doucette-Stamm, C. Deloughery, H. Lee, J. Dubois, T. Aldredge, R. Bashirzadeh, D. Blakely, R. Cook, K. Gilbert, D. Harrison, L. Hoang, P. Keagle, W. Lumm, B. Pothier, D. Qiu, R. Spadafora, R. Vicaire, Y. Wang, J. Wierzbowski, R. Gibson, N. Jiwani, A. Caruso, D. Bush, H. Safer, D. Patwell, S. Prabhakar, S. McDougall, G. Shimer, A. Goyal, S. Pietrokovski, G. M. Church, C. J. Daniels, J. Mao, P. Rice, J. Nölling, and J. N. Reeve.** 1997. Complete genome sequence of *Methanobacterium thermoautotrophicum* ΔH: functional analysis and comparative genomics. J Bacteriol **179:**7135-7155.

11. **Woese, C. R.** 1987. Bacterial evolution. Microbiol Rev **51:**221-271.

Table 2-1. Number of isORFs containing the 4Fe-4S motif $CX_2CX_2CX_3C$ in individual genomes

	Number of isORFs in the genomes of:[a]							
Functional category	*Ma*	*Mt*	*Mj*	*Af*	*Ph*	*Dh*	*Ec*	*Vc*
Methanogenesis	11	7	8	13[b]	0	0	0	0
Hydrogenases/formate dehydrogenases	5	9	9	2	2	7	6	1
Ferredoxin-dependent oxidoreductases	3	4	4	4	4	1	1	2
Ferredoxins/polyferredoxins	9	13	13	10	4	9	7	2
Reductases	3	1	1	10	0	20	7	1
Dehydrogenases	0	1	0	1	0	2	4	2
Other	5	11	3	12	0	10	12	4
Unidentified[c]	38	6	1	15	4	15	2	2
Total isORFs	74	52	39	67	14	64	39	14

[a] Abbreviations (genome size, x 10^6 bp, in parentheses): *Ma*, *Methanosarcina acetivorans* (5.8); *Mt*, *Methanothermobacter thermautotrophicus* (1.8); *Mj*, *Methanocaldococcus jannaschii* (1.7); *Af*, *Archaeoglobus fulgidus* (2.2); *Ph*, *Pyrococcus horikoshii* (1.7); *Dh*, *Desulfitobacterium hafniense* (4.5); *Ec*, *Escherichia coli* K-12 (4.6); *Vc*, *Vibrio cholerae* El Tor N16961 (4.0)

[b] Includes genes in the tetrahydromethanopterin pathway.

[c] Hypothetical ORFs of no known function.

Table 2-2. Numbers of the 4Fe-4S iron-sulfur motif $CX_2CX_2CX_3C$ within the genomes of various prokaryotic groups

Physiological and phylogenetic groups	No. of genomes[a]	Avg. no. of motifs/ 1000 ORFs[a]	SD[a]
ARCHAEA, all	22	14.8	8.6
non-methanogens	11	7.4	2.1
aerobes	6	6.4	2.5
faculatative anaerobes	2	8.6	0.4
anaerobes	3	8.6	0.5
non-methanogens, non-hyperthermophiles	4	6.2	2.9
methanogens (+ *Archaeoglobus fulgidus*[b])	11	22.2	5.5
hydrogenotrophs	6	25.3	3.6
methylotrophs	4	16.4	2.6
HYPERTHERMOPHILES, all	12	12.2	6.7
archaea	10	12.5	7.4
non-methanogenic archaea	7	8.1	1.3
bacteria	2	10.6	1.3
BACTERIA, all	98	3.7	3.1
aerobes	49	2.8	2.1
facultative anaerobes	38	3.7	2.7
anaerobes	11	7.4	5.4
mesophiles	93	3.6	3.0
thermophiles	3	2.6	0.7
photosynthetic	10	4.7	3.5
pathogens	66	3.1	2.6
proteobacteria	50	4.3	2.3

[a] Abbreviations: No., number; Avg., average; ORFs, open reading frames; SD, standard deviation.

[b] *Archaeoglobus fulgidus* is included in the methanogen category because it contains many of the genes of the tetrahydromethanopterin pathway.

Figure 2-1. Number of motifs found with varying numbers of "bridging" amino acids in *Escherichia coli* K-12, *Chlorobium tepidum* TLS, and *Methanococcus maripaludis* S2. Symbols: black bars, $CNCX_2CX_3C$, where N ranged from 0-8; open bars, CX_2CNCX_3C, where N ranged from 0-17; slanting right bars, CX_2CX_2CNC, where N ranged from 0-12.

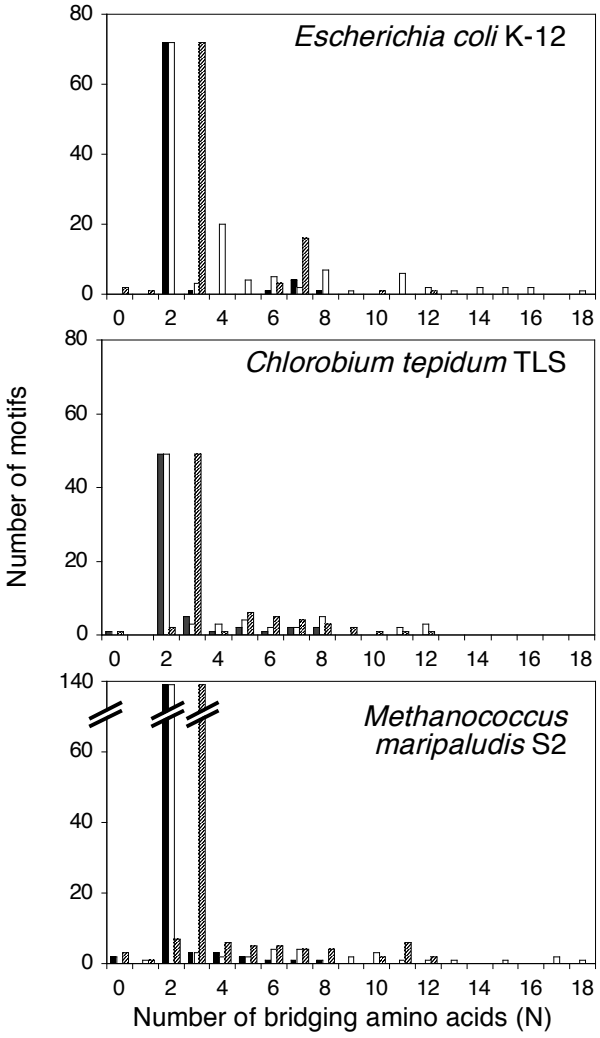
Escherichia coli K-12
Chlorobium tepidum TLS
Methanococcus maripaludis S2
Number of motifs
Number of bridging amino acids (N)

Figure 2-2. Comparison between prokaryotic genome size and number of open reading frames containing the Fe-S motif $CX_2CX_2CX_3C$. Symbols: ○, ● bacteria; ◇ photosynthetic bacteria; □, ■ non-methanogenic archaea; △, ▲ methanogenic archaea and *Archaeoglobus fulgidus*. Solid symbols represent hyperthermophiles. Solid line, linear correlation for bacteria (n = 98), y = 0.0036x + 0.99, r = 0.57; dashed lines, one standard deviation from best fit; dotted lines, two standard deviations. *Af*, *Archaeoglobus fulgidus*; *Cb, Clostridium botulinum; Cd, Clostridium difficile; Ct, Chlorobium tepidum; Dh*, *Desulfitobacterium hafniense*; *Ec*, *Escherichia coli* K-12; *Ma*, *Methanosarcina acetivorans*; *Mj*, *Methanocaldococcus jannaschii*; *Mt*, *Methanothermobacter thermautotrophicus*; *Ph*, *Pyrococcus horikoshii*; *Vc*, *Vibrio cholerae* El Tor N16961.

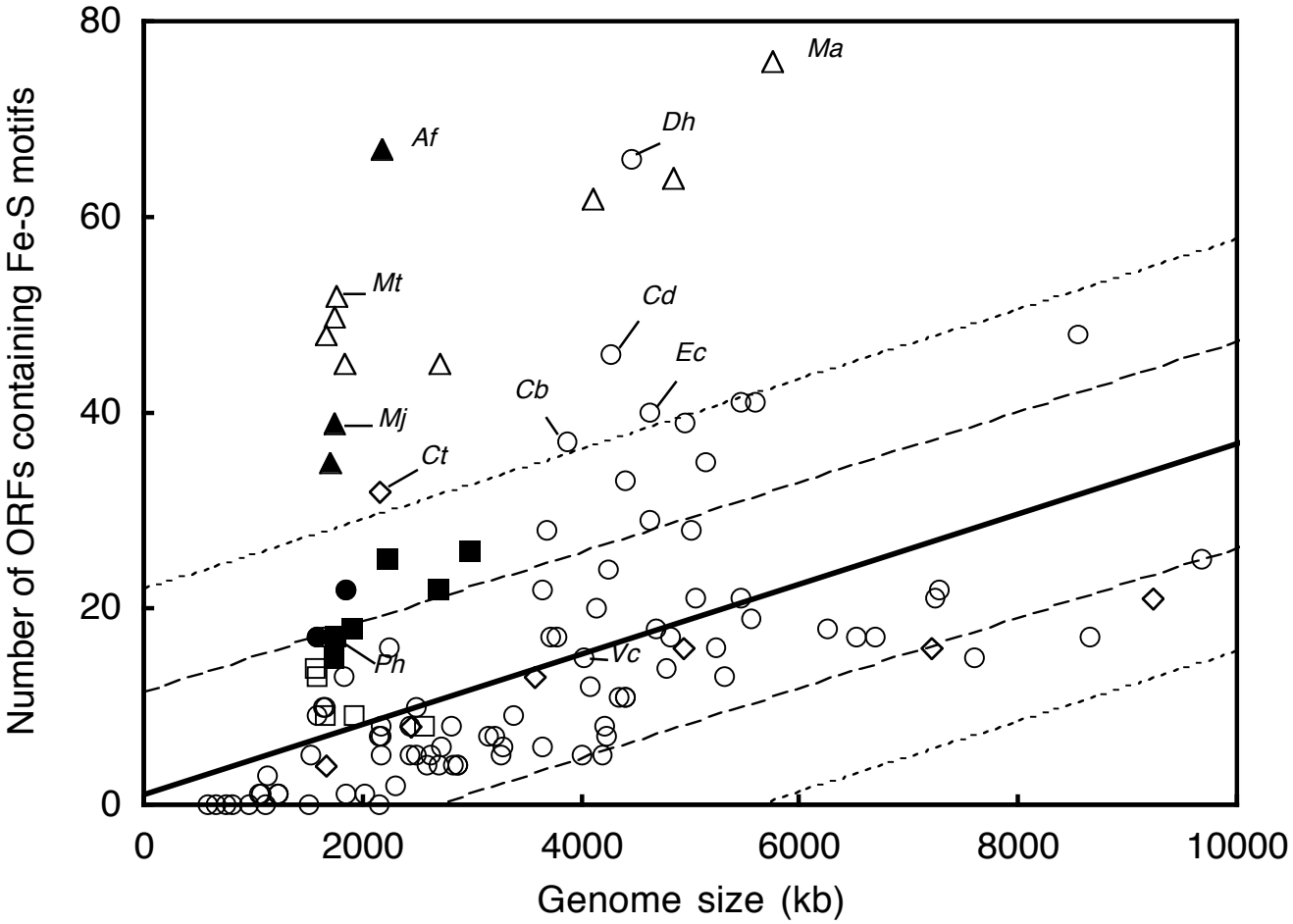
Number of ORFs containing Fe-S motifs
Genome size (kb)
0
20
40
60
80
0
2000
4000
6000
8000
10000
Ma
Af
Dh
Mt
Cd
Ec
Cb
Mj
Ct
Ph
Vc

CHAPTER 3

STRUCTURAL AND FUNCTIONAL ANALYSIS OF THE ENERGY CONSERVING HYDROGENASE B (EHB) IN *METHANOCOCCUS MARIPALUDIS* BY GENE DELETION: PHYSIOLOGICAL EVIDENCE THAT THE EHB IS COUPLED TO AMINO ACID BIOSYNTHESIS[2]

[2]Major, T.A. and W.B. Whitman. To be submitted to *J. Bacteriol.*

Abstract

The *Methanococcus maripaludis* energy conserving hydrogenase B (Ehb) generates low potenetial electrons for enzymes involved in autotrophy. Relative to the *Methanothermobacterium thermautotrophicum ehb* operon, *M. maripaludis* contains 17 *ehb* genes; however, only 9 of the genes are contiguous. To analyze the importance of individual subunits in Ehb structure and function, markerless in-frame deletions were made in several of the *ehb* genes. These genes encode an ion translocator (*ehbF*), a polyferredoxin and ferredoxin (*ehbK* and *ehbL*, respectively), the large and small hydrogenase subunits (*ehbN* and *ehbM*, respectively), and a conserved putative membrane-spanning protein (*ehbO*). When grown in minimal medium plus acetate (McA), *ehb* mutants displayed growth inhibition at varying severities. The membrane-spanning ion translocator deletion strain S940 and the large hydrogenase deletion strain S965 displayed the greatest growth inhibition. In contrast, the Δ*ehbO* strain had little growth inhibition in minimal medium. Since most strains had moderate growth defects, it is likely that there are isozymes capable of functionally complementing the deleted proteins. Furthermore, the Δ*ehbN* strain S965 could not grow in McA containing aryl acids. Typically aryl acids are converted to the aromatic amino acids via the indolepyruvate oxidoreductase (Ior) pathway. The second pathway for aromatic amino acid biosynthesis is blocked in the presence of aryl acids. This is the first physiological evidence that the Ehb is directly coupled to the Ior.

Introduction

Energy conserving hydrogenases (Ech) are multi-subunit, membrane-bound Ni-Fe hydrogenases. These enzymes have several conserved subunits, including large and small hydrogenase subunits, a 2[4Fe-4S] motif-containing protein (ferredoxin), and integral membrane proteins. Representatives of the Ech subfamily can either cleave or generate hydrogen gas; however, in order to be "energy conserving" an ion gradient must be generated that is coupled to ATP production. The Ech also play an important role in respiration as these enzymes either generate or utilize electrons, depending on the physiology of the organism analyzed.

Energy conserving hydrogenases have been identified in a wide variety of organisms. These include *Escherichia coli, Desulfovibrio vulgaris*, *Pyrococcus furiosus*, *Rhodospirillum rubrum*, *Methanosarcina barkeri,* and *Methanococcus maripaludis*. The energy conserving hydrogenases are homologous to the carbon monoxide-induced hydrogenase and the type 3 and 4 hydrogenase of *E. coli* (1, 4, 9, 10, 16, 29). Ech subunits also display similarity to the *Escherichia coli* NADH:ubiquinone oxidoreductase and the mitochondrial respiratory complex (6, 16, 37).

Neither the phylogeny, the function, nor the composition of the energy conserving hydrogenases would suggest that the Ech enzymes are closely related. Phylogenetic comparisons of the Ech large hydrogenase subunits demonstrate that these enzymes are remarkably dissimilar (Figure 3-1). The deep branching of the tree shows that the function of an individual Ech is not apparent by phylogeny. By comparisons of the whole *ech* operons, Calteau *et al.* (5) determined that the 6 gene *ech* operon was horizontally transferred to the *T. tengcongensis* and *Desulfovibrio* species from a *Methanosarcina*. In a second independent horizontal operon transfer, it appears that the pyrococcal Mbx has been transferred to bacteria

(5). Even within the same organism, the various Ni-FeS hydrogenases are not closely related. This is particularly apparent in the *P. furiosus* energy conserving hydrogenases, Mbx and Mbh, which do not cluster together despite the suggestion that these may be gene duplications (5). Furthermore, as seen in Figure 3-1, the energy conserving hydrogenases do not cluster with other Ni-FeS hydrogenases such as the *E. coli* type 1 and 2 or the methanogen F_{420}-reducing or F_{420}-nonreducing hydrogenases. In addition, the phylogenetic tree does not show a relationship between Ech with similar function. For example, the *M. maripaludis* Eha and Ehb large hydrogenase subunits are not closely related to the *M. mazei* Ech even though these hydrogenases are predicted to perform similar functions (22, 24).

Furthermore, the physiological roles of the Ech found in the individual organsims varies widely. For example, the *Pyrococcus furiosus* Ech (denoted Mbx) couples glyceraldehyde 3-phosphate oxidation to hydrogen gas production. ATP is produced *via* a proton motive force generated by the hydrogenase (28). In *Methanosarcina barkeri* the Ech can either utilize or generate hydrogen gas, depending on whether an electron sink is needed in aceticlastic methanogenesis or if low potential electrons are needed during hydrogenotrophic methanogenesis or autotrophy (22).

Even the subunit composition of the Ech's vary widely. *Methanosarcina barkeri* has only 6 genes in the *ech* operon, whereas the *Methanothermobacter thermautotrophicus eha* and *ehb* gene clusters contain 20 and 17 open reading frames, respectively. The Mbh, Mbx, Eha, and Ehb hydrogenases encode multiple membrane-spanning subunits whose functions are unknown (12, 27, 28, 31, 33). The *E. coli* type 3 and 4 hydrogenases and the carbon monoxide hydrogenases do not have a gene that encodes for an ion translocator but are coupled to other proton pumps (2, 9, 10, 34). Therefore, it is not reasonable to assume that one or two

characterized energy conserving hydrogenases are representative of all the energy conserving hydrogenases, particularly when the structures and functions of these hydrogenases differ greatly.

Methanococcus maripaludis is a hydrogenotrophic methanogen that can either synthesize amino acids autotrophically or assimilate amino acids and some amino acid precursors. In the Ehb functional model for *M. maripaludis*, the Ehb is predicted to couple the generation of a proton motive force to the production of low potential electrons utilized in autotrophic reactions (24). Ferredoxins reduced by the Ehb shuttle electrons to various enzymes utilized in autotrophic growth and amino acid production. These include the carbon monoxide dehydrogenase/acetyl-CoA synthase (CODH/ACS), the pyruvate oxidoreductase (Por), the α-ketoglutarate oxidoreductase (Kor), the indolepyruvate oxidoreductase (Ior) and the 2-oxoisovalerate oxidoreductase (Vor). The reduction of the CODH/ACS or Por by a ferredoxin is an energetically unfavorable reaction ($E^{\circ\prime} = -420$ mV; 3, 11). Hydrogenases have a midpoint potential of approximately -290 mV at physiologically relevant conditions. Therefore, an additional source of energy is required to drive the reduction of ferredoxin. This energy source is the ion gradient (either proton or Na^+/H^+ antiport) generated by the Ehb. Thus, the Ehb couples proton translocation with ferredoxin reduction.

Previous results with an *M. maripaludis ehb* insertion strain S40 demonstrated that the Ehb plays a strong role in autotrophy (24). Growth of the S40 strain in mineral medium was severely limited; however both yeast extract and Casamino acids could return growth of the S40 strain to wild-type levels (24). Proteomic and transcriptomic results demonstrated that the CODH/ACS and Por, which perform the first two steps of carbon assimilation in *M. maripaludis*, were upregulated in the S40 strain (24).

In this work, several markerless, in-frame *ehb* deletions were made in order to further characterize the function and structure of the Ehb. Growth experiments of the *ehb* mutants were performed to ascertain the relative importance of the Ehb subunits during growth under autotrophic conditions. Furthermore, the Ehb large hydrogenase subunit deletion strain S965 was analyzed for its ability to utilize the indolepyruvate oxidoreductase pathway to convert aryl acids to aromatic amino acids (AroAA). This work emphasizes the importance of the Ehb hydrogenase in autotrophy for hydrogenotrophic methanogens.

Materials and methods

Strains, media and growth conditions. Strains used in this study are listed in Table 3-1. *Methanococcus maripaludis* cultures were grown in media as described by Jones *et al.* (13). The media used in this study included McA, minimal medium plus 10 mM sodium acetate; McCA, McA plus 0.2 % (w/v) Casamino acids; and McCAV, McCA plus 1 % (v/v) vitamin mixture (38). Additional substrates used in growth studies are described in the text. *M. maripaludis* cultures were maintained under 275 kPa of a 80 %:20 % mixture of H_2:CO_2. The antibiotics puromycin (2.5 μg ml^{-1}) or neomycin (500 μg ml^{-1} in plates and 1 mg x ml^{-1} in broth) were used where necessary. For growth experiments, prewarmed McCA tubes were inoculated from frozen stocks. Cultures were grown to an absorbance (600 nm) of 0.4 to 0.5, then diluted in McA. The McA subcultures were used to start the experimental growth cultures with inocula sizes as described in the text.

Escherichia coli TOP10 strains were obtained from Invitrogen (Carlsbad, CA). *E. coli* cultures were maintained in low-salt (0.5 % w/v) Luria-Bertani medium.

Construction of ehb *plasmids.* Standard molecular biology techniques were used. The pWDK60 plasmid, which generates an *ehbO*::*pac* gene insertion into the *M. maripaludis*

chromosomal DNA, was constructed as described in Kim (14). Other *ehb* mutants were constructed using the marklerless in frame deletion method of Moore and Leigh (23). The pCRPrtNeo vector contains two multiple cloning regions for generating in-frame, markerless deletions in *M. maripaludis*. Upstream and downstream *ehb* gene flanking regions were cloned in tandem on the pCRPrtNeo vector at one of these multiple cloning sites. Primers for DNA amplification of *ehb* flanking regions are described in Table 3-2. With the exception of the *ehbF* primers, most primers were designed to contain a *Hin*dIII site on the 5' upstream primer, a *Bam*HI site on the 3' upstream primer and the 5' downstream primer and an *Afl*II site on the 3' downstream primer for insertion into the pCRPrtNeo vector. The *ehbF* primers contained *Eco*O109, *Xba*I and *Not*I restriction sites, respectively. The amplified flanking regions retained the ATG start codon, contained either the GGATCC of *Bam*HI or the TCTAGA from *Xba*I, and contained the relevant stop codon.

M. maripaludis genomic DNA was purified using the Wizard Genomic DNA Purification Kit (Promega, Madison, WI). DNA was amplified using Herculase Enhanced DNA Polymerase (Stratagene, La Jolla, CA) using quantities of DNA, primers and polymerase. PCR samples were aliquotted into three tubes, which were amplified (using the gradient function of the thermocycler) at different temperatures within the thermocycler. The cycling program proceeded as follows. To begin, there was a 1 min denaturation at 92 °C. The following steps were performed for 15 cycles. First, a denaturation step was performed at 92 °C for 30 seconds. Second, a gradient extenstion step of 45-55 °C was performed for 30 s with an increase of 1 °C per cycle (such that during the first cycle one tube was incubaed at 45 °C, one tube was incubated at 50 °C and one tube was incubated at 55 °C; during the second cycle, the tubes were at incubated at 46 °C, 51 °C, and 56 °C, etc.). Third, a gradient annealing step was performed at

60-70 °C for 1 min with an increase of 0.5 °C per cycle (where during the first cycle the tubes were incubated at 60 °C, 65 °C, and 70 °C, respectively; during the second cycle the tubes were incubated at 60.5 °C, 65.5 °C, and 70.5 °C; etc.). The first 15 cycles were immediately followed by a second round of 25 cycles (for a total program of 40 cycles). The second round of 25 cycles included a denaturation step at 92 °C for 30 s, which was followed by an extension step for 30 s at 52 °C. Finally, a gradient annealing step was performed at 63-73 °C for 1 min with a 10 s increase in duration per cycle (such that the tubes were incubated at 63 °C, 68 °C, and 73 °C during every cycle but the incubation was 1 minute during the first cycle, 1 min, 10 s during the second cycle, etc.). PCR amplification was verified via agarose gel electrophoresis.

Amplified DNA was subcloned into the TOPO TA Cloning Kit (Invitrogen, Carlsbad, CA) for ease of subsequent molecular manipulation. Plasmids were purified using either the Wizard Plus Minipreps DNA Purification System (Promega, Madison, WI) for plasmids larger than 10 kb or the Qiaprep Spin Miniprep Kit (Qiagen, Valencia, CA) for plasmids < 10 kb. Vectors containing the *ehb* flanking regions were digested with the appropriate restriction enzyme, gel extracted (if necessary) using the Qiaquick gel extraction kit (Qiagen, Valencia, CA) and ligated into the pCRPrtNeo vector. The upstream and downstream *ehb* flanking regions were inserted into the pCRPrtNeo vector in a stepwise manner, where typically the upstream flanking region was digested, ligated into the pCRPrtNeo vector, electroporated and cloned. Correct constructs containing the upstream flanking region were then digested for insertion of the downstream flanking region.

Ehb mutants were complemented using the pMEV2 vector containing the relevant *ehb* gene (20). Individual *ehb* genes were amplified as described above using the primers described

in Table 3-2. Primers were constructed to contain an *Nsi*I site at the 5' start site of the gene and an *Xba*I site at or after the 3' terminus of the gene to facilitate cloning into the pMEV2 vector.

Correct plasmid construction was confirmed by sequencing performed at the University of Michigan Sequencing Core Facility (Ann Arbor, MI). Primers used for sequenicng are available upon request.

Transformations. *M. maripaludis* transformations were performed as previously described (35). Selection of in-frame deletion mutants was performed as described by Moore and Leigh (23). *E. coli* were transformed as described by Lin and Whitman (20).

Confirmation of ehb *mutant genotypes*. Southern hybridization was used to confirm the Δ*ehbO*::*pac* mutation. The DIG High Prime DNA Labeling and Detection Starter Kit I (Roche, Mannheim, Germany) was used for Southern blotting. The S40 probe was generated by digestion of pWDK60 using *Eco*RV/*Kpn*I to generate the downstream flanking region of the *ehbO* gene (approximately 880 bp). Genomic DNA was digested using *Eco*RV. Markerless *ehb* mutants were confirmed via PCR screening and DNA sequencing.

Preparation of cell extracts and membranes. All steps were performed anaerobically. *M. maripaludis* cultures (200 ml) were used to generate cell-free extracts for enzyme assays. Cultures were grown to a final density of approximately 0.4-0.5 (mid-exponential phase) in McCA medium in 1 L adapted Wheaton bottles. Cells were harvested by centrifugation at 5,000 x g for 20 minutes at 4 °C. The cell pellets were frozen at -20 °C for one hour to lyse the cells. The pellets were resuspended in 11 ml of Por buffer: 20mM Tricine-KOH (pH 8.6), 5 mM $MgCl_2$, 0.5 mM dithiothreitol, 0.1 mM thiamine pyrophosphate (TPP), 10% (v/v) glycerol, and 0.5 mg DNase (19). A second centrifugation step (10,000 x g for 30 minutes at 4 °C) was used to remove whole cells. An aliquot (1 ml) of the supernatant was reserved for enzyme activity

and protein concentration, while the other approximately 10 ml was centrifuged at 150,000 x g for 2 hours at 4 °C to further purify the membranes. The pellet was resuspended in 3 ml of Por buffer. Enzyme assays were performed immediately after extract preparations. Protein determination was performed using the BCA Protein Assay Kit (Pierce, Rockford, IL).

Enzyme assays. All assays were performed anaerobically. Hydrogenase activity was analyzed as described by Ladapo and Whitman (18), except 10 mM methylviologen was prepared in a buffer composed of 100 mM Tricine-KOH (pH 8.6), 2mM $MgCl_2$ and I mM TPP. Hydrogenase assays were performed on the cell extract prior to the high speed centrifugation as well as on the supernatant and pellet following the high speed centrifugation. Carbon monoxide dehydrogenase (CODH) activity was performed as described in Shieh and Whitman (30), except the methylviologen buffer is as described above for the hydrogenase assay. Pyruvate oxidoreductase activity was performed as described by Lin *et al*. (19).

Phylogenetic analysis. The amino acid sequences of large hydrogenase subunits and relevant homologs were acquired from the NIH National Center for Biotechnology Information database. Sequences were aligned within the MEGA3.1 program using the ClustalX algorithm (15). Phylogenetic trees were generated using the Minimum Evolution algorithm under default MEGA3.1 settings.

Results

Growth phenotypes of ehb *mutants vary in severity*. In this work, various *ehb* genes were deleted using the in-frame, markerless deletion method of Moore and Leigh (23). This method involves the amplification and cloning of the upstream and downstream flanking regions of the gene of interest into the pCRPrtNeo plasmid. This plasmid contains a neomycin cassette and the *hpt* gene, which confers 8-azahypoxanthine base analog sensitivity to an *M. maripaludis* strain

lacking the *hpt* gene (S900). After transformation of the plasmid into S900, a recombination event must occur between the flanking regions of the plasmid and the genomic DNA, generating a merodiploid strain that is neomycin resistant. A second recombination event causes the plasmid DNA to "loop out" of the genomic DNA. This second cross-over event generates the deleted gene of interest only if one of the two independent recombination events occurs within the upstream flanking region of the plasmid and the genomic DNA and the other cross-over occurs between the downstream flanking regions. If the individual recombinations both occur within the same flanking region, then a wild type genotype is regenerated. This method of gene deletion should not affect the transcription of genes downstream of the deletion.

The *ehb* gene cluster in *M. maripaludis* contains nine genes designated *ehbEFGHJKLMO*. Notably, the *ehbN*, which is predicted to encode the Ehb large hydrogenase subunit, is not part of this gene cluster. The *ehb* genes selected for deletion have putative functional and/or structural roles in the Ehb complex. These genes include the *ehbF* (ion translocator), *ehbKL* and *ehbL* (the polyferredoxin and ferredoxin), the *ehbN* and *ehbM* (encoding the large and small hydrogenase subunits), and the conserved integral membrane protein *ehbO*. Previous results demonstrated that a *pac* insertion into the *ehbF* gene generated an acetate auxotroph (S40) with severe growth deficiencies in acetate-containing minimal medium (Figure 3-2B, 24). Because the pIJA03 plasmid has a terminator sequence downstream of the *pac* cassette, it was assumed that a *pac* insertion would generate a polar mutation. However, reverse transcriptase PCR demonstrated that the genes downstream of the *pac* insertion were expressed at nearly five-fold greater quantities than wild type (24). Evidently, the termination sequence does not stop transcription. The *ehb* genes downstream of *ehbF* appear to encode most of the "active" subunits of the complex, including the small hydrogenase subunit, a ferredoxin

and a polyferredoxin. It is unclear what increases in the levels of these proteins would cause *in vivo*. The *ehbO* gene encodes a membrane-spanning subunit with no known function. It is possible that an increase in the amount of this subunit could weaken the integrity of the cell membrane. The role of the other *ehb* genes has not been elucidated. To eliminate the possibility that the increased expression of the *ehbGHJKLMO* genes affected the S40 growth phenotype, a strain with an in-frame *ehbF* deletion (S940) was generated. Growth of the S940 strain was analyzed in McA and McCA to determine whether autotrophic growth was inhibited (Figure 3-2A). The S940 strain has little growth in McA medium, suggesting that the *ehbF* deletion alone is responsible for the growth phenotype. The S940 strain was complemented with the methanococcal plasmid pMEV2 containing a copy of the *ehbF* gene, generating strain S943. Growth of S943 in McA medium exceeds that of the S900 parent strain, suggesting that recombinant EhbF is bound and functional within the Ehb complex.

The *ehbO* gene encodes a predicted membrane-spanning protein of unknown function that is related to the NuoH of the NADH:ubiquinone oxidoreductase and the EchB, CooK, HycD and HyfC subunits of the membrane-bound hydrogenases (33). Deletion of the *ehbO* gene was performed by insertion of the *pac* cassette via double homologous recombination. This construct also deleted the C-terminal 17 amino acids of the *ehbM* gene, which encodes the small hydrogenase subunit. EhbM sequence alignments showed that this deletion is downstream of the Fe-S binding cysteinyl motifs (data not shown).

To determine whether the conserved membrane-spanning subunit EhbO has a structural role in the Ehb, the *pac* cassette was inserted into the *ehbO* gene. Since the *ehbO* gene is the last gene in the *ehb* cluster, there should be no polar effects associated with this mutation. As seen in Figure 3-2A and Table 3-3, S42 does not show a dramatic growth phenotype relative to wild type

in the absence of amino acids; however, it does have a slight lag. Presumably, the EhbO is a "scaffold" protein, whose role is either to provide structural stability to the Ehb or to act as a "dock" for proteins that interact with the Ehb. It would appear that the EhbO does not perform an active role (i.e., proton translocation) with the Ehb hydrogenase as the *ehbO* deletion does not substantially inhibit autotrophic growth.

The *ehbK* and *ehbL* genes encode a polyferredoxin and ferredoxin, respectively. These genes are predicted be involved in electron transport between the Ehb active site and ferredoxins (24). It is interesting that the *ehb* operon encodes both a ferredoxin and a polyferredoxin when the *Methanosarcina barkeri ech* encodes only a ferredoxin (16). To determine whether the polyferredoxin-ferredoxin of the Ehb are functionally redundant, a *ehbKL* strain (S945) was generated. An *ehbL* deletion strain (S955) was also generated. Growth phenotypes of the Δ*ehbKL* (S945) and Δ*ehbL* (S955) strains are shown in Figure 3-3 relative to the Δ*hpt* parent strain S900. In complex medium, all strains display a similar growth phenotype. However, in McA medium, the two mutant strains display growth inhibition. Interestingly, the Δ*ehbKL* and Δ*ehbL* strains displays a similar growth deficiency. This suggests that the EhbK and EhbL are not functionally redundant because strains S955 and S945 have a similar growth phenotype despite the presence of EhbK in strain S955.

Attempts were also made to generate an *ehbK* mutant. Two plasmids containing *ehbK* flanking regions were constructed, one with flanking regions approximately 750 bp in length and the other with 1000 bp flanking regions. Unfortunately, an *ehbK* merodiploid could not be isolated despite repeated attempts (>5 transformations). Obviously, as it was possible to generate an Δ*ehbKL* mutant, the *ehbK* mutation is not lethal. It is unclear why recombination

between either of the *ehbK* flanking regions of the plasmid and the genomic DNA was unsuccessful.

The S945 and S955 were both complemented using the pMEV2 plasmid containing the *ehbL* gene. Unfortunately, attempts to clone the *ehbKL* proved difficult because these genes contain multiple internal *Nsi*I sites. Cloning into the pMEV2 requires an N-terminal *Nsi*I site and a C-terminal *Xba*I or *Bgl*II site; thus, despite partial digestions, a full-length clone of the *ehbKL* genes was not obtained.

Interestingly, complementation of the Δ*ehbKL* with the *ehbL* gene restored growth to the level of the S900 parent strain (Figure 3-3). It appears that the loss of the EhbL confers the deficient growth phenotype of the Δ*ehbKL* strain S945. This further suggests that the EhbL has the more important role in the function of the Ehb. The complementation of the Δ*ehbL* mutation with the *ehbL*-containing plasmid results in a strain that grows better in minimal medium than the parent strain. Notably, both the S948 and S958 strains did not grow as well as the S945 and S955 mutant strains in complex media. This appears to be the case with all the complemented strains in repeated experiments. One explanation of this is that all the complemented strains were grown in the presence of neomycin in order to retain the pMEV2 plasmid. Neomycin phosphotransferase is encoded by the *neo* gene found on the pMEV2 vector. The inactivation of neomycin is likely to be taxing to the cells and may cause a growth limitation, as evidenced by the lower maximum growth density of the complemented strains relative to the S900 parent strain or the mutant strains.

It was predicted that low potential electrons generated by the Ehb are required for the first steps of carbon assimilation in *M. maripaludis* (24). As both the large and small hydrogenase subunits are required to generate and shuttle electrons generated from hydrogen

cleavage, deletions of either the *ehbM* or *ehbN* gene should abolish Ehb activity. As expected, mutants with deletions in either the *ehbM* or the *ehbN* gene displayed inhibited growth phenotypes in the absence of exogenous amino acids (Figure 3-4). The Δ*ehbN* strain S965 had a more severe growth deficiency than the Δ*ehbM* S960 strain. This result suggests that the Ehb large hydrogenase subunit is unique to the Ehb, such that the Ehb function cannot be replaced by another protein. Despite the 49.2% amino acid similarity of the Eha large hydrogenase subunit (EhaO) to the EhbN, it would appear that the EhaO cannot replace the EhbN in function. In contrast, the ability of strain Δ*ehbM* small subunit strain S960 to grow in the absence of amino acids suggests that some of the Ehb activity is retained. Perhaps the Eha small hydrogenase subunit can replace the EhbM, as these proteins display 60.6% amino acid similarity.

Enzyme activities. A previous deletion of the *ehbF* gene showed no difference in the levels of hydrogenase activity but approximately a 3-fold increase in the levels of pyruvate oxidoreductase and carbon monoxide dehydrogenase specific activity (24). The increase in the specific activity may be explained because the physiological role of the Ehb is both to generate low potential electrons and generate a proton motive force. With the deletion of the *ehbF*, protons are no longer shuttled by the Ehb. Therefore, the energy conservation aspect of the Ehb is lost and cells become carbon limited. One response to this may be the up-regulation of the Por and CODH-ACS enzymes, which play key roles in carbon fixation (24). In contrast, hydrogenase activity only requires the large hydrogenase subunit (not the proton translocator). When purifying the *M. barkeri* Ech, methylviologen-dependent Ech activity was difficult to measure because there are several hydrogenases in *M. barkeri* capable of reducing methylviologen (21). To determine whether the Ehb catalyzes measurable amounts of hydrogen oxidation for methylviologen reduction, the Δ*ehbN* strain S965 was analyzed for hydrogenase

activity. The S965 strain was also analyzed for pyruvate (Por) and carbon monoxide oxidation (CODH/ACS) specific activities.

Table 3-4 shows the specific activity of the three methylviologen-based assays. No difference was noted in hydrogenase activity of the membrane fraction, where the Ehb would reside. This suggests that, like the *M. barkeri* hydrogenases, the level of methylviologen reduction is low relative to soluble or membrane-associated hydrogenases (21). There was approximately a 2-fold increase in the levels of pyruvate oxidoreductase and carbon monoxide dehydrogenase activity. These results corraborate the evidence that the Ehb is coupled to pyruvate and acetyl-CoA biosynthesis (24).

Assimilation of aryl acids and biosynthesis of aromatic amino acids in the EhbN mutant. Two pathways exist for the biosynthesis of aromatic amino acids (AroAA) in *M. maripaludis.* The first pathway is the *de novo* AroAA pathway, which involves a novel 6-deoxy-5-ketofructose 1-phosphate pathway to generate the intermediate chorismate (25). Chorismate is then converted to the aromatic amino acids via canonical pathways (26).

The second aromatic amino acid biosynthesis pathway is the aryl acid pathway, where exogenous aryl acids are transported and converted to aromatic amino acids (26). One of the enzymes involved in this pathway is the indolepyruvate oxidoreductase, which is predicted to be coupled to the Ehb. Previous studies show that the deletion of the *iorA2* gene inhibits *M. maripaludis* growth on the aryl acids phenylacetate, indoleacetate and *p*-hydroxyphenylacetate (26). This effect is predicted to occur due to transcriptional regulation of enzymes involved in the *de novo* aromatic amino acid biosynthesis pathway in the presence of aryl acids (26). In this study, to confirm the Ehb is coupled to the Ior, the S965 strain was analyzed for its ability to assimilate aryl acids for growth (Figure 3-5).

If the Ehb is required for electron transport to the Ior, strain S965 is not expected to utilize aryl acids to generate aromatic amino acids. Furthermore, since aryl acids prevent the expression of the *de novo* AroAA biosynthetic pathway, strain S965 should not be able to to grow in the presence of aryl acids. As seen in Figure 3-5, S965 cannot grow in the presence of aryl acids, demonstrating that the EhbN is coupled to the Ior *in vivo*. In the presence of the aromatic amino acids, S965 grows at approximately the same rate as in McA medium. Therefore, growth inhibition is not due to the formation of the aromatic amino acids. With both the aryl acids and the amino acids, there is a substantial growth defect, suggesting both that the aryl acids are inhibiting the *de novo* pathway and that insufficient aromatic amino acids are taken up from the medium. In particular, growth inhibition is probably due to tyrosine limitation, as *M. maripaludis* does not take up exogenous tyrosine well (26).

Discussion

The physiological role of the Ehb is predicted to be an electron source for anabolic enzymes that require low potential electrons. The low-potential electrons are generated by an ion gradient that is coupled to H_2 oxidation. The inability of the Ehb to complete either of this role will cause a deficiency in autotrophic growth. This work sought to characterize several of the individual Ehb subunits that are predicted to have functional roles in the Ehb. Growth inhibition in minimal medium plus acetate (McA) of the individual *ehb* mutants proves that the subunits play important roles in Ehb function. Of the genes deleted in this study (*ehbF, ehbKL, ehbL, ehbM, ehbN,* and *ehbO*), only the Δ*ehbO* deletion had little effect on autotrophic growth. This is not entirely unexpected as this subunit has no obvious role except as a membrane-spanning protein. Evidently, this subunit does not play a major part in stabilizing the Ehb in the membrane nor is it involved with proton translocation.

To identify subunits that are likely to be involed with Ehb function, it was first necessary to identify all the *ehb* genes. The *M. maripaludis ehb* genes were identified based on homology to the *Methanothermobacter thermautotrophicus ehb* genes (12, 33). *M. thermautotrophicus* has 17 *ehb* genes, all of which form one transcriptional unit (33). In contrast, only nine *ehb* genes cluster in *M. maripaludis*, although all 17 *M. thermautotrophicus ehb* homologs are found at various loci on the genome. Of note is that the *ehbN* gene is not part of the *ehb* gene cluster in *M. maripaludis*. The phenotype of the Δ*ehbN* strain strongly suggests that the EhbN is part of the Ehb complex. Furthermore, this result implies that the other putative *ehb* genes are likely to be associated with the Ehb cluster.

In the dimeric Ni-FeS hydrogenase of *Desulfovibrio gigas*, the large and small hydrogenase subunit interact to catalyze hydrogen oxidation and shuttle electrons to cytochromes (36). The nickel-iron active site for hydrogen binding and cleavage is located within the large hydrogenase subunit (36). The small hydrogenase subunit contains three Fe-S clusters, which are predicted to shuttle electrons away from the active site and to cytochromes associated with the hydrogenase (7). The *M. barkeri* EchE, *R. rubrum* CooL, *E. coli* HycG and the *M. thermautotrophicum* EhaN and EhbM small hydrogenase amino acid sequences only appear to encode the first of the iron-sulfur clusters displayed in the *D. gigas* small hydrogenase subunit (16). Clearly, these three hydrogenases still carry out hydrogenase activity without the other two iron-sulfur clusters. It seems unlikely that the lack of the two iron-sulfur clusters in the small hydrogenase subunit and the presence of a ferredoxin are unrelated. In fact, the ferredoxin in the *M. barkeri* Ech appears to be involved both in electron and proton transport according to site-directed mutagenesis and EPR studies (8, 17).

It is interesting that the different *ehb* deletion mutants display varying levels of growth inhibition. Theoretically, the large hydrogenase, small hydrogenase, ferredoxin, and proton translocating subunit are all required for Ehb proton and electron transport. Elimination of either the proton motive force or electron transport to ferredoxin would inhibit the autotrophic enzymes. Thus, one would expect that a deletion in any of these subunits should produce mutants with no growth under autotrophic conditions. Obviously, this was not the case. The varying levels of growth inhibition by the different *ehb* mutants suggests that there is a functional replacement of the deleted *ehb* subunits by other proteins. Whether or not this is the case is currently being analyzed through a structural analysis of the Ehb complex in wild type and *ehb* mutant strains.

Acknowledgments

This work was funded by a grant from the U. S. Department of Energy.

References

1. **Andrews, S. C., B. C. Berks, J. McClay, A. Ambler, M. A. Quail, P. Golby, and J. R. Guest.** 1997. A 12-cistron *Escherichia coli* operon (*hyf*) encoding a putative pron-translocating formate hydrogenlyase system. *Microbiology* **143:**3633-3647.

2. **Bagramyan, K., and A. Trchounian.** 2003. Structural and functional features of formate hydrogen lyase, an enzyme of mixed-acid fermentation from *Escherichia coli*. Biochemistry **68:**1159-1170.

3. **Bock, A. K., J. Kunow, J. Glasemacher, and P. Schonheit.** 1996. Catalytic properties, molecular composition and sequence alignments of pyruvate:ferredoxin oxidoreductase from the methanogenic archaeon *Methanosarcina barkeri* (strain fusaro). Eur. J. Biochem. **237:**35-44.

4. **Böhm, R., M. Sauter, and A. Böck.** 1990. Nucleotide sequence and expression of an operon in *Escherichia coli* coding for formate hydrogenlyase components. Mol. Microbiol. **4:**231-243.

5. **Calteau, A., M. Gouy, and G. Perrière.** 2005. Horizontal transfer of two operons coding for hydrogenases between bacteria and archaea. J. Mol. Evol. **60:**557-565.

6. **Fearnley, I. M., and J. E. Walker.** 1992. Conservation of sequences of subunits of mitochondrial complex 1 and their relationships with other proteins. Biochim. Biophys. Acta. **1140:**105-134.

7. **Fontecilla-Camps, J. C., M. Frey, E. Garcin, C. Hatchikian, Y. Montet, C. Piras, X. Vernède, and A. Volbeda.** 1997. Hydrogenase: a hydrogen metabolizing enzyme. What do the crystal strucutres tell us about its mode of action? Biochimie **79:**661-666.

8. **Forzi, L., J. Koch, A. M. Guss, C. G. Radosevich, W. W. Metcalf, and R. Hedderich.** 2005. Assignment of the [4Fe-4S] clusters of Ech hydrogenase from *Methanosarcina barkeri* to individual subunits via the characterization of site-directed mutants. FEBS J. **272:**4741-4753.

9. **Fox, J. D., Y. He, D. Shelver, G. P. Roberts, and P. W. Ludden.** 1996. Characterization of the region encoding the CO-induced hydrogenase of *Rhodospirillum rubrum*. J. Bacteriol. **178:**6200-6208.

10. **Fox, J. D., R. L. Kerby, G. P. Roberts, and P. W. Ludden.** 1996. Characterization of the CO-induced, CO-tolerant hydrogenase from *Rhodospirillum rubrum* and the gene encoding the large subunit of the enzyme. J. Bacteriol. **178:**1515-1524.

11. **Grahame, D. A., and E. DeMoll.** 1995. Substrate and accessory protein requirements and thermodynamics of acetyl-CoA synthesis and cleavage in *Methanosarcina barkeri* Biochemistry **34:**4617-4624.

12. **Hendrickson, E. L., R. Kaul, Y. Zhou, D. Bovee, P. Chapman, J. Chung, E. Conway de Macario, J. A. Dodsworth, W. Gillett, D. E. Graham, M. Hackett, A. K. Haydock, A. Kang, M. L. Land, R. Levy, T. J. Lie, T. A. Major, B. C. Moore, I. Porat, A. Palmeiri, G. Rouse, C. Saenphimmachak, D. Söll, S. Van Dien, T. Wang, W. B. Whitman, Q. Xia, Y. Zhang, F. W. Larimer, M. V. Olson, and J. A. Leigh.** 2004. Complete genome sequence of the genetically tractable hydrogenotrophic methanogen *Methanococcus maripaludis*. J. Bacteriol. **186:**6956-6969.

13. **Jones, W. J., M. J. B. Paynter, and R. Gupta.** 1983. Characterization of *Methanococcus maripaludis* sp. Nov., a new methanogen isolated from salt marsh sediment. Arch. Microbiol. **135:**91-97.

14. **Kim, W.** 2003. Ph.D. Thesis. University of Georgia, Athens, GA.

15. **Kumar, S., K. Tamura, and M. Nei. 2004.** MEGA3: integrated software for molecular evolutionary genetics analysis and sequencwe alignment. Brief. Bioinform. **5:**150-163.

16. **Künkel, A., J. A. Vorholt, R. K. Thauer, and R. Hedderich.** 1998. An *Escherichia coli* hydrogenase-3-type hydrogenase in methanogenic archaea. Eur. J. Biochem. **252:**467-476.

17. **Kurkin, S., J. Meuer, J. Koch, R. Hedderich, and S. P. J. Albracht.** 2002. The membrane-bound [NiFe]-hydrogenase (Ech) from *Methanosarcina barkeri*: unusual properties of the iron-sulphur clusters. Eur. J. Biochem. **269:**6101-6111.

18. **Ladapo, J., and W. B. Whitman.** 1990. Method for isolation of auxotrophs in the methanogenic archaebacteria: role of the acetyl-Coa pathway of autotrophic CO_2 fixation in *Methanococcus maripaludis*. Proc. Natl. Acad. Sci. USA **87:**5598-5602.

19. **Lin, W. C., Y.-L. Yang, and W. B. Whitman.** 2003. The anabolic pyruvate oxidoreductase from *Methanococcus maripaludis*. Arch. Microbiol. **179:**444-456.

20. **Lin, W. C., and W. B. Whitman.** 2004. The importance of *porE* and *porF* in the anabolic pyruvate oxidoreductase of *Methanococcus maripaludis*. Arch. Microbiol. **179:**444-456.

21. **Meuer, J., S. Bartoschek, J. Koch, A Künkel, and R. Hedderich.** 1999. Purification and catalytic properties of Ech hydrogenase from *Methanosarcina barkeri*. Eur. J. Biochem. **265:**325-335.

22. **Meuer, J., H. C. Kuettner, J. K. Zhang, R. Hedderich, and W. W. Metcalf.** 2002. Genetic analysis of the archaeon *Methansarcina barkeri* fusaro reveals a central role for Ech hydrogenase and ferredoxin in methanogenesis and carbon fixation. Proc. Natl. Acad. Sci. USA **99:**5632-5637.

23. **Moore, B. C., and J. A. Leigh.** 2005. Markerless mutagenesis in *Methanococcus maripaludis* demonstates roles for alanine dehydrogenase, alanine racemase, and alanine permease. J. Bacteriol. **187:**972-979.

24. **Porat, I., W. Kim, E. L. Hendrickson, Q. Xia, Y. Zhang, T. Wang, F. Taub, B.C. Moore, I. J. Anderson, M. Hackett, J. A. Leigh, and W. B. Whitman.** 2006. Disruption of the operon encoding Ehb hydrogenase limits anabolic CO_2 assimilation in the archaeon *Methanococcus maripaludis*. J. Bacteriol. **188:**1373-1380.

25. **Porat, I., M. Sieprawska-Lupa, Q. Teng, F. J. Bohanon, R. H. White, and W. B. Whitman.** 2006. Biochemical and genetic characterization of an early step in a novel pathway for the biosynthesis of aromatic amino acids and p-aminobenzoic acid in the archaeon *Methanococcus maripaludis*. Submitted J. Bacteriol.

26. **Porat, I., B. W. Waters, Q. Teng, and W. B. Whitman.** 2004. Two biosynthetic pathways for aromatic amino acids in the archaeon *Methanococcus maripaludis*. J. Bacteriol. **186:**4940-4950.

27. **Sapra, R., M. F. J. M. Verhagen, and M. W. W. Adams.** 2000. Purification and characterization of a membrane-bound hydrogenase from the hyperthermophilic archaeon *Pyrococcus furiosus*. J. Bacteriol. **182:**3423-3428.

28. **Sapra, R., K. Bagramyan, and M. W. W. Adams.** 2003. A simple energy-conserving system: proton reduction coupled to proton translocation. Proc. Natl. Acad. Sci. USA **100**:7545-7550.

29. **Sauter, M., R. Böhm, and A. Böck.** 1992. Mutational analysis of the operon (*hyc*) determining hydrogenase 3 formation in *Escherichia coli*. Mol. Microbiol. **6:**1523-1532.

30. **Shieh, J. S., and W. B. Whitman.** 1988. Autotrophic acetyl-conezyme A biosynthesis in *Methanococcus maripaludis*. J. Bacteriol. **170:**3072-3079.

31. **Silva, P. J., E. C. D. van den Ban, H. Wassink, H. Haaker, B. de Castro, F. T. Robb, and W. R. Hagen.** 2000. Enzymes of hydrogen metabolism in *Pyrococcus furiosus*. Eur. J. Biochem. **267:**6541-6551.

32. **Stathopoulos, C., W. Kim, T. Li, I. Anderson, B. Deutsch, S. Palioura, W. Whitman, and D. Söll.** 2001. Cysteinyl-tRNA synthetase is not essential for viability of the archaeon *Methanococcus maripaludis*. Proc. Natl. Acad. Sci. USA **98:**14292-14297.

33. **Tersteegen, A., and R. Hedderich.** 1999. *Methanobacterium thermoautotrophicum* encodes two multisubunit membrane-bound [NiFe] hydrogenases. Eur. J. Biochem. **264:**930-943.

34. **Trchounian, A.** 2004. *Escherichia coli* proton-translocating F_0-F_1-ATP synthase and its association with solute secondary transporters and/or enzymes of anaerobic oxidation-reduction under fermentation. Biochem. Biophys. Res. Commun. **315:**1051-1057.

35. **Tumbula, D. L, R. A. Makula, and W. B. Whitman.** 1994. Transformation of *Methanococcus maripaludis* and identification of a *Pst*I-like restriction system. FEMS Microbiol. Lett. **121:**309-314.

36. **Volbeda, A., M.-H. Charon, C. Piras, E. C. Hatchikian, M. Frey, and J. C. Fontecilla-Camps.** 1995. Crystal structure of the nickel-iron hydrogenase from *Desulfovibrio gigas*. Nature **373:**580-587.

37. **Weidner, U., S. Geier, A. Ptock, T. Friedrich, H. Leif, and H. Weiss.** 1993. The gene locus of the proton-translocating NADH:ubiquinone oxidoreductase in *Escherichia coli*. Organization of the 14 genes and relationship between the derived proteins and subunits of mitochondrial complex I. J. Mol. Biol. **233:**100-122.

38. **Whitman, W. B., J. S. Sheih, S. H. Sohn, D. S. Caras, and U. Premachandran.** 1986. Isolation and characterization of 22 mesophilic methanococci. System. Appl. Microbiol. **7:**235-240.

Table 3-1. Bacterial strains and plasmids.

Bacterial strain or plasmid	Genotype or description	Source or reference
M. maripaludis		
S2	Wild type	(38)
S40	Δ*ehbF*::*pac*	(24)
S42	Δ*ehbO*::*pac*	This work
S900	Δ*hpt*	(23)
S940	Δ*hpt* Δ*ehbF*	This work
S943	Δ*hpt* Δ*ehbF*/pMEV2+*ehbF*	This work
S945	Δ*hpt* Δ*ehbKL*	This work
S948	Δ*hpt* Δ*ehbKL*/pMEV2+*ehbL*	This work
S955	Δ*hpt* Δ*ehbL*	This work
S958	Δ*hpt* Δ*ehbL*/pMEV2+*ehbL*	This work
S960	Δ*hpt* Δ*ehbM*	This work
S963	Δ*hpt* Δ*ehbM*/pMEV2+*ehbM*	This work
S965	Δ*hpt* Δ*ehbN*	This work
S968	Δ*hpt* Δ*ehbN*/pMEV2+*ehbN*	This work
E. coli TOP10	*F*$^-$ *mcrA* Δ(*mrr-hsdRMS-mcrBC*) Φ80*lacZ*Δ*M15* Δ*lacX74 recA1 deoR araD139* Δ(*ara-leu*)*7697 galU galK rpsL* (Str^r) *end A1 nupG*	Invitrogen
Plasmids		
pIJA03	Pur^R methanogen integration vector	(32)
WDK60	pIJA03 with the upstream and downstream regions of the *ehbO* gene	This work
pCRPrtNeo	*hmv* promoter-*hpt* fusion + Neo^R cassette in pCR2.1 TOPO for methanococcal in-frame deletions	(23)
pCRPrtNeo-*ehbF*	pCRPrtNeo with the upstream and downstream regions of *ehbF*	This work
pCRPrtNeo-*ehbL*	pCRPrtNeo with the upstream and downstream regions of *ehbL*	This work
pCRPrtNeo-*ehbKL*	pCRPrtNeo with the upstream and downstream regions of *ehbKL*	This work
pCRPrtNeo-*ehbM*	pCRPrtNeo with the upstream and downstream regions of *ehbM*	This work
pCRPrtNeo-*ehbN*	pCRPrtNeo with the upstream and downstream regions of *ehbN*	This work
pMEV2	Neo^R methanogen shuttle vector	(20)
pMEV2+*ehbF*	pMEV2 with *ehbF* gene	This work
pMEV2+*ehbL*	pMEV2 with *ehbL* gene	This work
pMEV2+*ehbM*	pMEV2 with *ehbM* gene	This work
pMEV2+*ehbN*	pMEV2 with *ehbN* gene	This work

Table 3-2. Oligonucleotide primers used.

Primer	Sequence 5' → 3'
Deletions	
5'upehbF	GGGTCCCAAAATGAGCCTCTGTTTTTCTCCACCACCACTT
3'upehbF	GGCTCTAGATGGAAGTGCTAACAATAGAATAGC
5'dnehbF	GGCTCTAGAGCGGTATTTTCACTTGCAGTTTTA
3'dnehbF	GGCTGCGGCCGCATAAGGAATAATTCCAGTATTTTC
5'upehbK	CCCAAGCTTGGTGGTAAAATGACTCAAAAAAGAGAAATCGCAG
3'upehbK	CCCGGATCCCATATTATCGCCCGGAAATACCTTTAATTCCAC
5'upehbL	CCCAAGCTTAATTGTAAAACCTGCTGAAAGAAAGTTAAG
3'upehbL	CCCGGATCCCATGATTATCCCTTTGCTTAAATTATTTGG
5'dnehbL	CCCGGATCCTAAGGTGTAGTCATGTTAAAAGAGCTTT
3'dnehbLM	CCCCTTAAGTAAAATGCCCTGATATTTTCCAG
5'upehbM	CCCAAGCTTTATGTAATACTTGCGTTAAAGAGTGCCCGC
3'upehbM	CCCGGATCCCATGACTACACCTTACACTTTTGAGTTCGC
5'dnehbM	CCCGGATCCTGAGGAGATAATTATGTTTGAAAATATTTTAAC
5'upehbN	CCCAAGCTTAAATTCCAACTTTTTTACAGAAATTAAG
3'upehbN	CCCGGATCCCATGATTTTTCCCTTTTTCAAAAATAAA
5'dnehbN	CCCGGATCCTAATCACATTAAATAATATGTATATACTAATC
3'dnehbN	CCCCTTAAGATATAATTTTTACAAGATTTTTGCCTATAT
Complementations	
CehbFfor	CCCATGCATGAACTTACTTCCCCTGATTGTAG
CehbFrev	CCCTCTAGATCAGACTATAAAGTCCATACCCTTC
CehbKfor	CCCATGCATGATAGTAACAGACATCAAAAAAT
CehbKrev	CCCTCTAGAAATTATTTGGTTTTTTCATTCCATG
CehbLfor	CCCATGCATGACGTTAAAAGGACTTACAAAAG
CehbLrev	CCCTCTAGATTACACTTTTGAGTTCGCTTTCTTT
CehbMfor	CCCATGCATGTTAAAAGAGCTTTCAAGAAAAG
CehbMrev	CCCTCTAGAAAACATAATTATCTCCTCATCCATT
CehbNfor	CCCATGCATGTACGAAGGAGAAATTGCAATCG
CehbNrev	CCCTCTAGACAATCATAAAACCACCAAAAACTGC

Note: restriction endonuclease sites are underlined.

Table 3-3. Growth rates, lag times, and linear growth rates of *M. maripaludis* S2, S40 and S42 strains.

Growth rate (hr^{-1})						
Strain	McN		McA		McCA	
	mean	SD	mean	SD	mean	SD
S2	0.29	0.01	0.28	0.00	0.31	0.01
S40	--	--	0.22	0.01	0.27	0.01
S42	0.27	0.01	0.28	0.04	0.24	0.02

Lag time (hr)						
Strain	McN		McA		McCA	
	mean	SD	mean	SD	mean	SD
S2	14.36	1.03	10.80	0.00	7.32	0.00
S40	--	--	59.20	10.91	10.30	0.00
S42	18.43	2.67	22.75	1.73	10.08	0.00

Linear growth rate ($\Delta OD \times hr^{-1}$)						
Strain	McN		McA		McCA	
	mean	SD	mean	SD	mean	SD
S2	0.032	0.003	0.035	0.006	0.049	0.001
S40	--	--	0.018	0.004	0.025	0.002
S42	0.032	0.006	0.027	0.001	0.040	0.002

Table 3-4. Methylviologen-based hydrogenase, pyruvate oxidoreductase and carbon monoxide dehydrogenase specific activities.

Fraction	Specific activity (U x mg^{-1})					
	Hydrogenase[a]		POR[b]		CODH[b]	
	S2	S965	S2	S965	S2	S965
low speed supernatant	280 ± 40	300 ± 20	310 ± 80	660 ± 200	260 ± 80	530 ± 90
high speed supernatant	160 ± 30	190 ± 40	ND[c]	ND	ND	ND
high speed pellet	540 ± 190	600 ± 210	ND	ND	ND	ND

[a]Average of two assays from two independent samples; units: mmol methylviologen reduced min^{-1}.
[b]Average of two assays from three independent samples; units: µmol methylviologen reduced min^{-1}.
[c]ND, not determined.

Figure 3-1. Phylogenetic relationships of NiFe large hydrogenase subunits, NADH:ubiquionone oxidoreductase and F_{420}:H_2 dehydrogenase. Amino acid sequence alignments and trees were generated using the MEGA3.1 program. Alignments were generated using the ClustalW algorithm. The phylogenetic tree was generated using the Minimum Evolutionary distance matrix method although similar trees were generated using the Neighbor-joining and Maximum Parsimony methods (data not shown). The bootstrap values are indicated by circles at the branch points: ●, > 70%; ○, 50 ≥ 70%; unlabeled, < 50%. The scale bar is 0.2 expected amino acid substitutions per site. Accession numbers for the amino acid sequences (from top to bottom of tree) are *Desulfovibrio vulgaris* AAS94913, *Methanosarcina mazei* AAM32020, *Pyrococcus furiosus* AAL81566, *Desulfovibrio vulgaris* AAS96764, *Escherichia coli* AAC75763, *Escherichia coli* AAC75540, *Pyrococcus furiosus* AAL81558, *Escherichia coli* AAC75346, *Methanosarcina mazei* AAM32184, *Methanococcus maripaludis* CAF31018, *Methanococcus maripaludis* CAF30709, *Escherichia coli* AAC76030, *Escherichia coli* AAC74058, *Methanosarcina mazei* AAM32009, *Methanococcus maripaludis* CAF31250, *Methanococcus maripaludis* CAF30379, *Methanosarcina mazei* NP_635069, *Methanococcus maripaludis* CAF30376 and *Methanococcus maripaludis* CAF30938.

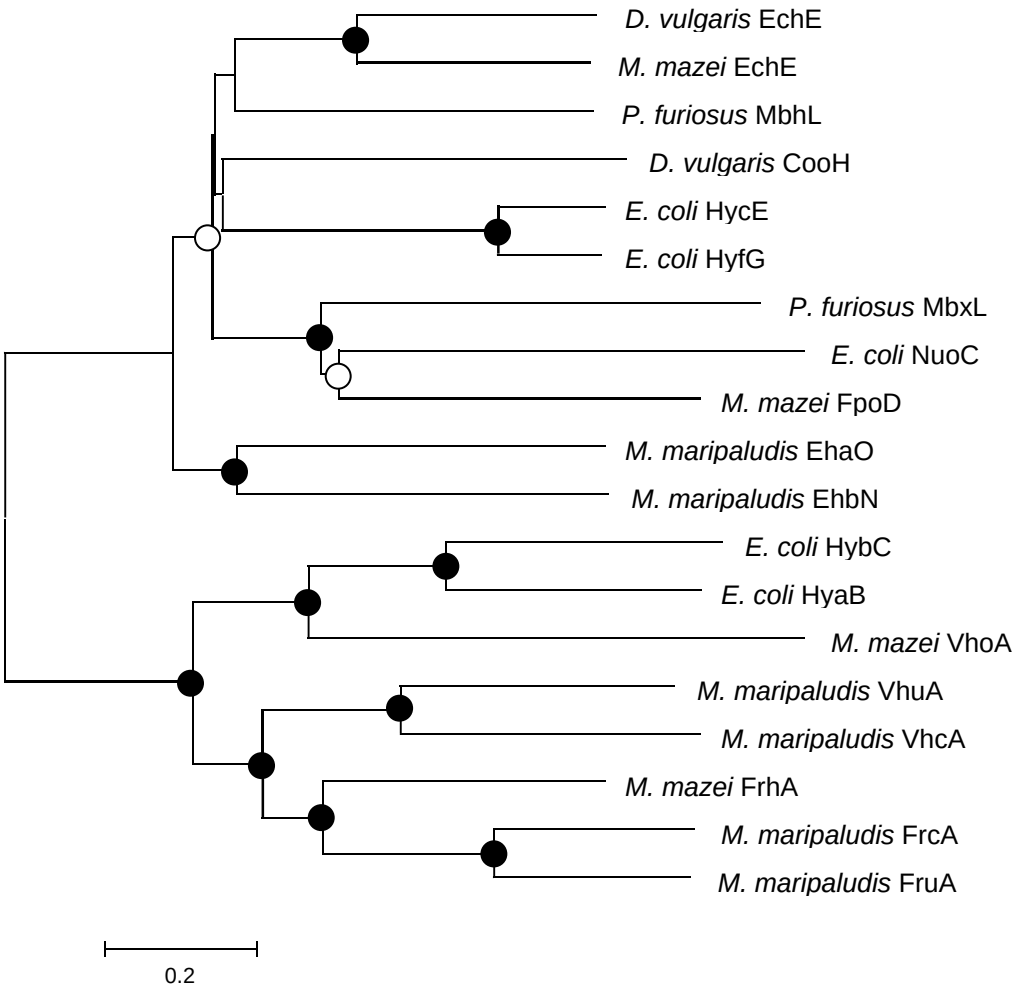
D. vulgaris EchE
M. mazei EchE
P. furiosus MbhL
D. vulgaris CooH
E. coli HycE
E. coli HyfG
P. furiosus MbxL
E. coli NuoC
M. mazei FpoD
M. maripaludis EhaO
M. maripaludis EhbN
E. coli HybC
E. coli HyaB
M. mazei VhoA
M. maripaludis VhuA
M. maripaludis VhcA
M. mazei FrhA
M. maripaludis FrcA
M. maripaludis FruA
0.2

Figure 3-2. Growth phenotypes of Δ*ehbF* (S940), Δ*ehbF*::*pac* (S40), and Δ*ehbO*::*pac* (S42) strains in McA medium (open symbols) and McCA medium (closed symbols). The *ehbO* and *ehbF* encode conserved integral membrane subunits, where EhbF is predicted to be a proton/Na^+ translocator. A. Growth of in-frame deletion parent strain (S900), Δ*ehbF* strain S940, and Δ*ehbF* complemented with pMEV2+*ehbF* strain S943. Approximately 1 x 10^5 cells were subcultured and inoculated into prewarmed media. Symbols: ● and ○, S900; ▲ and △, S940; ■ and □, S943. B. Growth of wildtype (S2) and Δ*ehbF*::*pac* (S40). Approximately 2 x 10^6 cells were subcultured and inoculated into prewarmed media. ● and ○, S2; ▲ and △, S40. C. Growth of S2 and Δ*ehbO*::*pac* (S42) strains. Approximately 2 x 10^6 cells were subcultured and inoculated into prewarmed media. Symbols are as in B except ■ and □, S42.

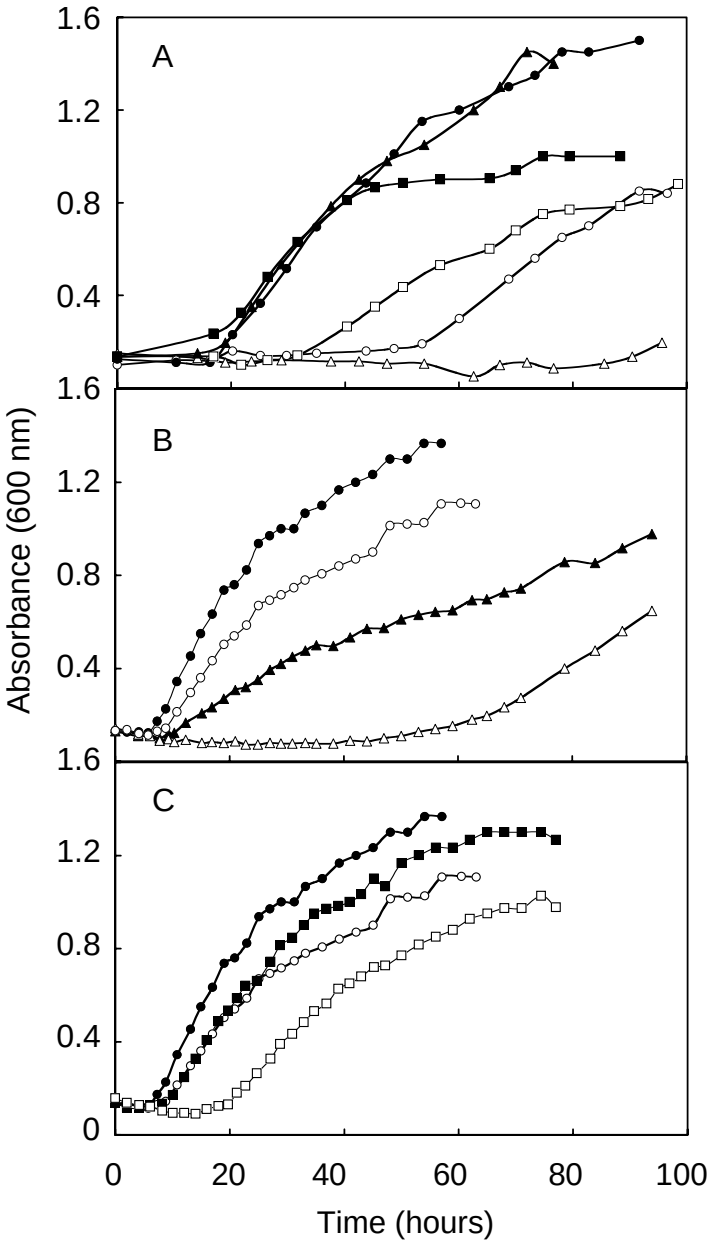
A
B
C
1.6
1.2
0.8
0.4
0
0
20
40
60
80
100
Absorbance (600 nm)
Time (hours)

Figure 3-3. Growth phenotypes of Δ*ehbKL* polyferredoxin-ferredoxin deletion strain and Δ*ehbL* ferredoxin deletion strain and their complementations. Cultures were inoculated with approximately 1 x 10^5 cells into prewarmed McA (open symbols) and McCA (closed symbols). A. Growth of S900 (parent strain), polyferredoxin-ferredoxin deletion strain (S945) and Δ*ehbKL* complemented with pMEV2+*ehbL* strain (S948). Symbols: ● and ○, S900; ■ and □, S945; ▲ and △, S948. B. Growth of S900, Δ*ehbL* ferredoxin deletion strain (S955), and Δ*ehbL* complemented with pMEV2+*ehbL* strain (S958). Symbols: ● and ○, S900; ■ and □, S955; ▲ and △, S958.

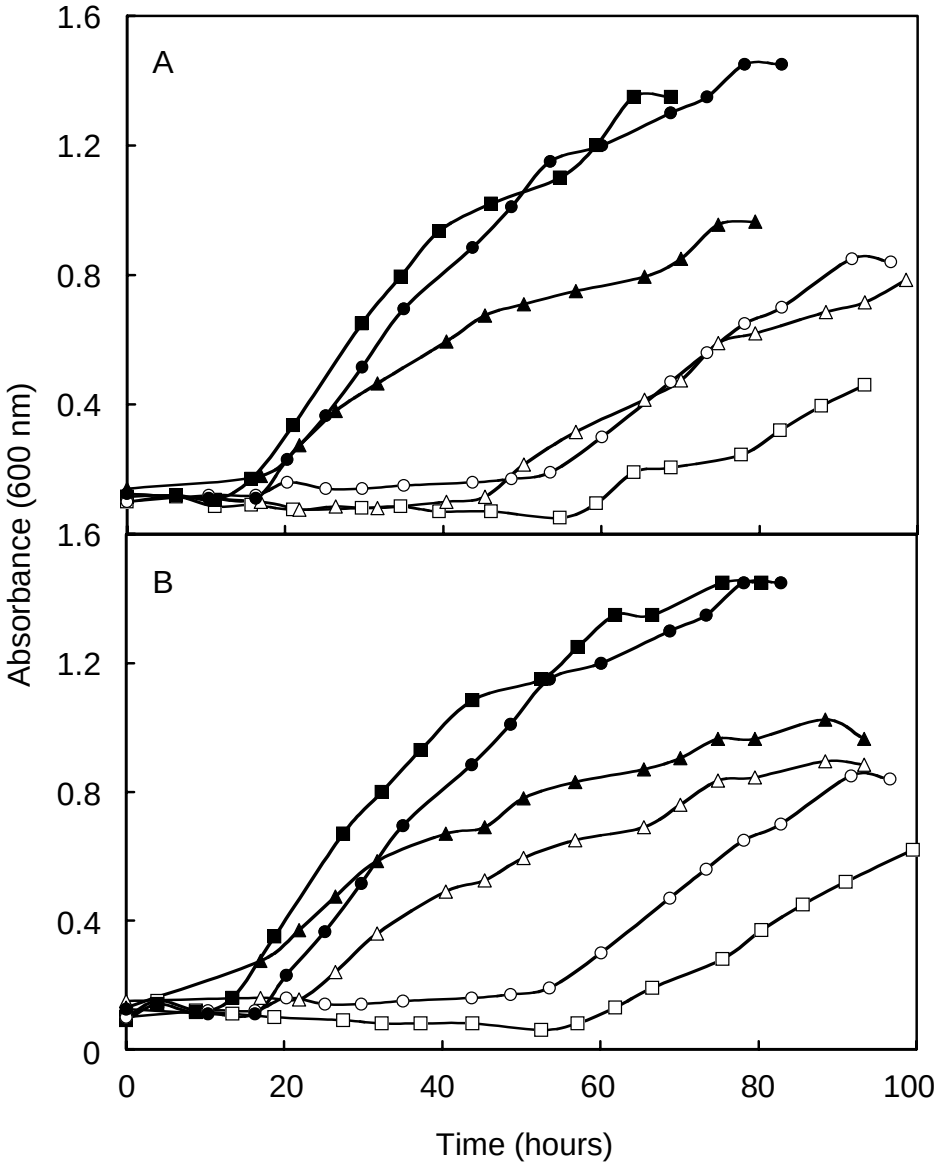
A
B
Absorbance (600 nm)
Time (hours)
0
0.4
0.8
1.2
1.6
0
20
40
60
80
100

Figure 3-4. Growth phenotypes of Δ*ehbM* small hydrogenase mutants and Δ*ehbN* large subunit mutants and their complementations. Prewarmed McA (open symbols) and McCA (closed symbols) media were inoculated with approximately 1 x 10^5 cells. A. Growth of Δ*ehbM* strain S960 and Δ*ehbM* complemented with pMEV2+*ehbM* strain S963. Symbols: ● and ○, S900; ■ and □, S960; ▲ and △, S963. B. Growth of Δ*ehbN* strain S965 and Δ*ehbN* complemented with pMEV2+*ehbN* strain S968. Symbols: ● and ○, S900; ■ and □, S965; ▲ and △, S968.

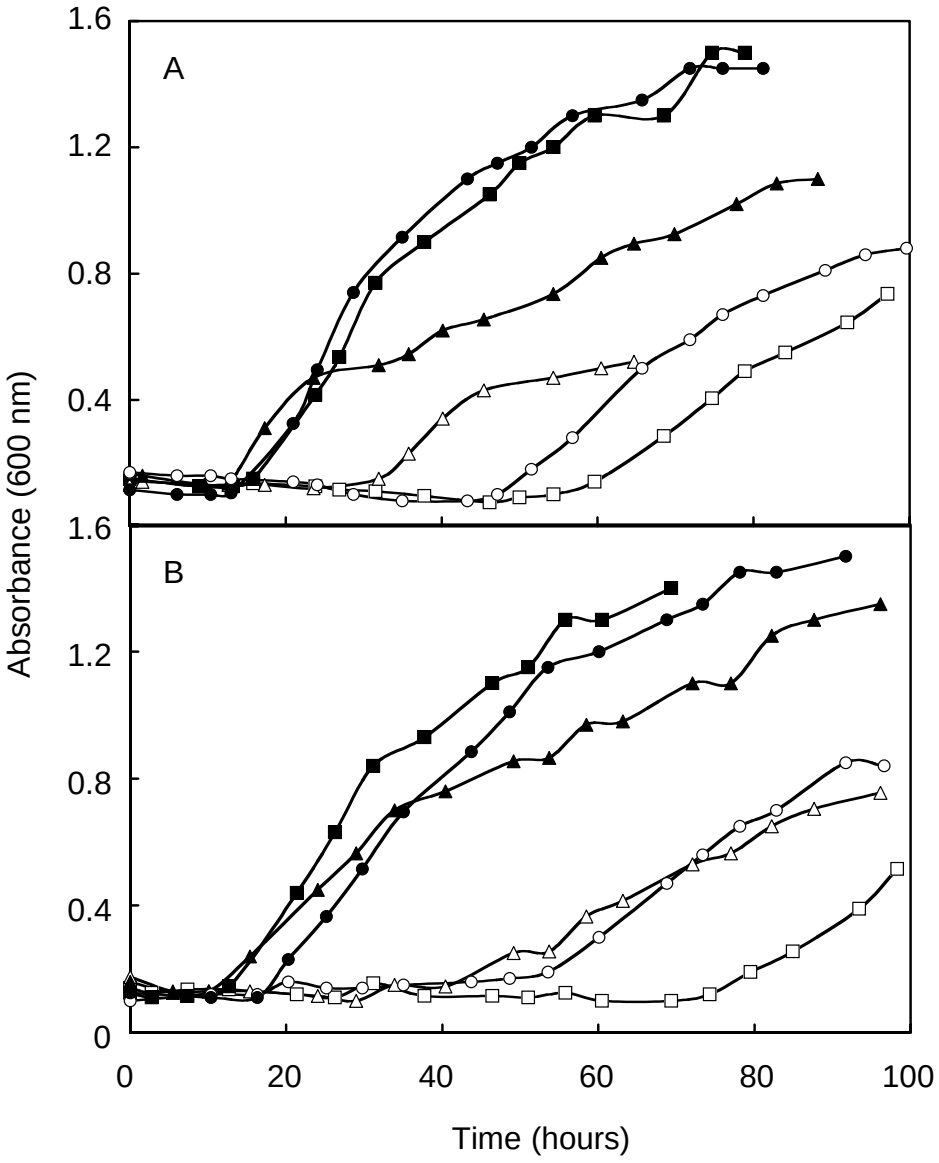
A
B
1.6
1.2
0.8
0.4
0
0
20
40
60
80
100
Absorbance (600 nm)
Time (hours)

Figure 3-5. Effects of aryl acids and aromatic amino acids on growth of *M. maripaludis* strains S2 and S965. Aryl acids (1 mM phenylacetate, indoleacetate and *p*-hydroxyphenylacetate) and aromatic amino acids (1 mM tyrosine, phenylalanine and tryptophan) were added to McA medium as indicated. Inocula were approximately 1.2 x 10^5 cells. A. Growth of wild type strain S2. ●, McCA medium; ▲, amino acids; ■, both amino acids and aryl acids; ◆, aryl acids; ○, McA. B. Growth of Δ*ehbN* strain S965. Media symbols are as indicated in A.

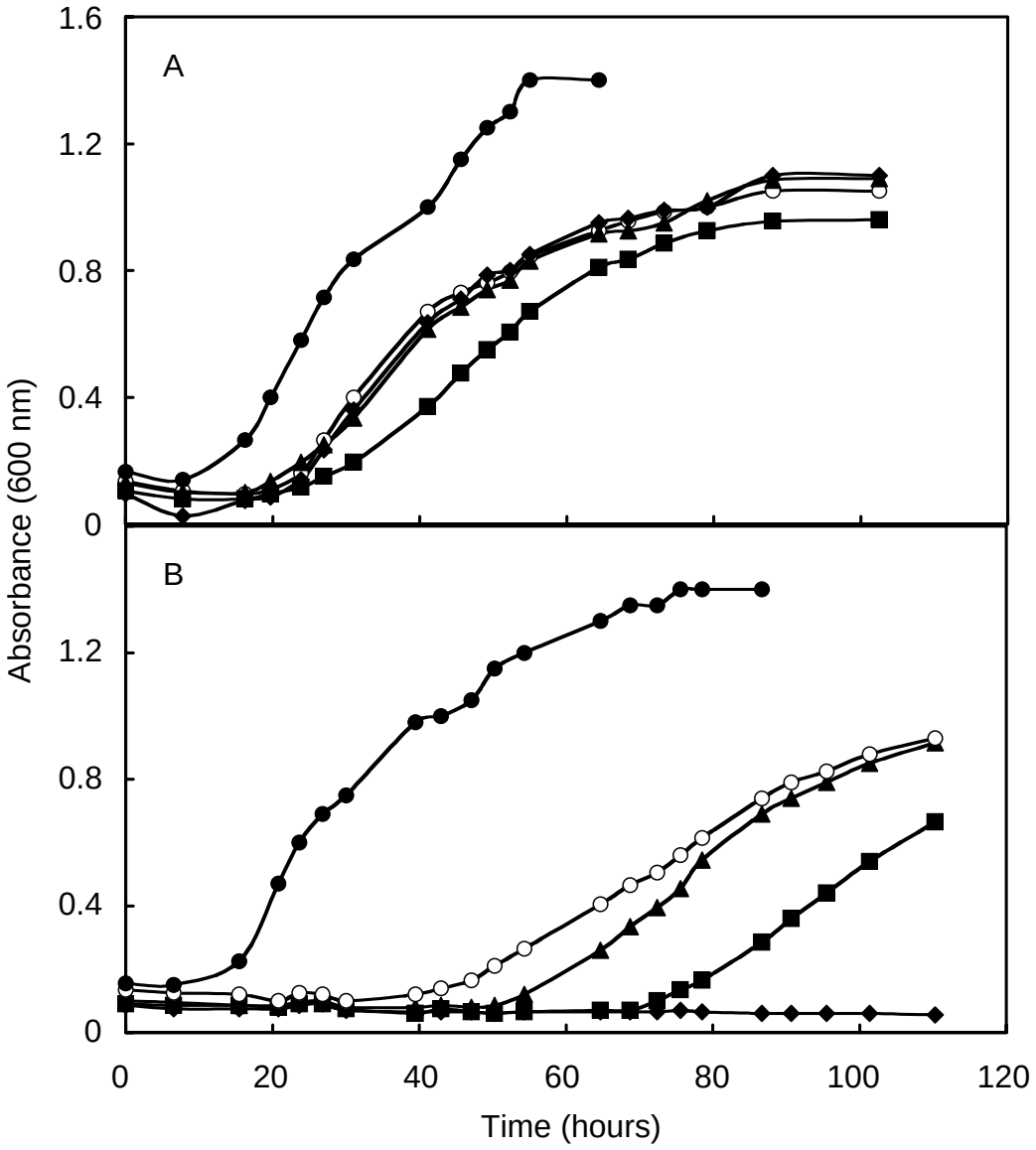
A
B
Absorbance (600 nm)
Time (hours)
0
0.4
0.8
1.2
1.6
0
20
40
60
80
100
120

CHAPTER 4

ELECTRON TRANSPORT FROM THE ENERGY CONSERVING HYDROGENASE B TO THE PYRUVATE OXIDOREDUCTASE IN *METHANOCOCCUS MARIPALUDIS*: CHARACTERIZATION OF RECOMBINANT HISTIDINE-TAGGED PORE AND PORF[3]

[3]Major, T.A. and W.B. Whitman. To be submitted to *J. Bacteriol*.

Abstract

The pyruvate oxidoreductase (Por) in *Methanococcus maripaludis* catalyzes the reductive carboxylation of acetyl-CoA for pyruvate biosynthesis. The *M. maripaludis* Por enzyme is unique in that a fifth polypeptide, PorE, copurifies with the Por complex (Lin, W. C., Y.-L. Yang, and W. B. Whitman. 2003. The anabolic pyruvate oxidoreductase from *Methanococcus maripaludis*. Arch. Microbiol. 179:444-456). The gene encoding the PorE was found in the *por* gene cluster, along with sixth open reading frame designated *porF*. These genes appear to encode ferredoxins. To characterize these proteins, recombinant 6x-histidine-tagged PorE and PorF were produced in *E. coli*. Attempts to purify natively-folded proteins were unsuccessful due to the formation of inclusion bodies. The histidine-tagged *porE* and *porF* were then cloned into the pMEV2 expression vector of *M. maripaludis* for expression in the proteins' native host. Due to the low levels of protein expression from this vector, it is unlikely that inclusion bodies are formed; however, too little protein is produced to be visible on SDS-PAGE gels.

The predicted role of the PorE and PorF ferredoxins is to shuttle low-potential electrons from the energy conserving hydrogenase B (Ehb) to the Por. To characterize the electron transport pathway between the Ehb and the PorE or PorF, two enzymatic assays were designed. The Δ*porEF* mutant strain JJ150 was used to generate a cell-free extract where the pyruvate-linked ferredoxin reduction assay could be tested with the recombinant proteins. Unfortunately, this mutant strain still had pyruvate-linked ferredoxin activity, suggesting that the Por utilizes iron-sulfur clusters to directly reduce the metronidazole dye used in this assay. A second assay that linked hydrogen-oxidation to ferredoxin activity was also unsuccessful, presumably because the membrane-bound hydrogenases contain Fe-S clusters that can directly reduce metronidazole.

Introduction

Electron transport is vital for respiration in any organism. Typically, electron transport chains in anaerobic prokaryotes are composed of quinones, cytochromes, ferredoxins, and flavodoxins. Methylotrophic methanogens utilize the quinone analog coenzyme F_{420}, cytochromes, ferredoxins and methanophenazine for electron transport (1, 9, 24, 25). The hydrogenotrophic methanogens, however, do not contain methanophenazine or cytochromes (10). Obviously, an electron transport chain is equally important in hydrogenotrophic methanogens as it is in any other organism. As the genomes of methanogens contain large numbers of ferredoxins and polyferredoxins, it would appear that the hydrogenotrophic methanogens must primarily utilize these proteins in their electron transport pathway (13).

In particular, carbon fixation in the hydrogenotrophic methanogens is a process requiring several reductive steps. One of the primary reactions requiring low-potential electrons is the reductive carboxylation of acetyl-CoA to pyruvate, which is performed by the pyruvate oxidoreductase (Por; 19). This reaction has a midpoint potential of the acetyl-CoA/pyruvate couple of approximately -500 mV under physiological conditions. Furthermore, the production of pyruvate by the Por is an energetically unfavorable reaction ($\Delta G' = +46.6$ kJ x mol^{-1}), requiring coupling to a proton motive force for pyruvate synthesis.

The pathway for coupling pyruvate production to low-potential electron generation and proton translocation was described in *Methanosarcina barkeri* (14). In this pathway, a membrane-bound hydrogenase designated Ech oxidizes hydrogen gas and uses energy in the proton motive force to generate low-potential electrons (14). An unidentified ferredoxin then shuttles these electrons to the Por (14). The hydrogenotrophic methanogens such as *M. maripaludis* also contain Ech, albeit two independent enzymes with remarkably different

operonic and subunit structure (7, 22). Results obtained with a mutant in one of the two *M. maripaludis* Ech operons (Ehb), determined that the carbon monoxide dehydrogenase/acetyl-CoA synthase (CODH/ACS) and the Por are both coupled to the Ehb (16).

Unlike in *M. barkeri*, it is more obvious in *M. maripaludis* which ferredoxins shuttle electrons from the Ehb to the Por. The purified Por of *M. maripaludis* contains a fifth polypeptide (PorE) whose corresponding gene was found in the *por* gene cluster (11). Further sequencing of the *por* operon identified a sixth open reading frame designated *porF* (11). The *porE* and *porF* genes contain $CX_2CX_2CX_3C$ amino acid motifs for binding 4Fe-4S clusters (11). To identify whether the *porE* and *porF* are required for Por activity, deletions of the *porEF* genes were made (12). The PorEF mutant displayed a growth deficiency in mineral medium or mineral medium containing acetate (12). Furthermore, pyruvate-dependent methanogenesis activity was inhibited; however, the methylviologen-dependent pyruvate oxidation activity was not affected in the mutants (12). These results suggest that the PorE and PorF proteins are not directly involved in the production of pyruvate but are involved in electron transport for the Por enzyme.

In order to better characterize the PorE and PorF proteins, recombinant histidine-tagged PorE and PorF were expressed in *E. coli*. Expression in *E. coli* was used for ease of production and purification of large quantities of protein. Assays were also designed to prove that the Ehb, Por and PorE and PorF are linked, as well as to characterize the electron transport between these systems.

Materials and methods

Bacterial strains, plamids, media and culture conditions. All bacterial strains and plasmids are listed in Table 4-1.

Methanococcus maripaludis strains were grown in 28 ml anaerobic culture tubes under 275 kPa H_2:CO_2 gas (80:20, v/v) at 37 °C as described in Jones *et al*. (8) and Whitman *et al*. (26). Media varied from the mineral medium (McN) of Jones *et al*. (8) by the following additions: 0.2 % Casamino acids, 10 mM sodium acetate, 1 % (v/v) vitamin mixture (26), McCAV; the above additions plus 0.2 % yeast extract, McYCAV. In some cases, neomycin was added at the concentration of 500 μg ml^{-1} in plates and 1000 μg ml^{-1} in broth.

Escherichia coli M15 and TOP10 were grown at 37 °C on low salt Luria-Bertani (LB) medium as described in the Invitrogen TA TOPO handbook (Carlsbad, CA). In one experiment, 0, 50, 200, 500, and 1000 mM glycyl-glycine was added to the Luria-Bertani medium, as described by Ghosh *et al*. (6). For anaerobic growth, LB was supplemented with 1 % glucose, 40 mM sodium fumarate, 100 μM $Fe(NH_4)_2(SO_4)_2$ and 200 μM Na_2S, as described by Gencic and Grahame (5). Kanamycin (50 μg ml^{-1}) and ampicillin (75 μg ml^{-1}) was added to M15 cultures, and ampicillin was added to media with TOP10 containing pMEV2.

Growth of *M. maripaludis* was monitored at 600 nm using a Spectronic 20 spectrophotometer (Bausch and Lomb, New York).

Transformations. *E. coli* was transformed by electroporation as described by Lin and Whitman (12). *M. maripaludis* was transformed by the polyethylene glycol method (23).

Construction of plasmids. The genes *porE* and *porF* were amplified from *M. maripaludis* S2 genomic DNA. Primers for amplification are listed in Table 4-2. The pQE2 vector (Qiagen, Valencia, CA) was used for *E. coli* protein expression. This vector contains an N-terminal

polyhistidine tag that can be removed after protein purification. Protein expression is controlled by the T5 promoter and two *lac* operator sequences for *lac* repressor binding. Primers for *porE* and *porF* amplification were designed including a 5' *Nde*I site and a 3' *Pst*I site for insertion into the pQE2 vector. PuReTaq Ready-To-Go PCR Beads (Amersham Biosciences, Piscataway, NJ) were utilized for DNA amplification as described in the manufacturer's instructions. Amplification of *porE* and *porF* was performed via polymerase chain reaction using the following program: 94 °C for five minutes, then 30 cycles of 94 °C for 30 seconds; 60 °C for 30 seconds, with a 0.5 °C decrease in temperature per cycle and an 8 °C gradient; 72 °C for 1.5 min, with a 0.3 °C temperature decrease per cycle and an 8 °C gradient. A final extention time of 65 °C for 7 minutes was included. PCR amplicons were subcloned into the TA TOPO vector according to the manufacturers instructions (Invitrogen, Carlsbad, CA), and *E. coli* TOP10 was used as a host for this plasmid. Colonies were selected by the blue/white screen as described in the TA TOPO instruction manual. Plasmids were gel extracted using the QIAquick gel extraction kit (Qiagen, Valencia, CA). The pQE2 vector and the plasmid containing the PCR products were digested with *Nde*I and *Pst*I and gel purified using the Qia kit (Qiagen, Valencia, CA). Ligations were perfomed using T4 DNA ligase (Promega, Madison, WI) in an overnight incubation at 14 °C.

The expression vector pMEV2 was utilized for histidine-tagged *porE* and *porF* expression in *M. maripaludis*. This vector contains a neomycin cassette for neomycin resistance in *M. maripaludis* and a *bla* gene for ampicillin resistance in *E. coli*. The N-terminally his-tagged *porE* and *porF* genes contained in the pQE2 vectors were amplified for cloning the his-tagged *porE* and *porF* into pMEV2. Primers for this PCR amplification contained the *Nsi*I and *Bgl*II restriction sites for insertion into pMEV2. Plasmids for production of C-terminally

histidine-tagged PorE and PorF were also designed. The 3' primers CporE3' and CporF3' contained six histidine codons and a stop codon upstream of the *Bgl*II restriction site. *M. maripaludis* genomic DNA was amplified to generate the C-terminally his-tagged *porE* and *porF*. Amplification was performed using Herculase Enhanced Polymerase (Stratagene, La Jolla, CA). PCR samples were aliquotted into three tubes, which were amplified (using the gradient function of the thermocycler) at different temperatures within the thermocycler. The cycling program proceeded as follows. To begin, there was a 1 min denaturation at 92 °C. The following steps were performed for 15 cycles. First, a denaturation step was performed at 92 °C for 30 seconds. Second, a gradient extenstion step of 45-55 °C was performed for 30 s with an increase of 1 °C per cycle (such that during the first cycle one tube was incubaed at 45 °C, one tube was incubated at 50 °C and one tube was incubated at 55 °C; during the second cycle, the tubes were at incubated at 46 °C, 51 °C, and 56 °C, etc.). Third, a gradient annealing step was performed at 60-70 °C for 1 min with an increase of 0.5 °C per cycle (where during the first cycle the tubes were incubated at 60 °C, 65 °C, and 70 °C, respectively; during the second cycle the tubes were incubated at 60.5 °C, 65.5 °C, and 70.5 °C; etc.). The first 15 cycles were immediately followed by a second round of 25 cycles (for a total program of 40 cycles). The second round of 25 cycles included a denaturation step at 92 °C for 30 s, which was followed by an extension step for 30 s at 52 °C. Finally, a gradient annealing step was performed at 63-73 °C for 1 min with a 10 s increase in duration per cycle (such that the tubes were incubated at 63 °C, 68 °C, and 73 °C during every cycle but the incubation was 1 minute during the first cycle, 1 min, 10 s during the second cycle, etc.). All other cloning procedures were performed as described above.

Induction of recombinant protein production and preparation of cell-free extracts. *E. coli* M15E or M15F cultures were inoculated into 5 ml cultures for overnight growth at 37 °C. Under aerobic conditions, a 100 ml culture was started with the overnight culture and allowed to grow until the optical density (600 nm) reached approximately 0.6. Different growth temperatures were tried in order to optimize soluble protein production, including 16 °C, 20 °C, room temperature (approximately 24 °C), 31 °C and 37 °C. Cultures were then induced with 1 mM isopropyl-beta-D-thiogalactopyranoside (IPTG), and 100 μM $Fe(NH_4)_2(SO_4)_2$ was added to the culture. Lower concentrations of IPTG (0.1 mM, 0.5 mM) were used in later experiments in order to moderate protein production. Cultures were allowed to grow for approximately 4-5 hours and were harvested by centrifugation at 4,000 x g for 15 minutes. Cultures were either frozen at -20 °C or -70 °C or were immediately used for analysis.

Several different buffers were used to resuspend the *E. coli* cells. For purification under denaturing conditions, cells were resuspended in 400 μl of Buffer B: 100 mM NaH_2PO_4, 10 mM Tris-Cl, 8 M urea, pH 8.0. For native purification, cells were resuspended in a Lysis Buffer composed of 50 mM NaH_2PO_4, 300 mM NaCl, and 10 mM imidazole, pH 8.0, as described in the QIA*expressionist* 6xHis-tagged protein expression and purification handbook (Qiagen, Valencia, CA). Other buffers used included a buffer containing 20 mM Tris-HCl, pH 7.4, 10 % (v/v) glycerol, 1 mM dithiothreitol (DTT), 0.5 mM phenylmethylsulfonylfluoride (PMSF), 0.1 % Triton X-100, 0.1 mg/ml lysozyme, 10 mM β-mercaptoethanol, containing either 0, 50 or 300 mM NaCl or 50 or 300 mM KCl. Another buffer tried contained 50 mM Tris-Cl (pH 8.0), 10 mM DTT, 10 mM β-mercaptoethanol, 0.5 mM PMSF and either 30 % (v/v) glycerol, 30 % (v/v) ethylene glycol, 30 % (w/v) ammonium sulfate, or 50 % methanol.

Cells were broken either through sonication or via French press. For sonication, cells were incubated on ice for 30 minutes with 1 mg ml^{-1} lysozyme and then sonicated six times for ten seconds with a 30 second cooling period between bursts. Under French press, cells were broken under 20,000 lb x in^2 pressure at 4 °C. Cells were pelleted in a microcentrifuge at maximum speed for 20 minutes, and the supernatant was saved for protein purification.

For anaerobic *E. coli* growth, one ml of an overnight culture was inoculated into an anaerobic 100 ml flask of medium and allowed to grow at 31 °C until the optical density (600 nm) reached approximately 0.7. IPTG, 0.4 mM, was added, along with the iron, for induction of protein production. After 5 hours (optical density around 2.0) cells were harvested anaerobically. Cells were resuspended in 1 ml of a nitrogen-sparged "POR buffer" composed of 20 mM potassium Tricine, pH 8.6, 5 mM $MgCl_2$, 0.1 mM thiamine pyrophosphate (TPP), 0.5 mM DTT, and 10% (v/v) glycerol (11). Resuspended cells were then passed through a French press as described above under anaerobic conditions at room temperature.

Purification of histidine-tagged proteins. E. coli containing recombinant his-tagged PorE and PorF were purified using the Qiagen Ni-NTA Spin Kit per the manufacturer's instructions (Valencia, CA). Under denaturing conditions, cell-free extracts were washed and eluted with buffers of the same chemical composition of Buffer B except the pH was adjusted to 6.3, 5.9, and 4.5. Under native conditions, cell-free extracts were washed with a buffer containing 50 mM NaH_2PO_4, 300 mM NaCl and 20 mM imidazole, pH 8.0. The elution buffer was composed of 50 mM NaH_2PO_4, 300 mM NaCl, and 250 mM imidazole, pH 8.0.

SDS-PAGE or native PAGE. Polyacrylimide gel electrophoresis (PAGE) was performed as described in Sambrook and Russell (18). Ready Gel Tris-HCl 4-20% or 15% (Biorad, Hercules, CA) precast gels were used.

Purification of membrane fractions for hydrogenase-linked activity assays. *M. maripaludis* cultures (200 ml) were grown to a final density of approximately 0.4-0.5 (mid-exponential phase) in McCA medium in 1 L bottles. Cells were harvested by centrifugation at 5,000 x g for 20 minutes at 4 °C. Cell pellets were frozen at -20 °C for one hour to lyse the cells. The pellets were resuspended in 11 ml of POR buffer. An aliquot (1 ml) of the supernatant was reserved for enzyme activity and protein concentration, while the other approximately 10 ml was centrifuged at 10,000 x g for 30 minutes at 4 °C to remove whole cells. An aliquot of the supernatant was reserved, and the other approximately 9 ml was centrifuged at 150,000 x g for 2 hours at 4 °C to further purify the membranes. The pellet was resuspended in 3 ml of POR buffer.

Preparation of supernatant fractions. Supernatant fractions were separated on a 10 ml capacity Sephadex G-50 column (Sigma-Aldrich, St. Louis, MO) in a Coy anaerobic chamber (Grass Lake, MI). The column was prepared by autoclaving 1.5 g resin in a dry cycle for 30 minutes. Resin was taken inside the chamber, along with nitrogen-sparged Por buffer excluding TPP and DTT and solid sucrose. Resin was allowed to swell overnight in 15 ml Por buffer minus TPP and DTT and then was packed into a 1 cm diameter column. Sucrose (0.1 g) was added to the cell-free extract derived from a 100 ml culture of JJ150 or S2, and was subsequently loaded onto the column. Por buffer including TPP and DTT was used to elute the proteins. Fractions were taken at one milliliter intervals.

Enzymatic assays. All enzyme assays were performed under strictly anaerobic conditions. Ferredoxin assays with hydrogen as electron donor were performed as described in Chen and Blanchard (2) using metronidazole as an electron acceptor. Ferredoxin assays with pyruvate as electron donor were performed as described by George and Smibert (4). These

assays monitor the spectrophotometric reduction of metronidazole at 320 nm. Units are recorded in μmol x (min x mg)$^{-1}$.

Pyruvate oxidoreductase and hydrogenase activities were monitored through the spectrophotometric reduction of methylviologen at 603 nm. The pyruvate oxidation reaction was performed as described in Shieh and Whitman (19), while the hydrogenase assay was performed as in Ragsdale and Ljungdahl (17).

Results and Discussion

Purification of recombinant PorE and PorF. Initial attempts to express and purify recombinant histidine-tagged PorE and PorF were performed using the protocols provided in the Qiagen Qia*expressionist* manual. The *porE* and *porF* genes were cloned and inserted into the Qiagen TAGZyme vector pQE2, which yields an N-terminal his-tag on the proteins of interest. This vector was chosen because the histidine tag could later be cleaved from PorE and PorF after purification using the Qiagen TAGZyme System (Valencia, CA). The expression of the *porE* and *porF* genes was verified by lysing the cells under denaturing conditions and electrophoresing the cell-free extract on an SDS-PAGE gel (Figure 4-1). Denaturing the cell-free extract clearly demonstrates that a large quantity of protein corresponding to the predicted sizes of the histidine tagged PorE and PorF was produced in *E. coli*. Furthermore, induced *E. coli* strains M13E and M13F were brown, whereas uninduced M13E or M13F were off-white. As Fe-S clusters are brown in color, it seems likely that the expressed PorE and PorF proteins contained Fe-S clusters.

As it is necessary to purify protein in its native conformation in order to retain enzymatic activity, subsequent purification was performed under non-denaturing conditions. Native purification using the methods described both in the Qia*expressionist* handbook and in

Sambrook and Russell (18) and subsequent purification using the Ni-NTA Spin Column Kit (Qiagen, Valencia, CA) did not yield his-tagged proteins (data not shown). The pellets generated from centifugation of the cell-free extracts were brown, suggesting that the recombinant Fe-S-containing proteins were not soluble. In one experiment, pellets were resuspended and centrifuged at 60%, 50%, and 35% of the maximum speed of the microcentrifuge (Figure 4-2). Under these conditions, little of the pellet formed as the centrifugation was insufficient to sediment the proteins. As seen in Figure 4-2, particularly in the M15E samples (lanes 3, 6, and 9), the band corresponding to PorE increases significantly as the protein pellet is less sedimented. The M15F samples yielded very little pellet under these conditions, which may explain why the band corresponding to PorF is visible in all three lanes (4, 7, and 10). These results strongly suggest that the recombinant PorE and PorF were forming inclusion bodies.

In order to be purified on either Ni-NTA Spin Columns (Qiagen, Valencia, CA) or on Ni-NTA (nickel-nitrilotriacetic acid) resin columns, the recombinant proteins must be soluble. Therefore, a variety of methods were performed to produce soluble PorE and PorF in a native conformation. First, media conditions were varied. Luria-Bertani broth was the standard medium used, with 5 μM $Fe(NH_4)_2(SO_4)_2$ added to provide iron and sulfur for 4Fe-4S cluster formation. In some cultures, glucose was added to the medium, as described in Sambrook and Russell (18). Glycylglycine was also added to medium in one experiment, as described by Ghosh *et al*. (6). *E. coli* was grown anaerobically as described by Gencic and Grahame (5). None of the media conditions affected the solubility of the recombinant proteins. Next, protein expression conditions were varied, such that less of the recombinant proteins were produced. The incubation temperature was varied from 37 °C to 16 °C, where most cultures were

incubated at 20 °C. Various concentrations of IPTG (used to induce recombinant protein production) were used in order to decrease the amount of recombinant PorE and PorF produced. Although less protein was produced, PorE and PorF were not soluble.

Another technique that was tried was based on the success of Nakamura *et al.* (15). In that work, ferredoxins of interest were coexpressed with the *isc* operon, which encodes the iron-sulfur cluster biosynthesis proteins (15). The production of five reporter holo-ferredoxins was increased due to the coexpression of the *isc* gene cluster (15). If PorE and PorF formed apo-ferredoxins that were misfolding due to the lack of Fe-S clusters, the co-expression of the Isc or Suf Fe-S cluster biosynthesis proteins should form holo-PorE and holo-PorF. Plasmids containing the *isc* and *suf* operons (pRKISC and pRKSUF017) were transformed to the *E. coli* hosts. These two operons encode proteins that assemble iron-sulfur clusters in a large number of ferredoxins (20, 21.) Although transformation of the Isc and Suf plasmids along with the pQE2 vectors was successful, the coexpression of these genes did not produce soluble recombinant PorE or PorF, suggesting that apo-protein production was not the cause of inclusion body formation.

Finally, the cell extracts were prepared using a variety of methods. Several methods were used to lyse cells, including lysozyme treatment, French press, and sonication. Most purifications were performed using sonication because that technique was recommended in the Qia*expressionist* handbook; however, there was no apparent difference with respect to solubility regardless of the lysis method used. In addition, a variety of buffers were used to resuspend the cell-free extract. First, the buffers used were those recommended in the QIA*expressionist* handbook. Subsequent buffers included the Por buffer used for purification of the Por native enzyme (11); buffers with various salt concentrations; the addition of DTT or β-

mercaptoethanol; the addition of the protease inhibitor PMSF; utilization of Triton X-100 to partially solubilize proteins; and the addition of ethylene glycol, glycerol, ammonium sulfate, or methanol in order to produce soluble proteins. The recombinant PorE and PorF proteins were not soluble using any of these buffers.

As purification of the histidine-tagged PorE and PorF expressed in *E. coli* was unsuccessful, it was decided to express the his-tagged proteins in *Methanococcus maripaludis*. There are several reasons to use the *M. maripaludis* as a vector for the histidine-tagged *porE* and *porF* expression. First, in the complementation of the Δ*porEF* strain JJ150, it was clear that the *porE* and *porF* genes encoded on the pMEV2 vector were expressed as growth and enzymatic defects were rescued (12). Second, the expression system in *M. maripaludis* maximally produces 1-2% of the total protein in the cell (3). At low levels of expression, inclusion bodies may not form. Third, any necessary chaperones or iron-sulfur insertion proteins necessary for PorE and PorF production would be present in *M. maripaludis*. Thus, the *porE* and *porF* genes were cloned into the pMEV2 vector. To generate *porE* and *porF* with N-terminal histidine tags, the pQE2+porE and pQE2+porF plasmids were used as a template for amplification of the pMEV2+porE and pMEV2+porF constructs. To generate C-terminal histidine-tagged PorE and PorF, 3'-primers were designed that contained the reverse complemented histidine codons. Therefore, amplification of the *porE* and *porF* genes directly from *M. maripaludis* included six histidine codons at the C-terminus of the genes. SDS-PAGE gels did not conclusively demonstrate whether or not histidine-tagged PorE and PorF were produced in *M. maripaludis*. In fact, the low level of protein expression from these vectors is not necessarily sufficient for visible bands on an SDS-PAGE gel. Western blotting using anti-histidine tag antibodies should be used to determine whether the PorE and PorF proteins are expressed.

Enzyme assays. The pyruvate oxidation (Por) activity in JJ150 (Δ*porEF*) cell-free extract was analyzed by Lin and Whitman (12). No significant difference was found in Por activity between the wild type (JJ) and the JJ150 strains (12). In this work, attempts were made to characterize the pyruvate-linked ferredoxin activity using metronidazole as the final electron acceptor. The PorE and PorF proteins are predicted to be ferredoxins that are associated with the Por enzyme (11). Physiologically, electrons are predicted to be carried by the PorE or PorF to the Por for pyruvate biosynthesis. In cell-free extracts, it is predicted that the Por can shuttle electrons yielded from pyruvate oxidation to the PorE or PorF, and thus, to metronidazole. Thus, the JJ150 strain, which lacks PorE and PorF, should have no pyruvate-linked ferredoxin activity. Subsequent addition of purified his-tagged PorE or PorF to the JJ150 cell-free extract could then be assayed. Unfortunately, the pyruvate-linked ferredoxin (metronidazole-reduction) activity is similar between the JJ150 and the wild type S2 strains (Table 4-3). One explanation may be that the PorABCD complex of *M. maripaludis* contains three cysteinyl motifs characteristic of 4Fe-4S clusters (11). In the metronidazole assay, ferredoxins donate electrons to the metronidazole dye. If the Por is capable of directly donating electrons from the Fe-S clusters to the dye, the metronidazole assay will not be specific for PorE or PorF activity. Another possibility is that non-specific ferredoxins were carrying electrons from the Por to the metronidazole. In case non-specific ferredoxins were binding to the Por, an anaerobic size exclusion purification of the cell-free extract was performed. Weakly associated proteins should be separated, as should the large and small proteins. The Por activity was found primarily in the early fractions. Qualitatively, in assays performed with JJ150 extract, early fractions containing Por activity did not contain pyruvate-linked ferredoxin reduction activity. The addition of later fractions, which contain smaller molecules, did cause the reduction of the metronidazole dye. In assays performed with

S2 extract, the Por and metronidazole activities were found in the same extracts, which is expected as the PorE and PorF are available. Unfortunately, the pyruvate-linked ferredoxin assay did not provide a linear reduction of metronidazole with which to accurately calculate activity. Furthermore, reproducible results were not obtained either with cell-free extract or fractions separated by size exclusion chromatography. Often, no pyruvate-linked ferredoxin activity was found, despite that pyruvate-linked methylviologen reduction (Por) activity was present. The presence of Por activity suggests that the cell extract had not been oxidized. Thus, the pyruvate-ferredoxin assay was not useful in monitoring PorE or PorF activity.

A second metronidazole-based assay was attempted to characterize the interaction between the PorE or PorF and the Ehb. Here, the hydrogenase-linked ferredoxin assay was used to monitor membrane-bound hydrogen oxidation coupled to ferredoxin reduction and subsequent metronidazole reduction. The membrane-bound proteins were separated from soluble proteins using an ultracentrifugation step. It was believed that this step would separate weakly-bound proteins from the membranes. Table 4-4 shows one experiment where the membrane-associated hydrogenase-ferredoxin activities were analyzed in wild type S2 extract. From this work, it would appear that both soluble and membrane-bound hydrogenases link hydrogen oxidation to ferredoxin reduction. However, it also appears that the membrane-bound hydrogenases can directly reduce the metronidazole dye, whether directly from ferredoxin or polyferredoxin subunits or from electron-shuttling ferredoxins that are tightly associated with the hydrogenases. The combination of the high speed supernatant to the high speed pellet fractions did not substantially affect the metronidazole activity (data not shown). Furthermore, many of the same difficulties were found with this assay that were problematic with the pyruvate-linked ferredoxin assay, such as irreproducibility and that the assay was not specific to the PorE and PorF proteins.

Conclusions

The focus of this work was to characterize the PorE and PorF proteins and the interactions between the PorE and PorF and the pyruvate oxidoreductase enzyme and the energy conserving hydrogenase b. Several attempts were made to produce soluble histidine-tagged PorE and PorF in *E. coli* using a variety of expression and protein purification strategies. Unfortunately, *E. coli* appears to overproduce these proteins and generate inclusion bodies, from which it is difficult to purify the proteins via Ni-NTA resin. Plasmids encoding histidine-tagged *porE* and *porF* were cloned into *M. maripaludis* to generate soluble proteins. Whether N- or C-terminal his-tagged PorE and PorF are produced in *M. maripaludis* has not been conclusively determined. Furthermore, attempts to develop specific assays between the PorE and PorF and the Por and the Ehb were made. Unfortunately, it would appear that the metronidazole dye is too fickle to be used to characterize the PorE and PorF electron transport. Perhaps a different chemical for assaying the reduction of ferredoxins will be identified, which will provide a quantitative analysis of the Por-ferredoxin or Ehb-ferredoxin reduction activity. Future work may involve the analysis of the histidine-tagged PorE and PorF derived from plasmid-based expression in *M. maripaludis* by Western blotting. Large-scale cultures of *M. maripaludis* can be used to produce sufficient quantities of protein for purification and characterization. Soluble proteins would be purified using Ni-NTA resin. Several techniques could then be utilized for analyzing the purified PorE and PorF proteins, including metal analysis, characterization of the Fe-S clusters by electron paramagnetic resonance spectrometry, and X-ray crystallography.

Acknowledgments

The authors would like to thank Yasuhiro Takahasi for his generous donation of the pRKSUF017, pRKISC and pRKNMC plasmids. This project was funded through a grant from the US Department of Energy.

References

1. **Abken, H. J., M. Tietze, J. Brodersen, S. Bäumer, U. Beifuss, and U. Deppenmeier.** 1998. Isolation and characterization of methanophenazine and funciton of phenazines in membrane-bound electron transport of *Methanosarcina mazei* Gö1. J. Bacteriol. **180:**2027-2032.

2. **Chen, J.-S., and D. K. Blanchard.** 1979. A simple hydrogenase-lined assay for ferredoxin and flavodoxin. Anal. Biochem. **93:**216-222.

3. **Gardner, W. L., and W. B. Whitman.** 1999. Expression vectors for *Methanococcus maripaludis*: overexpression of acetohydroxyacid synthase and β-galactosidase. Genetics **152:**1439-1447.

4. **George, H. A. and R. M. Smibert.** 1982. Pyruvate oxidation by the Reiter strain of *Treponema phagedenis*. J. Bacteriol. **152:**1060-1065.

5. **Gencic, S., and D. A. Graham.** 2003. Nickel in subunit β of the acetyl-CoA decarbonylase/synthase multienzyme complex in methanogens. Catalytic properties and evidence for a binuclear Ni-Ni site. J. Biol. Chem. **278:**6101-6110.

6. **Ghosh, S., S. Rasheedi, S. S. Rahim, S. Banerjee, R. K. Choudhary, P. Chakhaiyar, N. Z. Ehtesham, S. Mukhopadhyay, and S. E. Hasnain.** 2004. Method for enhancing solubility of the expressed recombinant proteins in *Escherichia coli*. Biotechniques **37:**418, 420, 422-423.

7. **Hendrickson, E. L., R. Kaul, Y. Zhou, D. Bovee, P. Chapman, J. Chung, E. Conway de Macario, J. A. Dodsworth, W. Gillett, D. E. Graham, M. Hackett, A. K. Haydock, A. Kang, M. L. Land, R. Levy, T. J. Lie, T. A. Major, B. C. Moore, I. Porat, A. Palmeiri, G. Rouse, C. Saenphimmachak, D. Söll, S. Van Dien, T. Wang, W. B. Whitman, Q. Xia, Y. Zhang, F. W. Larimer, M. V. Olson, and J. A. Leigh.** 2004. Complete genome sequence of the genetically tractable hydrogenotrophic methanogen *Methanococcus maripaludis*. J. Bacteriol. **186:**6956-6969.

8. **Jones, W. J., M. J. B. Paynter, and R. Gupta.** 1983. Characterization of *Methanococcus maripaludis* sp. nov., a new methanogen isolated from salt marsh sediment. Arch. Microbiol. **135:**91-97.

9. **Kühn, W., K. Fiebig, R. Walther, and G. Gottschalk.** 1979. Presence of a cytochrome b_{559} in *Methanosarcina* species. FEMS Lett. **105:**271-274.

10. **Kühn, W., and G. Gottschalk.** 1983. Characterization of the cytochromes occurring in *Methanosarcina* species. Eur. J. Biochem. **135:**89-94.

11. **Lin, W. C., Y.-L. Yang, and W. B. Whitman.** 2003. The anabolic pyruvate oxidoreductase from *Methanococcus maripaludis*. Arch. Microbiol. **179:**444-456.

12. **Lin, W., and W. B. Whitman.** 2004. The importance of *porE* and *porF* in the anabolic pyruvate oxidoreductase of *Methanococcus maripaludis*. Arch. Microbiol. **181:**68-73.

13. **Major, T. A., H. Burd, and W. B. Whitman.** 2004. Abundance of 4Fe-4S motifs in the genomes of methanogens and other prokaryotes. FEMS Microbiol. Lett. **239**:117-123.

14. **Meuer, J., H. C. Kuettner, J. K. Zhang, R. Hedderich, and W. W. Metcalf.** 2002. Genetic analysis of the archaeon *Methansarcina barkeri* fusaro reveals a central role for Ech hydrogenase and ferredoxin in methanogenesis and carbon fixation. Proc. Natl. Acad. Sci. USA **99:**5632-5637.

15. **Nakamura, M., K. Saeki, and Y. Takahashi.** 1999. Hyperproduction of recombinant ferredoxins in *Escherhcia coli* by coexpression of the ORF1-ORF2-*iscS-iscU-iscA-hscB-hscA-fdx*-ORF3 gene cluster. J. Biochem. **126:**10-18.

16. **Porat, I., W. Kim, E. L. Hendrickson, Q. Xia, Y. Zhang, T. Wang, F. Taub, B.C. Moore, I. J. Anderson, M. Hackett, J. A. Leigh, and W. B. Whitman.** 2006. Disruption of the operon encoding Ehb hydrogenase limits anabolic CO_2 assimilation in the archaeon *Methanococcus maripaludis*. J. Bacteriol. **188:**1373-1380.

17. **Ragsdale, S. W., and L. G. Ljungdahl.** 1984. Hydrogenase from *Acetobacterium woodii*. Arch. Microbiol. **139:**361-365.

18. **Sambrook, J., and S. W. Russell.** 2001. Molecular Cloning: A Laboratory Manual. 3rd edition. Cold Spring Harbor Laboratory Press, Cold Spring Harbor, New York.

19. **Shieh, J., and W. B. Whitman.** 1988. Autotrophic acetyl coenzyme A biosynthesis in *Methanococcus maripaludis*. J. Bacteriol. **170:**3072-3079.

20. **Takahashi, Y., and M. Nakamura.** 1999. Functional assignment of the ORF2-iscS-iscU-iscA-hscB-hscA-fdx-ORF3 gene cluster involved in the assembly of Fe-S clusters in Escherichia coli. J. Biochem. **126:**917-926.

21. **Takahashi, Y., and U. Tokumoto.** 2002. A third bacterial system for the assembly of iron-sulfur clusters with homologs in archaea and plastids. J. Biol. Chem. **277:**28380-28383.

22. **Tersteegen, A., and R. Hedderich.** 1999. *Methanobacterium thermoautotrophicum* encodes two multisubunit membrane-bound [NiFe] hydrogenases. Eur. J. Biochem. **264:**930-943.

23. **Tumbula, D. L, R. A. Makula, and W. B. Whitman.** 1994. Transformation of *Methanococcus maripaludis* and identification of a *Pst*I-like restriction system. FEMS Microbiol. Lett. **121:**309-314.

24. **Tzeng, S. F., R. S. Wolfe, and M. P. Bryant.** 1975. Factor 420-dependent pyridine nucleotide-linked hydrogenase system of *Methanobacterium ruminantium*. J. Bacteriol. **121:**184-191.

25. **Tzeng, S. F., R. S. Wolfe, and M. P. Bryant.** 1975. Factor 420-dependent pyridine nucleotide-linked formate metabolism of *Methanobacterium ruminantium*. J. Bacteriol. **121:**192-196.

26. **Whitman, W. B., J. S. Sheih, S. H. Sohn, D. S. Caras, and U. Premachandran.** 1986. Isolation and characterization of 22 mesophilic methanococci. System. Appl. Microbiol. **7:**235-240.

Table 1. Bacterial strains and plasmids.

Bacterial strain or plasmid	Genotype or description	Source or reference
M. maripaludis		
JJ150	Δ*porEF*::*pac*	(12)
S2	Wild type	(26)
S220	S2 containing pMEV2+Nhis-*porE*	This work
S221	S2 containing pMEV2+Nhis-*porF*	This work
S222	S2 containing pMEV2+Chis-*porE*	This work
S223	S2 containing pMEV2+Chis-*porF*	This work
E. coli		
M15	F$^-$ *lac ara gal mtl recA*	Qiagen
M15 -pQE2	M15 containing pQE2	This work
M15E	M15 containing pQE2+*porE*	This work
M15F	M15 containing pQE2+*porF*	This work
M15-isc-pQE2	M15 containing pQE2 and pRKISC	This work
M15E-isc	M15 containing pQE2+*porE* and pRKISC	This work
M15F-isc	M15 containing pQE2+*porF* and pRKISC	This work
M15-suf-pQE2	M15 containing pQE2 and pRKSUF017	This work
M15E-suf	M15 containing pQE2+*porE* and pRKSUF017	This work
M15F-suf	M15 containing pQE2+*porF* and pRKSUF017	This work
TOP10	F$^-$ *mcrA* Δ(*mrr-hsdRMS-mcrBC*) Φ80*lacZ*Δ*M15* Δ*lacX74 recA1 deoR araD139* Δ(*ara-leu*)*7697 galU galK rpsL* (Str^r) *end A1 nupG*	Invitrogen
Plasmids		
pQE2	6x histidine-tagging expression vector for *E. coli*	Qiagen
pQE2+*porE*	pQE2 with N-terminal histidine-tagged *porE*	This work
pQE2+*porF*	pQE2 with N-terminal histidine-tagged *porF*	This work
pMEV2	Neo^R shuttle vector for *M. maripaludis*	(12)
pMEV2+Nhis-*porE*	pMEV2 with N-terminal histidine-tagged *porE*	This work
pMEV2+Nhis-*porF*	pMEV2 with N-terminal histidine-tagged *porF*	This work
pMEV2+Chis-*porE*	pMEV2 with C-terminal histidine-tagged *porE*	This work
pMEV2+Chis-*porF*	pMEV2 with C-terminal histidine-tagged *porF*	This work
pRKSUF017	Tc^r, low copy number vector containing *sufABCDSE ynhG* genes	(21)
pRKISC	Tc^r, low copy number vector containing *iscSUA-hscBA-fdx*-ORF3	(15)
pRKNMC	Tc^r, low copy number vector	(15)

Table 4-2. Primers used for amplification in this study.

Primer	Description	Sequence 5' to 3'
5'porE2	Amplification of *M. maripaludis* S2 *porE* with *Nde*I site for use in pQE2	GCCGGCCATATGAAAAAAGTAATGATGGTTAGTGGAATC
3'porE2	Amplification of *M. maripaludis* S2 *porE* with ***Pst*I** site for use in pQE2	GCCGGC**CTGCAG**TTAAGGATTACATCTTGACGATGGAGTAAC
5'porF2	Amplification of *M. maripaludis* S2 *porF* with *Nde*I site for use in pQE2	GCCGGCCATATGAAGGTAATGCCAAATATTGACTTGTGC
3'porF2	Amplification of *M. maripaludis* S2 *porF* with ***Pst*I** site for use in pQE2	GTCCGGC**CTGCAG**TTATTTTCTTGAAGTTAATTTCTTAAGTTT
1MmporEF	Amplification of pQE2+*porE* or pQE2+*porF* plasmids with N-terminal his-tag with *Nsi*I site for use in pMEV2	CCGATGCATGAAACATCACCATCACCATCAC
2MmporEF	Amplification of pQE2+*porE* or pQE2+*porF* plasmids with N-terminal his-tag with ***Bgl*II** site for use in pMEV2	CCG**AGATCT**AAGCTCAGCTAATTAAGCTTCTGC
CporE5'	Amplification of *M. maripaludis*S2 *porE* with *Nsi*I site for use in pMEV2	CCCATGCATGAAAAAAGTAATGATGGTTAACG
CporE3'	Amplification of *M. maripaludis*S2 *porE* with ***Bgl*II** site and C-terminal his-tag for use in pMEV2	CCC**AGATCT***TTAGTGATGGTGATGGTGATGTTT*AGGATTACATCTTGACGATGCAGTA
CporF5'	Amplification of *M. maripaludis*S2 *porF* with *Nsi*I site for use in pMEV2	CCCATGCATAAGGTAATGCCAAATATTGACT
CporF3'	Amplification of *M. maripaludis*S2 *porF* with ***Bgl*II** site and C-terminal his-tag for use in pMEV2	CCC**AGATCT***TTAGTGATGGTGATGGTGATG*TTTTCTTGAAGTTAATTTCTTAAGT

Table 4-3. Pyruvate-linked ferredoxin-metronidazole assay from JJ150 and S2 cell-free extracts[a]

Fraction	Specific activity[b] (U mg^{-1})	Range[c] (U mg^{-1})
S2 cell-free extract	2.60	0.03
S2 low speed supernatant	1.73	0.00
JJ150 cell-free extract	1.81	0.21
JJ150 low speed supernatant	3.05	0.26

[a]In this assay, 15 or 20 μl cell-free extract was added to a sealed, nitrogen-sparged cuvette containing nitrogen-sparged 50 mM Tris-Cl pH 8.0 plus 0.1 mM metronidazole. To initiate the assay, 0.1 mM acetyl-CoA and 1.6 mM pyruvate were added to the cuvette. The ferredoxin-mediated reduction of metronidazole was monitored at 320 nm.

[b]Specific activity is the average of two assays; units are measured in mM metronidazole reduced $(min)^{-1}$.

[c]Range represents the difference between the two measurements.

Table 4-4. Membrane-associated hydrogenase-ferredoxin activities from *M. maripaludis* S2[a]

Fraction	Units[b]	Protein (mg)
cell extract[c]	37.6 +/- 4.7	32.57
low speed		
supernatant[c]	33.6 +/- 7.9	25.85
pellet[c]	2.1 +/- 0.3	5.61
high speed		
supernatant[d]	15.3 +/- 2.8	12.52
pellet[e]	16.0 +/- 4.7	11.33

[a]In this assay, cell-free extract was added to a sealed, hydrogen-sparged cuvette containing nitrogen-sparged 50 mM Tris-Cl pH 8.0 plus 0.1 mM metronidazole. This assay was intiated with cell-free extract, using between 10 ml (diluted 1:10) to 15 ml (undiluted), depending on the fraction. The ferredoxin-mediated reduction of metronidazole was monitored at 320 nm.

[b]Units are measured in μM metronidazole reduced x $(min)^{-1}$

[c]Data are the averages of three assays.

[d]Data are the averages of two assays.

[e]Data are the averages of four assays.

Figure 4-1. Expression of histidine-tagged PorE and PorF proteins in *Escherichia coli* and protein denaturation prior to loading on an SDS-PAGE gel. Predicted sizes of his-tagged PorE is 19.3 kDa and PorF is 16.4 kDa, but the negatively-charged histidine tag will cause the proteins to run slower. Histidine-tagged PorE is predicted to be the band in lane 3 at approximately 29 kDa and PorF is predicted to be the band in lane 5 at approximately 23 kDa. Dark bands at approximately 21 kDa are probably DNase. Lane 1, protein size markers (in kDa): 209, 124, 80, 49.1, 34.8, 28.9, 20.6, 7.1; lane 2, uninduced M13E; lane 3, induced M13E; lane 4, uninduced M13F; lane 5, induced M13F.

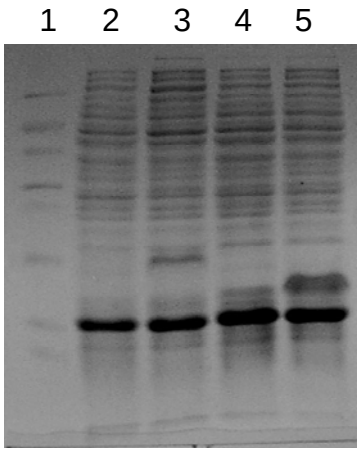
1 2 3 4 5

Figure 4-2. PorE and PorF are found in resuspended pellet fractions. Pellets were originally obtained from broken *E. coli* cells that were centrifuged at maximum speed in a microfuge for 20 minutes. The soluble protein fraction was analyzed for PorE and PorF protein but none was detected (data not shown). Here, the pellets were resuspended in 1 ml of Buffer B and were centrifuged for 20 minutes at 60% maximum speed (lanes 2, 3, and 4). Aliquots of the "soluble fraction" (20 μl) were removed and the pellets were resuspended and centrifuged for 20 minutes at 50% maximum speed (lanes 5, 6, and 7). Again, aliquots were removed, the pellets were resuspended and centrifuged for 20 minutes at 35% maximum speed. Lane 1, protein size markers (in kDa): 209, 124, 80, 49.1, 34.8, 28.9, 20.6, 7.1; lanes 2, 5, and 8, M15-pQE2; lanes 3, 6 and 9, induced M13E; lanes 4, 7, and 10, induced M13F.

1 2 3 4 5 6 7 8 9 10

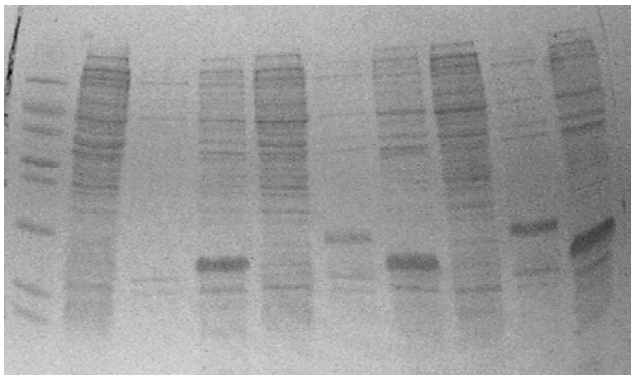

CHAPTER 5

CHARACTERIZATION OF THE EARLY STEPS OF *METHANOCOCCUS MARIPALUDIS* SULFUR ASSIMILATION: CYSTEINE UPTAKE, BIOSYNTHESIS AND METABOLISM[4]

[4]Major, T.A., K. Hong, D. Söll and W.B. Whitman. To be submitted to *J. Bacteriol*.

Abstract

A two-step pathway for Cys-tRNA^{Cys} loading and cysteine biosynthesis was proposed for several of the methanogenic archaea that do not contain the cognate pathways for cysteine biosynthesis (Sauerwald, A., W. Zhu, T. A. Major, H. Roy, S. Palioura, D. Jahn, W. B. Whitman, J. R. Yates, M. Ibba, and D. Söll. 2005. RNA-dependent cysteine biosynthesis in archaea. Science 307:1969-1972). To test this hypothesis, a mutation of the *Methanococcus maripaludis sepS* gene, which encodes the first step of the proposed cysteine biosynthesis pathway, was created. This strain is a cysteine auxotroph (strain S210). Further characterization of the S210 phenotype found that in mineral medium plus acetate, 190 μmol cysteine is required for a growth yield of 1 g cell dry weight. The total thiol concentration in *M. maripaludis* is approximately 283 μmol thiol x (g cell dry weight)$^{-1}$. Therefore, it appears that cysteine does not provide all the sulfur necessary for growth. Competition of cysteine uptake by the branched chain amino acids was also characterized in this work. In the presence of 100 μM cysteine, S210 growth is inhibited by the presence of 2 mM of the any of the branched chain amino acids. S210 growth is not inhibited by branched chain amino acids in medium containing 2 mM cysteine. Finally, attempts to generate a mutation in the gene encoding the second step of the proposed cysteine biosynthesis pathway (*pscS*) have been unsuccessful, suggesting that this may be a lethal mutation.

Introduction

Sulfur metabolism is an area that until recently has had little study. Assimilation of sulfur is vital for all organisms, as is the transport and regulation of sulfur concentration within the cell. Of the pathways involved in organic sulfur metabolism, perhaps the best described is cysteine biosynthesis, as it has been characterized in bacteria and mammals. In bacteria, cysteine is biosynthesized from serine (13) as described:

L-serine + acetyl-CoA ⟶ *O*-acetylserine + coenzyme A,

where serine is activated *via* the serine transacetylase (SAT) enzyme. In the second step of cysteine biosynthesis, the enzyme *O*-acetylserine sulfhydrylase (OASS-A or OASS-B) converts *O*-acetylserine to cysteine:

O-acetylserine + H_2S (or thiosulfate) ⟶ L-cysteine + acetate.

In mammals, methionine is used as a sulfur donor and serine acts as the carbon backbone in cysteine biosynthesis (6). First, methionine is converted to homocysteine by the methionine adenosyl transferase, S-adenosyl-L-methionine methyltransferase and adenosyl homocysteinase. Two further steps are utilized to convert homocysteine to cysteine: first, cystathionine β-synthase (CBS) catalyzes the following reaction to generate cystathionine:

L-homocysteine + L-serine ⟶ cystathionine + H_2O.

Second, cystathionine γ-ligase (CGL) converts cystathionine to cysteine as follows:

Cystathionine + H_2O ⟶ L-cysteine + NH_3 + 2-ketobutyrate.

The ability to biosynthesize cystiene is vital not only for protein generation, but also because free cysteine is utilized as a sulfur source. Free cysteine is the sulfur source for iron-sulfur clusters, thiamine, biotin, 4-thiouridine and molybdopterins (9, 11, 14, 16, 23). Cysteine desulfurases catalyze the breakdown of cysteine as well as transport and assembly of the thiol into sulfur-containing substrates (30, 31). This class of enzyme is homodimeric, pyridoxal 5'-phosphate-dependent, and catalyzes the production of L-alanine and sulfane sulfur via the formation of an enzyme-bound persulfide intermediate (30, 31). The four cysteine desulfurases described in bacteria are the NifS, IscS, the CsdA, and SufS enzymes (18, 24, 30, 31). The SepCysS protein is a distant homolog of this group of enzymes that was recently identified in methanogens (21). Another recently-described protein capable of cysteine catalysis is the

cysteine desulfidase (25). This protein was identified from *Methanocaldococcus jannaschii* and was recombinantly expressed in *E. coli* (25). This protein catalyzes the breakdown of cysteine into pyruvate, ammonia, and sulfide (25). It has been suggested that this enzyme may be involved in the biosynthesis of Fe-S clusters (25).

In the methanogens, even less is known about sulfur metabolism than in other organisms. Genomic data has not provided clear evidence for any particular pathway of cysteine biosynthesis or metabolism. The genome sequences of *Methanocaldococcus jannaschii, Methanothermobacter thermautotrophicum*, *Methanopyrus kandleri* and *M. maripaludis* are missing some or most of the homologs to enzymes typically used in cysteine production (1). These include SAT, OASS-A and -B, and CGL. Whether cysteine is used as the primary organic sulfur source is also mystery. The only NifS homolog found in *M. maripaludis* is the SepCysS protein, which is predicted to be involved in cysteine-tRNA^{Cys} biosynthesis. Interestingly, many proteins involved in biotin, molybdopterin and thiamine biosynthesis, which utilize organic sulfur derived from cysteine, have been identified in *M. maripaludis* (Table 5-1). The presence of these biosynthetic genes suggest that despite differences in the early steps of sulfur assimilation between the methanogens and other organisms, some later steps of sulfur-containing protein biosynthesis are similar to those already described (9, 11, 14, 23).

The efforts to elucidate the early steps of organic sulfur metabolism in *Methanococcus maripaludis* presented in this work have largely been focused on cysteine biosynthesis and metabolism. The two-step method for cysteine loading onto tRNA proposed by Sauerwald *et al.* (21) seems to be the sole method for generating cysteinyl residues in hydrogenotrophic methanogens. In this proposed pathway, *O*-phosphoserine is loaded onto tRNA^{cys} by a class II-type *O*-phosphoseryl-tRNA synthetase (SepRS, encoded by *sepS*). In *M. maripaludis*, deletion

of the *sepS* gene generated a cysteine auxotroph (21). In this work, the phenotype of the *M. maripaludis* Δ*sepS* strain is further explored. In the second step of cysteinyl-tRNA loading, the Sep-tRNA^{cys} is then converted to Cys-tRNA^{cys} by Sep-tRNA:Cys-tRNA synthase (SepCysS, encoded by *pscS*). The *in vitro O*-phosphoserine-tRNA^{Cys}:cysteine-tRNA^{Cys} activity of the SepCysS protein was demonstrated (21). In this work, attempts were made to isolate a Sep-tRNA:Cys-tRNA mutant in *M. maripaludis* for *in vivo* characterization.

Although there is evidence that the SepRS/SepCysS is the likely method for producing Cys-tRNA^{Cys}, other pathways for cysteine biosynthesis have not been excluded. An alternative pathway for cysteine biosynthesis has been proposed by White (28). In his study, GC-MS was used to quantify isotopically-labeled predicted intermediates (homocysteine, *O*-phosphoserine, L-cystathionine) relative to other, known cysteine biosynthesis pathways. A model was formed in which *O*-phosphohomoserine plus an unidentified sulfur source produces L-homocysteine. Homocysteine reacts with *O*-phosphoserine to form L-cystathionine, and cysteine is produced by the cleavage of L-cystathionine. While this pathway is plausible, it does not account for the cysteine auxotrophy of to the Δ*sepS* mutant (21). Conversely, one of the compelling arguments for the White model is the availability of free cysteine as the organic sulfur source. In the case of the Sauerwald model, it is unclear how cysteine metabolism and the biosynthesis of thiol-containing prosthetic groups and cofactors occurs if all the cysteine produced is shuttled into protein synthesis.

Another possibility is that cysteine is not used as the primary organic sulfur source in the methanogens. The rationale for using cysteine as a sulfur carrier is this compound can be monitored and transported by the cell, and cysteine is much less toxic than sulfide. The question arises as to how sulfide is sequestered by the cells, transported into the cells and shuttled to the

SepCysS. Methanogens are typically found in areas containing millimolar concentrations of sulfide. It seems illogical, therefore, that organisms should bind sulfide to cysteine, which is directly used in protein synthesis, then convert the cysteinyl residues back into free sulfide for synthesizing prosthetic groups or cofactors. Clearly, a great deal is unknown about sulfur metabolism in these organisms.

To clarify the pathway for organic sulfur anabolism, it is relevant to quantify the levels of free cysteine and homocysteine in *M. maripaludis*. If the White model is the primary method for cysteine biosynthesis in *M. maripaludis*, then there should be measurable quantities of free cysteine and homocysteine in the cells. If the Sauerwald model is the only method for cysteine biosynthesis in the hydrogenotrophic methanogens, then there should be negligible free cysteine in the cells. A lack of free cysteine would also suggest that cysteine is not the organic sulfur source. A high-pressure liquid chromatography technique is used in this work to quantify the levels of free cysteine and homocysteine in *M. maripaludis.*

Materials and methods

Strains, media and growth conditions. Table 5-2 lists the strains utilized in this study. *Methanococcus maripaludis* strain S2 was grown in 28 ml anaerobic culture tubes under 275 kPa H_2:CO_2 gas (80:20, v/v) at 37 °C as described in Jones *et al*. (8) and Whitman *et al*. (29). Media varied from the mineral medium (McN) of Whitman *et al*. (29) by the following additions: 10 mM sodium acetate, McA; sodium acetate plus 3 mM DTT as a reductant, McAD; sodium acetate, 0.2% Casamino acids, 1% (v/v) vitamin mixture (29), McCAV; the above additions plus 0.2% yeast extract, McYCAV. In some cases, neomycin was added at the concentration of 500 μg ml^{-1} in plates and 1000 μg ml^{-1} in broth. For free cysteine and homocysteine analyses, 12.5 ml of *M. maripaludis* cultures were grown in 160 ml sidearm bottles with 275 kPa H_2/CO_2 gas

(80:20 v/v) at 37 °C in McAD medium (8, 29). Growth of *M. maripaludis* was monitored at 600 nm using a Spectronic 20 spectrophotometer (Bausch and Lomb, New York).

Escherichia coli TOP10 was grown at 37 °C on low salt Luria-Bertani medium as described by Invitrogen (Carlsbad, CA). Kanamycin (50μg ml^{-1}) and/or ampicillin (75 μg ml^{-1}) was added to cultures containing pCR2.1 or pCRPrtNeo.

Plasmid construction. Standard cloning methods were used. The *sepS* plasmid construction was described in Sauerwald (21). Two *pscS* deletion plasmids were constructed using the pCRPrtNeo vector (19). The pCRPrtNeo vector contains two multiple cloning regions, either of which can be used for generating in-frame, markerless deletions in *Methanococcus maripaludis*. Alternatively, this vector can be used to create *neo* insertion mutants. The first plasmid, pHBA-1240, had the *pscS* flanking regions in tandem with the purpose of generating an in-frame deletion. The second *pscS* deletion plasmid, pCRPrtNeo-D*pscS*, was created for generating a gene insertion containing the neomycin resistance cassette. Primers for DNA amplification of *pscS* flanking regions are described in Table 5-3. To generate the in-frame deletion, primers were designed to contain a *Hin*dIII site on the 5' upstream primer, a *Bam*HI site on the 3' upstream primer and the 5' downstream primer, and an *Afl*II site on the 3' downstream primer for insertion into the pCRPrtNeo vector. The flanking regions were each approximately 600 bp in length, and the resulting Δ*pscS* gene was 441 bp in length. In the construction of the insertion plasmid, the *Hin*dIII and *Bam*HI sites were again used for the upstream flanking region, while *Not*I and *Xba*I sites were used in the downstream primers. *M. maripaludis* genomic DNA was purified using the Wizard Genomic DNA Purification Kit (Promega, Madison, WI). DNA was amplified using Herculase Enhanced DNA Polymerase (Stratagene, La Jolla, CA) and the Eppendorf Mastercycler gradient thermocycler. PCR samples were aliquotted into three tubes,

which were amplified (using the gradient function of the thermocycler) at different temperatures within the thermocycler. The cycling program proceeded as follows. To begin, there was a 1 min denaturation at 92 °C. The following steps were performed for 15 cycles. First, a denaturation step was performed at 92 °C for 30 seconds. Second, a gradient extenstion step of 45-55 °C was performed for 30 s with an increase of 1 °C per cycle (such that during the first cycle one tube was incubaed at 45 °C, one tube was incubated at 50 °C and one tube was incubated at 55 °C; during the second cycle, the tubes were at incubated at 46 °C, 51 °C, and 56 °C, etc.). Third, a gradient annealing step was performed at 60-70 °C for 1 min with an increase of 0.5 °C per cycle (where during the first cycle the tubes were incubated at 60 °C, 65 °C, and 70 °C, respectively; during the second cycle the tubes were incubated at 60.5 °C, 65.5 °C, and 70.5 °C; etc.). The first 15 cycles were immediately followed by a second round of 25 cycles (for a total program of 40 cycles). The second round of 25 cycles included a denaturation step at 92 °C for 30 s, which was followed by an extension step for 30 s at 52 °C. Finally, a gradient annealing step was performed at 63-73 °C for 1 min with a 10 s increase in duration per cycle (such that the tubes were incubated at 63 °C, 68 °C, and 73 °C during every cycle but the incubation was 1 minute during the first cycle, 1 min, 10 s during the second cycle, etc.). PCR amplification was verified via agarose gel electrophoresis. Genotypes of *pscS* merodiploids were analyzed by PCR amplification using the 1240f and 1240r primers listed in Table 5-2.

Amplified DNA was subcloned into the TOPO TA Cloning Kit (Invitrogen, Carlsbad, CA) for ease of subsequent molecular manipulation. Plasmids were purified using either the Wizard Plus Minipreps DNA Purification System (Promega, Madison, WI) for plasmids larger than 10 kb or the Qiaprep Spin Miniprep Kit (Qiagen, Valencia, CA) for plasmids < 10 kb. Vectors containing the *pscS* flanking regions were digested with the appropriate restriction

enzyme, gel purified using the Qiaquick gel extraction kit (Qiagen, Valencia, CA) and ligated into the pCRPrtNeo vector. The upstream and downstream *pscS* flanking regions were inserted into the pCRPrtNeo in a stepwise manner, where typically the upstream region was digested, ligated into the vector, electroporated and cloned. The resulting plasmid was then purified for the subsequent insertion of the downstream flanking region.

Transformations. *M. maripaludis* transformations were performed as previously described (26). Selection of in-frame deletion mutants was performed as described by Moore and Leigh (19). *E. coli* was transformed as described by Lin (17).

HPLC sample preparation. Cell extracts were prepared as described by Fahey and Newton (5) and Fahey *et al*. (4) with the following exceptions. Cultures (25 ml) were grown in McAD medium and were anaerobically pelleted but not frozen. Thiol positive controls included cysteine, homocysteine, and coenzyme M at approximately 50 nmol/reaction. Solutions were sparged with nitrogen gas instead of argon. Fifty microliters of a solution containing 100 mM HEPPS (pH 8.0), 5 mM EDTA, and 2 mM monobromobimane (mBBr) was added to cell pellets or thiol standards and allowed to incubate at room temperature for five minutes. Acetonitrile (50 µl) was added to the samples and incubated at 60 °C in a water bath for 15 minutes. All steps up to the addition of acetonitrile were performed in an anaerobic chamber (Coy Laboratory Products, Inc., Grass Lake, MI). Samples were homogenized for one minute using a Mini-BeadBeater (Biospec Products, Bartlesville, OK). Glacial acetic acid (1 µl) was added to the samples to stop the mBBr reaction. *M. maripaludis* samples were pelleted by centrifugation at maximum speed in a microcentrifuge for 10 minutes. The sample was diluted 1:1 with 1 % (v/v) acetic acid and centrifuged for an additional five minutes. Samples were either immediately

injected onto the HPLC or were stored at -20 °C. Frozen samples were thawed and centrifuged for 5 minutes prior to loading onto the HPLC.

For a negative control, DTNB was added to cell pellets to bind all cellular thiols. In this reaction, 2 mM DTNB was substituted for mBBr in the labeling reaction. As DTNB does not appear to be taken up by the cells, best results were obtained if DTNB was added to the cell pellet, and the mBBr solution was added following the acetonitrile step.

Instrumentation and HPLC analysis. HPLC analyses were performed using a Hitachi 655A-40 autosampler (Yokohama, Japan,) a Beckman 114M pump (San Ramon, CA), an Alltech 4.6 x 250 mm Alltima 5 μm C-18 column (Deerfield, IL), an RF-10AXL fluorescence detector (Shimadzu, Kyoto, Japan), and an HP 3390A Reporting Integrator (Hewlett-Packard, Avondale, PA). An isocratic elution of 10% HPLC-grade methanol, 0.25% acetic acid (in water) was used for cysteine analysis; 16.5% HPLC-grade methanol, 0.25% acetic acid was used for homocysteine analysis; and 18% HPLC-grade methanol, 0.25% acetic acid was used for coenzyme M analysis. The column was operated at a 1 ml/min flow rate. Fluorescence excitation and emission wavelengths were monitored at 400 nm and 490 nm, respectively.

Results and Discussion

*Strain S210 (*ΔsepS*) is a cysteine auxotroph*. In order to determine whether the two-step tRNA loading pathway was utilized for cysteine biosynthesis in the hydrogenotrophic methanogens, a deletion was made in the *M. maripaludis sepS* gene. *M. maripaludis* is the only hydrogenotrophic methanogen that has a well-developed genetic system, making gene deletions possible. Furthermore, *M. maripaludis* fortuitously has a copy of the cognate bacterial *cysS* gene, which, along with the uptake of exogenous cysteine, should allow this organism to grow without the proposed two-step cysteine biosynthetic pathway. It is known that the *cysS* gene is

not required for growth in *M. maripaludis* because deletion of that gene had no effect on the growth phenotype (22). Therefore, there must be another route for loading cysteine onto tRNA, which is predicted to be the same as in other hydrogenotrophic methanogens lacking the *cysS* gene (i.e., the proposed two-step pathway).

Construction of the S210 Δ*sepS* strain was described in Sauerwald *et al*. (21). Briefly, the flanking regions of the *sepS* gene were cloned into the integration vector pIJA03 around the puromycin transacetylase (*pac*) cassette. Following transformation, a double homologous recombination between the plasmid and genomic DNA generated the Δ*sepS* strain S210, which containes the *pac* cassette in place of the *sepS* gene. This strain requires exogenous cysteine for growth, demonstrating that *sepS* is necessary for cysteine biosynthesis in *M. maripaludis* (Figure 5-1; 21).

Further growth characterization of S210 strain. The cysteine auxotrophy of strain S210 in McAV +/- cysteine was previously presented by Sauerwald *et al*. (21). The growth phenotype of the S210 mutant strain in complex medium +/- cysteine was also analyzed (Figure 5-1). Slight growth variations were noted, particularly between the wild type +/- cysteine in the different media. These variations may be due to high concentrations of cysteine. These *M. maripaludis* cultures contained 3 mM cysteine, and *M. maripaludis* cultures have been grown in medium containing > 23 mM cysteine (data not shown). Cysteine has been shown to have an inhibitory effect in some strains of *E. coli* at 0.16 mM (7). This was due to down-regulation of the expression of the threonine deaminase enzyme, apparently during transcription (7). The threonine deaminase is necessary for isoleucine production in *E. coli*, but it is not part of the pathway for isoleucine biosynthesis in *M. maripaludis* (3), which may explain why *M. maripaludis* is resistant to high concentrations of cysteine.

In optimizing chemostats growing *M. maripaludis* S2, it was found that growth was inconsistant without cysteine in the medium (J. Leigh, pers. comm.) The S210 cysteine auxotroph was analyzed for the amount of exogenous cysteine necessary for growth (Figure 5-2). In McA medium, 190 μmol cysteine was required for a cellular yield of one gram cell dry weight. The predicted quantity of thiols in *M. maripaludis* is approximately 283 μmol thiol x g cell dry weight^{-1}. This calculation was based on reported quanties of thiol-containing vitamins, prosthetic groups and cofactors in methanogens, as well as the cysteine and methionine amino acid pool of *E. coli* (Table 5-4). This result suggests that cysteine cannot provide the total sulfur for the cells and that *M. maripaludis* utilizes an uncharacterized method for sulfur assimilation.

Interestingly, in complex medium, nearly twice the concentration of cysteine was required for growth yields similar to that seen in minimal medium (Figure 5-2). To identify the source of the growth inhibitor present in Casamino acids, growth experiments were performed using a slightly limiting concentration of cysteine (0.1 mM) plus 2 mM of the following: cysteamine, homocysteine, cysteic acid, serine, histidine, methionine, alanine, leucine and threonine. Only homocysteine and leucine inhibited growth of S210 (data not shown, Figure 5-3). In McA medium containing homocysteine, the S210 lag time was approximately 20 hours greater than that of S210 grown in McA medium alone. It is unclear how well exogenous homocysteine is taken up by *M. maripaludis*. It is possible that homocysteine and cysteine are taken up by the same transport mechanism, which would explain why growth of S210 was delayed in the presence of exogenous homocysteine. It is also possible that homocysteine acts as a transcriptional regulator of a protein involved in the biosynthesis of cysteine or as an alternative substrate for the SepCysS, which could also explain why homocysteine retards S210 growth.

Cysteine has previously been shown to inhibit the branched chain amino acid transport in *Salmonella typhimurium* (10). Because leucine inhibited the growth of the S210 mutant, additional experiments were performed with the other branched chain amino acids. These growth curves were performed with the S210 mutant in media containing either 2 mM or 0.1 mM cysteine in the presence or absence of the individual branched chain amino acids (Figure 5-3). Here, it was found that S210 growth was limited by the addition of any of the three branched chain amino acids in the presence of 0.1 mM cysteine. However, growth is restored in the presence of 2 mM cysteine. This result is consistant with the hypothesis of competition between amino acids during transport.

Attempts to generate a pscS *mutant in* Methanococcus maripaludis. The SepCysS protein was identified as a component of the protein fraction that catalyzed cysteine-$tRNA^{Cys}$ loading (21). The SepCysS protein is encoded by the *pscS* gene. Recombinant SepCysS catalyzed the conversion of *O*-phosphoserine-$tRNA^{Cys}$ to cysteine-$tRNA^{Cys}$ *in vitro* (21).

To confirm the function of the *pscS* gene product *in vivo*, plasmids were designed to delete the *pscS* gene. If the SepCysS converts *O*-phosphoserine-$tRNA^{Cys}$ to cysteine-$tRNA^{Cys}$, then a mutation in the *pscS* gene will generate a cysteine auxotroph. It is also possible that *pscS* is an essential gene, particularly if the SepCysS has other roles in sulfur metabolism, such as insertion of sulfur into prosthetic groups. The first attempt to delete the *pscS* gene was through an in-frame deletion (Figure 5-4). The in-frame, markerless deletion system in *M. maripaludis* was first described in Moore and Leigh (19). The vector used to make *M. maripaludis* in-frame deletions, pCRPrtNeo, contains two multiple cloning regions, which are separated by a neomycin cassette and the *hpt* gene, which confers 8-azahypoxanthine sensitivity. The upstream and downstream flanking regions of the gene of interest are cloned in tandem such that typically only

the start site of the gene, the six base restriction site, and the stop codon of the gene are transcribed. These flanking regions are cloned into the pCRPrtNeo vector within the same multiple cloning site, as follows: the upstream flanking DNA region of the *pscS* gene was amplified containing a 5' *Hin*dIII site and a 3' *Bam*HI site, where the ATG start codon for the *pscS* gene is immediately upstream of the *Bam*HI recognition site. The downstream flanking region contained a 5' *Bam*HI site and a 3' *Afl*II site, where the stop codon occurred immediately after the *Bam*HI site. The plasmid is then transformed into *M. maripaludis*. A homologous recombination event between one of the flanking regions of the plasmid and the corresponding flanking region of the chromosomal DNA is necessary to generate a merodiploid, as shown in Figure 5-4B. This strain is neomycin resistant. To generate a double-cross-over strain, the merodiploid strain is incubated overnight in medium without neomycin, then plated on medium containing the counterselection agent, 8-azahypoxanthine. The second recombination event must occur between the other plasmid flanking region and the chromosomal DNA in order to generate a gene deletion. Alternatively, if the second recombination occurs in the same flanking region as the original cross-over, a wild-type copy of the gene is retained. Under optimal conditions, the wild type:mutant phenotype ratio in the screen for the second cross-over event is 50:50. However, as mutants generally have growth deficiencies, it is more common to identify wild type colonies. Unfortunately, in the case of the *pscS*, >100 colonies screened had the wild-type *pscS* genotype despite 8-azahypoxanthine resistance (data not shown). Due to the difficult nature of screening under anaerobic conditions, it was unclear if the failure to isolate the mutant was due to the generation of the deletion at a low frequency or whether the deletion of the *pscS* was lethal.

A second Δ*pscS* plasmid was constructed to attempt to generate a neomycin cassette insertion into the *pscS* gene (Figure 5-5). Deletion by insertion of the neomycin cassette does not require a secondary cross-over/screening step as the in-frame deletions do, which makes the transformation process easier. Several attempts to delete the *pscS* by insertion were also unsuccessful. Although neomycin-resistant colonies were obtained, these colonies all had the wild-type genotype. Furthermore, independent attempts to generate a *pscS* mutant using a different vector were also unsuccessful (M. Hohn and D. Söll, pers. comm.). Therefore, no further endeavors to delete the *pscS* gene were undertaken.

Attempts to quantify free cysteine and homocysteine levels in Methanococcus maripaludis. The levels of various biologically-derived thiols have been previously quantified using the method of Fahey (4, 5). Although a minor amount of cysteine was identified in *Methanococcus voltae* (< 0.2 mM), it is unclear whether this cysteine was due to exogenous cysteine in the medium (5). A goal of this study is to quantify the levels of free cysteine and homocysteine in *M. maripaludis* S2.

The technique described by Fahey (5) utilizes monobromobimane to label free thiols. Not only does this compound selectively react with thiols, it also penetrates cell membranes, which minimizes thiol oxidation that occurs upon cell lysis (4, 12). The Fahey method utilizes reverse-phase HPLC and fluorescence detection to separate the labeled cellular thiols. A series of isocratic elutions are used to separate the labeled thiols on the C18 column. In this study, we did not have access to a similar HPLC aparatus, so attempts were made to optimize the Fahey method with the available system. Elution of a control containing cysteine was best performed using a 10:0.25:89.75 % (v/v) methanol-acetic acid-water running phase, while homocysteine best eluted with a 16.5:0.25:83.25 % (v/v) running phase. Unfortunately, when performing the

thiol labeling with *M. maripaludis* cells, there was a contaminating cell-derived peak overlapping the cysteine peak. Further optimization of the protocol, including quantification of free cellular coenzyme M (as an internal control), the removal of *M. maripaludis* protein, and the separation of small soluble particles *via* column chromatography are currently being performed.

Conclusion

The cysteine auxotrophy caused by the deletion of the *sepS* gene strongly suggests that the two-step Cys-tRNA^{Cys} pathway is the method of cysteine biosynthesis in *M. maripaludis*. Although not definitive, the difficulty in generating a *pscS* mutant also argues for the importance of this gene/protein in the cell. Based on calculations of the total cellular thiol content and the concentration of cysteine necessary for growth, it would appear that cysteine alone cannot support the total sulfur requirement. This suggests that the hydrogenotrophic methanogens utilize a novel method for thiol storage and insertion into cofactors and prosthetic groups. The preliminary work on thiol quantification in *M. maripaludis*, with a few more improvements, is likely to be successful in quantifying the levels of cysteine and homocysteine in *M. maripaludis*. If the quantity of free cysteine is less than the amount necessary for protein biosynthesis, the hypothesis that the two-step method for cysteine biosynthesis is the sole method of cysteine biosynthesis in *M. maripaludis* is supported.

Acknowledgments

The authors would like to thank James Henriksen for his help in using the HPLC. This work was supported by a grant from the U. S. Department of Energy.

References

1. **Ambrogelly, A., S. Kametkar, A. Sauerwald, B. Ruan, D. Tumbula-Hansen, D. Kennedy, I. Ahel, D. Söll.** 2004. Cys-tRNA^{Cys} formation and cysteine biosynthesis in methanogenic archaea: Two faces of the same problem? Cell. Mol. Life Sci. **61:**2437-2445.

2. **Balch, W. E., and R. S. Wolfe.** 1979. Transport of coenzyme M (2-mercaptoethanesulfonic acid) in *Methanobacterium ruminantium*. J. Bacteriol. **137:**264-273.

3. **Eikmanns, B. D. Linder, and R. K. Thauer.** 1983. Unusual pathway of isoleucine biosynthesis in *Methanobacterium thermoautotrophicum*. Arch. Microbiol. **136:**111-113.

4. **Fahey, R. C., R. M. Buschbacher, and G. L. Newton.** 1987. The evolution of glutathione metabolism in phototrophic microorganisms. J. Mol. Evol. **25:**81-88.

5. **Fahey, R. C., and G. L. Newton.** 1983. Occurrence of low molecular weight thiols in biological systems. *In:* Functions of Glutathione: Biochemical, Physiological, Toxicological, and Clinical Aspects, pp. 251-260. Larsson, A., S. Orrenius, A. Holmgren, and B. Mannervik (eds.), Raven Press, New York.

6. **Griffith, O. W.** 1987. Mammalian sulfur amino acid metabolism: an overview. Methods Enzymol. **143:**366-376.

7. **Harris, C. L.** 1981. Cysteine and growth inhibition of *Escherichia coli*: Threonine deaminoase as the target enzyme. J. Bacteriol. **145:**1031-1035.

8. **Jones, W. J., M. J. B. Paynter, and R. Gupta.** 1983. Characterization of *Methanococcus maripaludis* sp. Nov., a new methanogen isolated from salt marsh sediment. Arch. Microbiol. **135:**91-97.

9. **Kambampati, R., and C. T. Lauhon.** 1999. IscS is a sulfurtransferase in the *in vitro* biosynthesis of 4-thiouridine in *Escherichia coli* tRNA. Biochemistry **38:**16561-16568.

10. **Kiritani, K., and K. Ohnishi.** 1977. Repression and inhibition of transport systems for branched-chain amino acids in *Salmonella typhimurium*. J. Bacteriol. **129:**589-598.

11. **Kiyasu, T., A. Asakura, Y. Nagahashi, and T. Hoshino.** 2000. Contribution of cysteine desulfurase (NifS protein) to the biotin synthase reaction of *Escherichia coli*. J. Bacteriol. **182:**2879-2885.

12. **Kosower, E. M., B. Pazhenchevsky, and E. Hershkowitz.** 1978. 1,5-diazabicyclo[3.3.0]-octadiones (9,10-dioxabimanes). Strongly fluorescent syn isomers. J. Am. Chem. Soc. **100:**6516-6518.

13. **Kredich, N. M.** 1996. Biosynthesis of cysteine. *In: Escherichia coli* and *Salmonella*: Cellular and Molecular Biology, pp. 517-527. Neidhardt, F. C. (chief ed.), ASM Press, Washington, D.C.

14. **Lauhon, C. T., and R. Kambampati.** The *iscS* gene in *Escherichia coli* is required for the biosynthesis of 4-thiouridine, thiamin, and NAD. J. Biol. Chem. **26:**20096-20103.

15. **Leigh, J. A.** 1983. Levels of water-soluble vitamins in methanogenic and non-methanogenic bacteria. Appl. Environ. Microbiol. **45:**800-803.

16. **Leimkuhler, S., and K. V. Rajagopalan.** 2001. A sulfurtransferase is required in the transfer of cysteine sulfur in the *in vitro* synthesis of molybdopterin from precursor Z in *Escherichia coli*. J. Biol. Chem. **276:**22024-22031.

17. **Lin, W. C., and W. B. Whitman.** 2004. The importance of *porE* and *porF* in the anabolic pyruvate oxidoreductase of *Methanococcus maripaludis*. Arch. Microbiol. **179:**444-456.

18. **Mihara, H., T. Kurihara, T. Yoshimura, K. Soda, and N. Esaki.** 1997. Cysteine sulfinate desulfinase, a NIFS-like protein of *Escherichia coli* with selenocysteine lyase and cysteine desulfurase activities. Gene cloning, purification, and characterization of a novel pyridoxal enzyme. J. Biol. Chem. **272:**22417-22424.

19. **Moore, B. C., and J. A. Leigh.** 2005. Markerless mutagenesis in *Methanococcus maripaludis* demonstates roles for alanine dehydrogenase, alanine racemase, and alanine permease. J. Bacteriol. **187:**972-979.

20. **Neidhardt, F. C., and H. E. Umbarger.** 1996. Chemical composition of *Escherichia coli*. *In*: *Escherichia coli* and *Salmonella*: Cellular and Molecular Biology, pp.13-16. Neidhardt, F. C. (chief ed.), ASM Press, Washington, D.C.

21. **Sauerwald, A., W. Zhu, T. A. Major, H. Roy, S. Palioura, D. Jahn, W. B. Whitman, J. R. Yates, M. Ibba, and D. Söll.** 2005. RNA-dependent cysteine biosynthesis in archaea. Science **307:**1969-1972.

22. **Stathopoulos, C., W. Kim, T. Li, I. Anderson, B. Deutsch, S. Palioura, W. Whitman, and D. Söll.** 2001. Cysteinyl-tRNA synthetase is not essential for viability of the archaeon *Methanococcus maripaludis*. Proc. Natl. Acad. Sci. USA **98:**14292-14297.

23. **Takahashi, Y., and M. Nakamura.** 1999. Functional assignment of the ORF2-*iscS*-*iscU*-*iscA*-*hscB*-*hscA*-*fdx*-ORF3 gene cluster involved in the assembly of Fe-S clusters in *Escherichia coli*. **126:**917-926.

24. **Takahashi, Y., and U. Tokumoto.** 2002. A third bacterial system for the assembly of iron-sulfur clusters with homologs in archaea and plastids. J. Biol. Chem. **277:**28380-28383.

25. **Tchong, S., H. Xu, and R. H. White.** 2005. L-Cysteine desulfidase: an [4Fe-4S] enzyme isolated from *Methanocaldococcus jannaschii* that catalyzes the breakdown of L-cysteine into pyruvate, ammonia, and sulfide. Biochemistry **44:**1659-1670.

26. **Tumbula, D. L, R. A. Makula, and W. B. Whitman.** 1994. Transformation of *Methanococcus maripaludis* and identification of a *Pst*I-like restriction system. FEMS Microbiol. Lett. **121:**309-314.

27. **White, R. H.** 1989. Steps in the conversion of α-ketosuberate to 7-mercaptoheptanoic acid in methanogenic bacteria. Biochemistry **28:**9417-9423.

28. **White, R. H.** 2003. The biosynthesis of cysteine and homocysteine in *Methanococcus maripaludis*. Biochim. Biophys. Acta **1624:**46-53.

29. **Whitman, W. B., J. S. Shieh, S. H. Sohn, D. S. Caras, and U. Premachandran.** 1986. Isolation and characterization of 22 mesophilic methanococci. System. Appl. Microbiol. **7:**235-240.

30. **Zheng, L., R. H. White, V. L. Cash, R. F. Jack, and D. R. Dean.** 1993. Cysteine desulfurase activity indicates a role for NIFS in metallocluster biosynthesis. Proc. Natl. Acad. Sci. USA **90:**2754-2758.

31. **Zheng, L, R. H. White, V. L. Cash, and D. R. Dean.** 1994. Mechanism for the desulfurization of L-cysteine catalyzed by the *nifS* gene product. Biochemistry **33:**4714-4720.

Table 5-1. Homologs of thiamine, biotin and molybdopterin biosynthesis genes in *Methanococcus maripaludis* and *Methanocaldococcus jannaschii*.

Gene	Protein Name	*M. maripaludis* Homolog	*M. jannaschii* Homolog
thiC	thiamine biosynthesis protein	MMP0187	MJ1026
thiD	phosphomethylpyrimidine kinase	MMP1639	MJ0236
thiE	thiamine phosphate pyrophosphorylase	MMP1139	NF[a]
thiF	thiamine biosynthesis protein	MMP1234	NF
thiI	thiamine biosynthesis protein	MMP1354	MJ0931
thiJ	thiamine monophosphate kinase	MMP0559	MJ0967
thiL	thiamine phosphate kinase	MMP1124	NF
thiM	hydroxyethylthiazole kinase	MMP1138	MJ0028
bioA	aminotransferase class III	MMP0865	MJ1300
bioB	biotin synthase	MMP0126, MMP1238[b]	MJ1296, MJ0785[b]
bioW	6-carboxyhexanoate-CoA ligase	MMP1575	MJ1297
bioF	8-amino-7-oxononanoate synthase	MMP1574	MJ1298
bioD	dethiobiotin synthetase	MMP1573	MJ1299
moaA	molybdopterin synthase	MMP0571	MJ0824
moaB	molybdopterin synthase	MMP1485	MJ0167
moaC	molybdopterin synthase	MMP1066	MJ1135
moaD	molybdopterin synthase	MMP1357	MJ0018
moaE	molybdopterin synthase	MMP1235	MJ0717
moeA	molybdopterin synthase	MMP0545	MJ0886
moeB	molybdopterin synthase	MMP1234	MJ1661

[a]Not found.

[b]One of these open reading frames may correspond to the *lipA* (lipoic acid biosynthesis) gene.

Table 5-2. Bacterial strains and plasmids.

Strain	Genotype	Source or reference
M. maripaludis		
S2	Wild type	(28)
S900	Δ*hpt*	(19)
S210	Δ*hpt* Δ*sepS*	(21)
E. coli TOP10	*F⁻ mcrA* Δ(*mrr-hsdRMS-mcrBC*) Φ80*lacZ*Δ*M15* Δ*lacX74 recA1 deoR araD139* Δ(*ara-leu*)*7697 galU galK rpsL* (Str^r) *end A1 nupG*	Invitrogen
Plasmids	**Description**	**Source or reference**
pIJA03	Pur^r methanogen integration vector	(22)
pCRPrtNeo	*hmv* promoter-*hpt* fusion + Neo^r cassette in pCR2.1 TOPO for methanococcal in-frame deletions	(19)
pHBA-1240	pCRPrtNeo with tandem upstream and downstream flanking regions of *pscS* for in-frame deletion	This work
pCRPrtNeo-D*pscS*	pCRPrtNeo with upstream and downstream regions of *pscS* separated by *neo* and *hpt* genes, for insertion	This work

Table 5-3. Oligonucleotide primers used.

Primer	Sequence 5' → 3'
5uppscS	CCCCAAGCTTTTAACGAATCAAACATAATTTCTCCC
3uppscS	CGCGGATCCGGACATGTCTTCTAAAAATTCGTTTATAGG
5dnpscS	CGCGGATCCATAAACCACGATATCATAAGATTTGAAACCC
3dnpscS	CCCCTTAAGTTATTCTTCTTTTACGTAATATTTTACCATTTCTTC
5'upDpscS	CCCAAGCTTCAATTAACTCCACTGATGCATTGAA
5'dnDpscS	CCCGGATCCCATAAAATCACCAATTCTCGCGTAA
5'dnDpscS	CCCGCGGCCGCTGAATTTAATGAGTTCTAAGTATGT
3'dnDpscS	CCCTCTAGAGAAATTATACTTGAAGCAAAGAAAA
1240f	GATTCGATAGAAAGAATAAATACGG
1240r	CCCTGATTAAATGTAACTCCTAAAA

Note: Restriction endonuclease sites are underlined.

Table 5-4. Thiol-containing vitamins, prosthetic groups and cofactors in methanococci.

Thiol	Cellular quantity (μmol thiol x g cell dry wt.$^{-1}$)	Reference
biotin	0.001	(15)
thiamine	0.047	(15)
pantothenate	0.041	(15)
coenzyme M	0.5	(2)
Fe-S clusters	50	(27)
cysteine	87	(20)
methionine	146	(20)

Figure 5-1. Growth of *M. maripaludis* wild type (S2) and Δ*sepS* (S210) strains. About 2 x 10^3 cells were subcultured and inoculated into prewarmed medium containing 3 mM coenzyme M for a final cysteine concentration of <0.16 µM (□, ○) or into the same medium with 3 mM cysteine (■ and ●). Wild type S2 (● and ○), and *sepS* mutant S210 (■ and □). A. Growth in the mineral medium plus acetate and vitamins (McAV) (21). B. Growth in complex medium containing Casamino acids plus acetate and vitamins (McCAV).

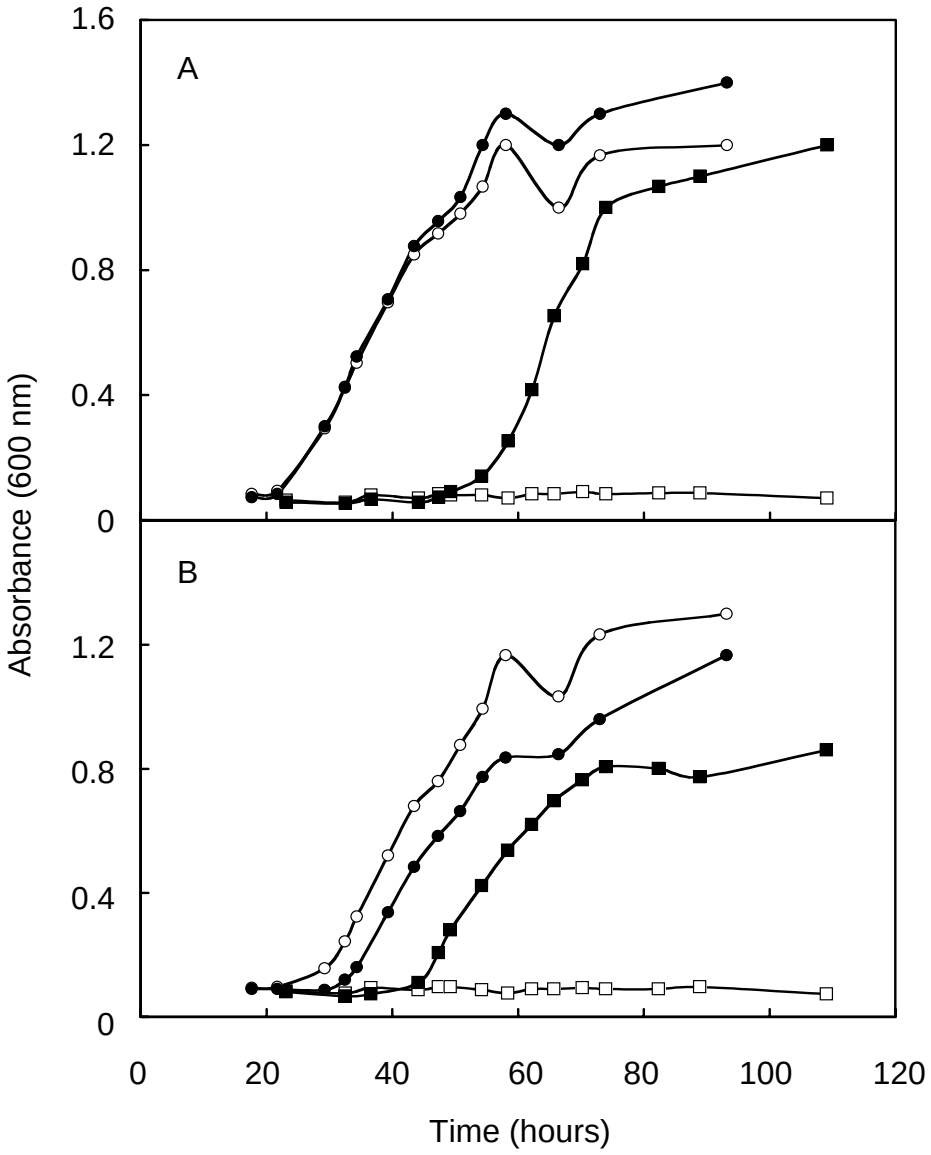
A
B
1.6
1.2
0.8
0.4
0
0
20
40
60
80
100
120
Absorbance (600 nm)
Time (hours)

Figure 5-2. Maximum absorbance (600 nm) of S210 upon the addition of limiting concentrations of cysteine. A cysteine stock solution was prepared in McAV medium and was nitrogen-sparged and filter-sterilized. Cysteine was added to the prewarmed cultures prior to inoculation. A. Growth of S210 with a limiting amount of cysteine in McAV medium (■). Line of best fit: Maximum absorbance = 0.3677 ln [cys] - 0.7838, R^2 = 0.926. B. Growth of S210 with a limiting amount of cysteine in McCAV medium (●). Line of best fit: Maximum absorbance = 0.526 ln [cys] - 1.9636, R^2 = 0.9885.

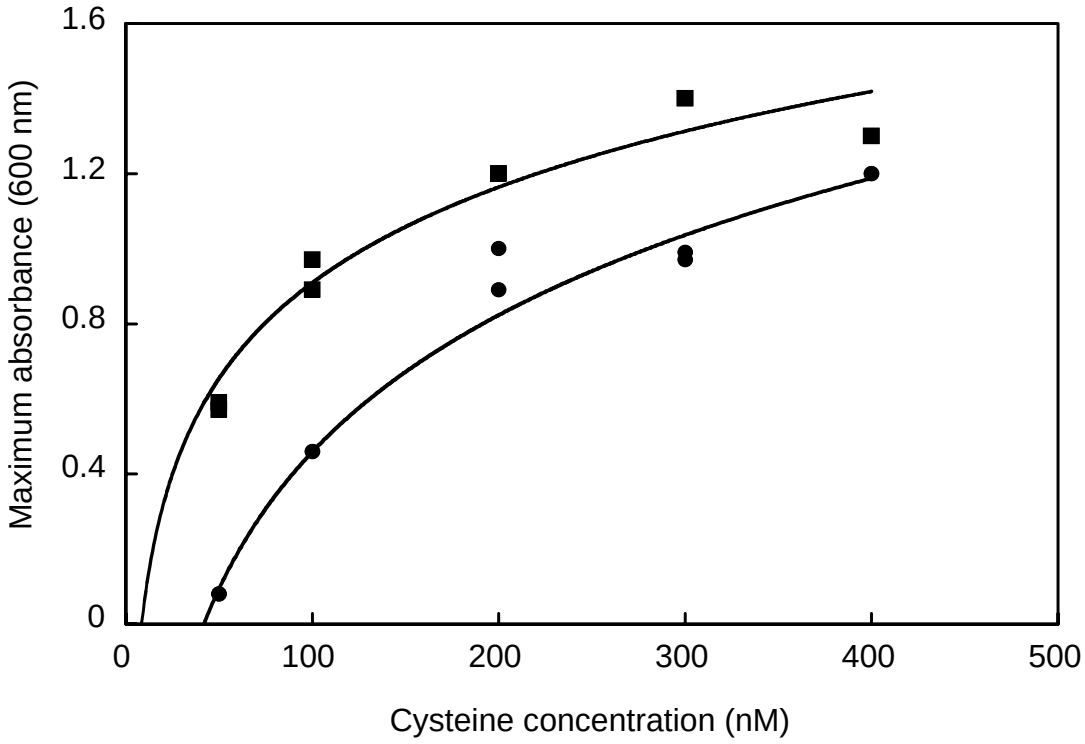
1.6
1.2
0.8
0.4
0
Maximum absorbance (600 nm)
0
100
200
300
400
500
Cysteine concentration (nM)

Figure 5-3. S210 growth is inhibited by branched chain amino acids when the cysteine concentration is limiting. McAV medium was supplemented with 2 mM isoleucine (■), leucine (▲), valine (◆), no branched chain amino acid (●), no cysteine or branched chain amino acid added (○). A. S210 growth in media containing 2 mM cysteine. B. S210 growth in media containing 0.1 mM cysteine.

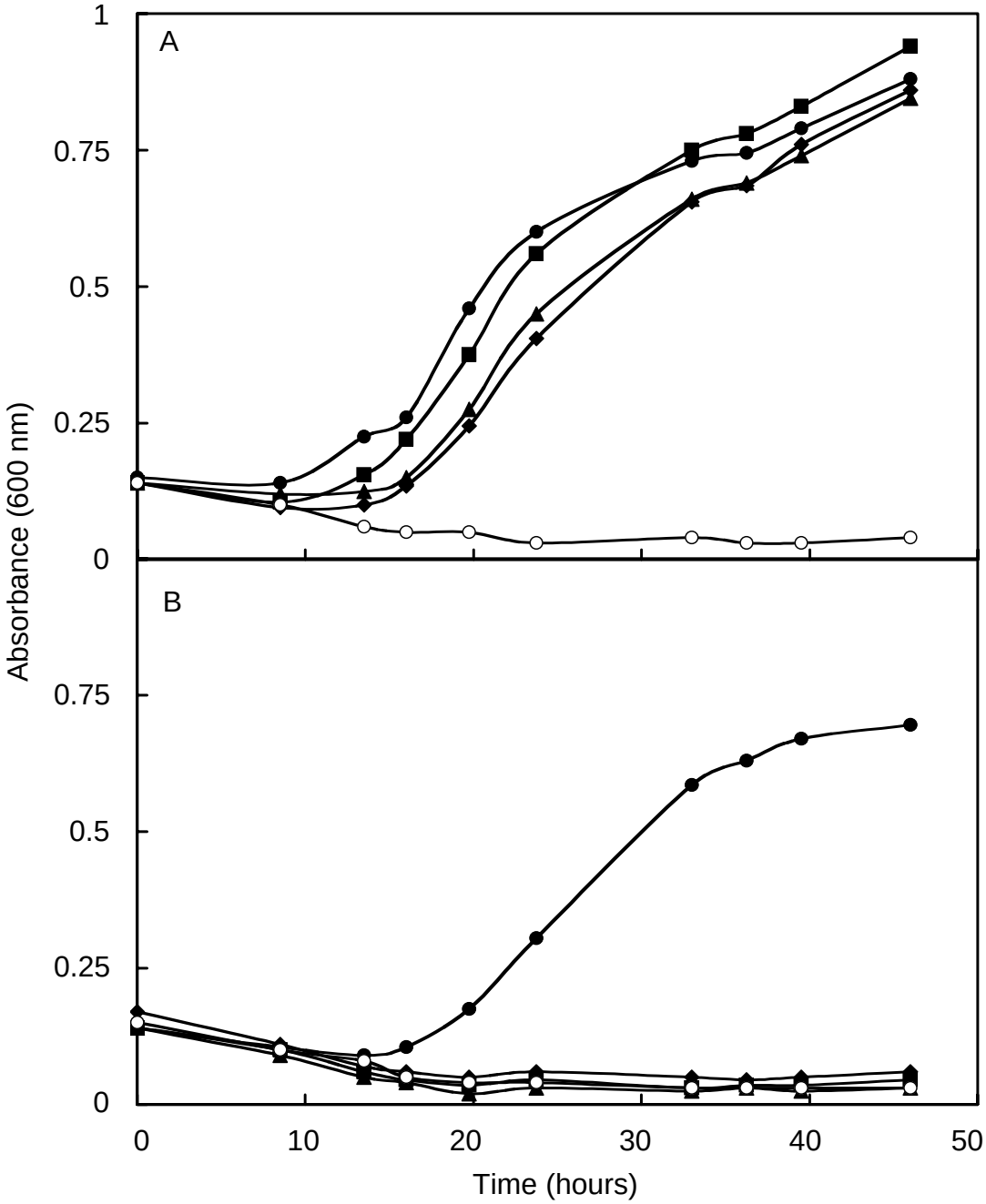
A
B
1
0.75
0.5
0.25
0
0
10
20
30
40
50
Absorbance (600 nm)
Time (hours)

Figure 5-4. A. Model of deletions in the *pscS* gene. The pCRPrtNeo plasmid for generating in-frame deletions contains the neomycin cassette (neo), conferring neomycin resistance, and the *hpt* gene, which confers 8-azahypoxanthine sensitivity. Flanking regions for the *pscS* gene are cloned into one of the multiple cloning sites of the plasmid. The plasmid is transformed into *M. maripaludis* as described by Tumbula *et al.* (26). A single recombination event between the plasmid and the genomic DNA yields a neomycin-resistant strain containing both the wild-type and deleted version of the *pscS*. Shown here is the crossing-over event between homologous regions of the MMP1239 genes and the N-terminus of the *pscS* gene. Alternatively, this recombination event could also occur at the MMP1241 (dotted) gene (not shown). Incubation of this merodiploid strain in the absence of neomycin causes the plasmid to loop out via a second cross-over event. Counterselection with the base analog 8-azahypoxanthine (8-zhyp) yields only cells that have "looped out" the plasmid, i.e., lost the *hpt* gene. This step yields either the Δ*pscS* genotype (if the second crossing-over event occurred between the dotted genes as shown) or wild-type (if crossing over occurred in the thatched genes, not shown). B. Merodiploid containing both wild-type and Δ*pscS* genes. Lane 1, PCR amplification from the pHBA-1240 plasmid; lane 2, wild type *M. maripaludis* genomic DNA; lane 3, PCR amplification of genomic DNA from a merodiploid mutant culture.

A

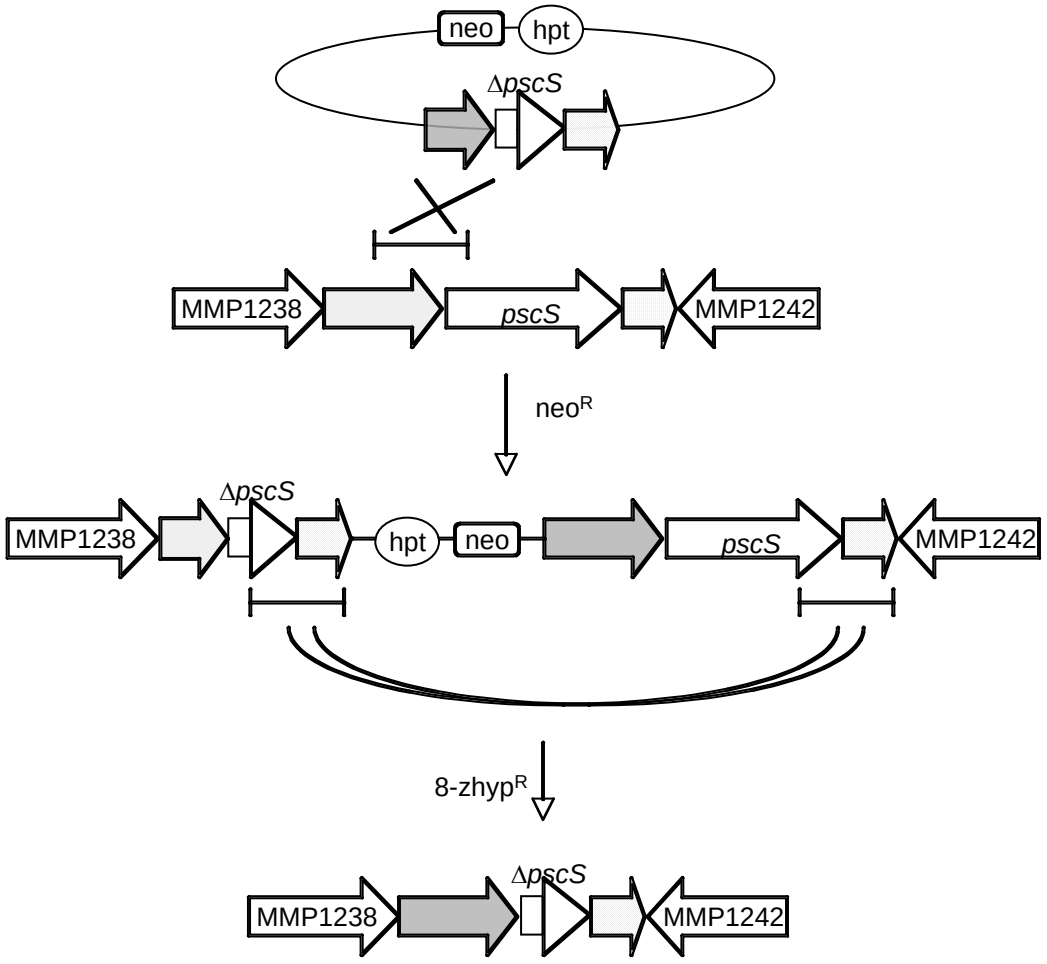
neo
hpt
ΔpscS
MMP1238
pscS
MMP1242
neoR
ΔpscS
MMP1238
hpt
neo
pscS
MMP1242
8-zhypR
ΔpscS
MMP1238
MMP1242

B

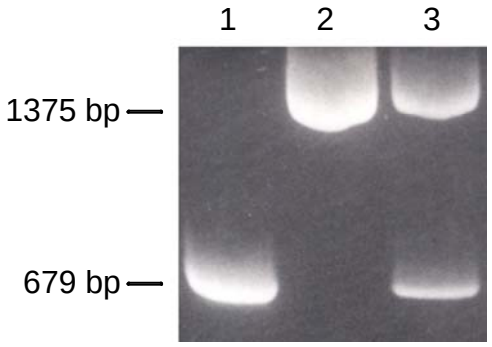
1
2
3
1375 bp
679 bp

Figure 5-5. Model of the strategy to generate a double homologous recombination event generating a *pscS*::*neo* insertion. Flanking regions to the *pscS* gene were amplified and inserted into the pCRPrtNeo plasmid, generating pCRPrtNeo-D*pscS*. After transformation into *M. maripaludis*, a double homologous recombination event between the plasmid and the genomic DNA will generate a neomycin resistant transformant lacking the *pscS* gene. Since the plasmid was not linearized prior to transformation into *M. maripaludis*, it is also possible to generate a single cross-over event to generate a merodiploid strain (not shown), although this event was not observed.

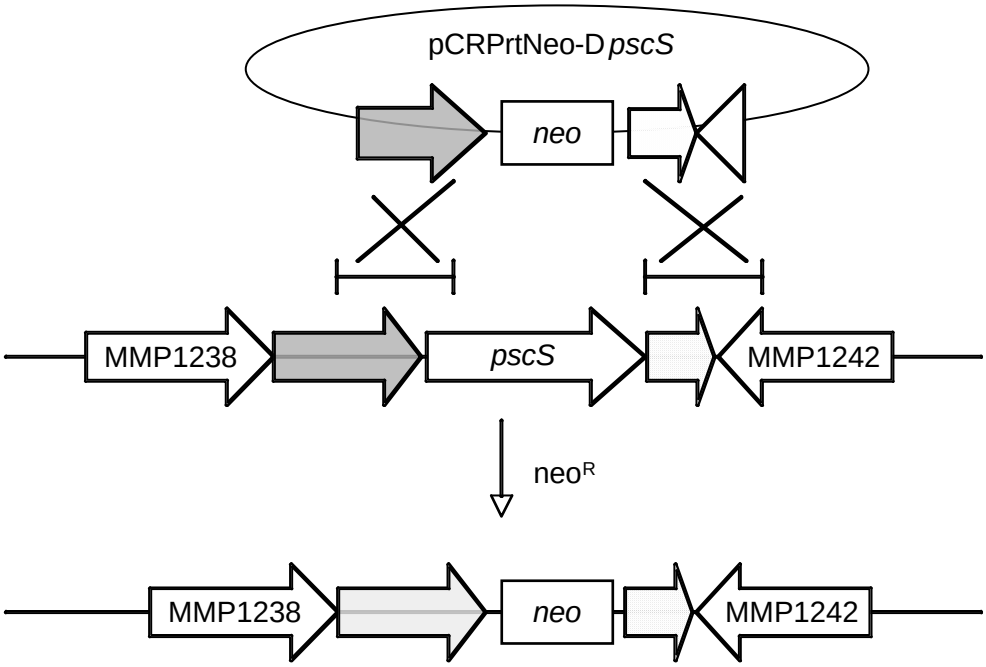
pCRPrtNeo-D*pscS*
neo
MMP1238
pscS
MMP1242
neo^{R}
MMP1238
neo
MMP1242

CHAPTER 6

CONCLUSION

Electron transport in the hydrogenotrophic methanogen *Methanococcus maripaludis* is confounded by the lack of cytochromes and methanophenazine, which are the electron carriers in aceticlastic methanogens. However, the large number of ferredoxins and polyferredoxins found in the genomes of methanogens suggests that these proteins are the primary vehicle for electron transport in these organisms. The energy conserving hydrogenase b (Ehb) generates electrons for enzymes involved in autotrophy such as the carbon monoxide dehydrogenase/acetyl-CoA synthase (CODH/ACS), the pyruvate oxidoreductase (Por) and the indolepyruvate oxidoreductase (Ior). Furthermore, the Ehb generates a proton motive force to drive the endergonic autotrophic reactions forward. In order to characterize the function of the Ehb, several *ehb* deletion strains were made. With the exception of a gene encoding a membrane-spanning protein of unknown function, deletions in genes encoding a ferredoxin, polyferredoxin, proton translocator, and the large and small hydrogenase subunits all produced mutant strains whose growth under autotrophic conditions was limited. However, the ability of the *ehb* mutants to grow autotrophically suggests that either another enzyme can replace the function of the Ehb, albeit poorly, or that the deleted subunits can be replaced by other proteins to rescue the growth defects. In addition, the large hydrogenase mutant strain S965 was incapable of growth in minimal medium containing aryl acids. Aryl acids inhibit the *de novo* pathway of aromatic amino acid biosynthesis but can be converted to aromatic amino acids by the indolepyruvate

oxidoreductase. Therefore, the S965 growth defect demonstrates that there is a direct physiological association between the Ehb and the Ior.

The Por is also coupled to the Ehb. In *M. maripaludis*, the operon encoding the Por was found to contain two extra open reading frames that appear to encode ferredoxins. These ferredoxins were hypothesized to shuttle electrons between the Ehb and Por. Expression and purification of histidine-tagged PorE and PorF from *E. coli* were attempted in order to characterize these proteins. Enzyme assays were also designed to characterize the interactions between the PorE and PorF, the Ehb, and the Por. Although the data suggests that both the Por and Ehb can reduce the ferredoxin-linked dye metronidazole, other results are inconclusive. Future work may include the use of Western blotting to confirm *M. maripaludis* histidine-PorE and –PorF expression and purification.

Finally, sulfur assimilation is required to generate cysteine, which in turn donates sulfur to iron-sulfur clusters and other thiol-containing cofactors and prosthetic groups. In most organisms, the assimilation of sulfur begins with cysteine biosynthesis and metabolism. Cysteine biosynthesis in hydrogenotrophic methanogens appears to occur *in vitro* via a two-step cysteine-tRNA^{Cys} loading mechanism. This pathway utilizes the *sepS* gene, which encodes a protein that binds *O*-phosphoserine to the tRNA, and the *pscS* gene, which encodes a protein that converts *O*-phosphoserine to cysteine. A *sepS* deletion strain S210 was a cysteine auxotroph. Attempts to delete the *pscS*, which encodes the second step of the cysteine biosynthesis pathway, were unsuccessful, suggesting that this gene may be essential. The minimum amount of cysteine necessary for growth is less than the calculated amount of thiols within *M. maripaludis*. This supports the hypothesis that the two-step pathway is the sole pathway for cysteine biosynthesis in the hydrogenotrophic methanogens. However, it is unclear how sulfur-containing cofactors and

prosthetic groups are formed as the sulfur is typically donated by free cysteine, which in the two-step pathway would not exist. In order to ascertain whether *M. maripaludis* has a pool of free cysteine, which would suggest that there is another cysteine biosynthesis pathway, an HPLC protocol was adapted that uses the thiol-binding fluorescent molecule monobromobimane to label all cellular free thiols. Current efforts are underway to optimize this method.